OCS Study
BOEM 2019-034

Multidisciplinary Assessment of Deepwater Coral Ecosystems: Tools to Detect Impacts of Sub-lethal Stress

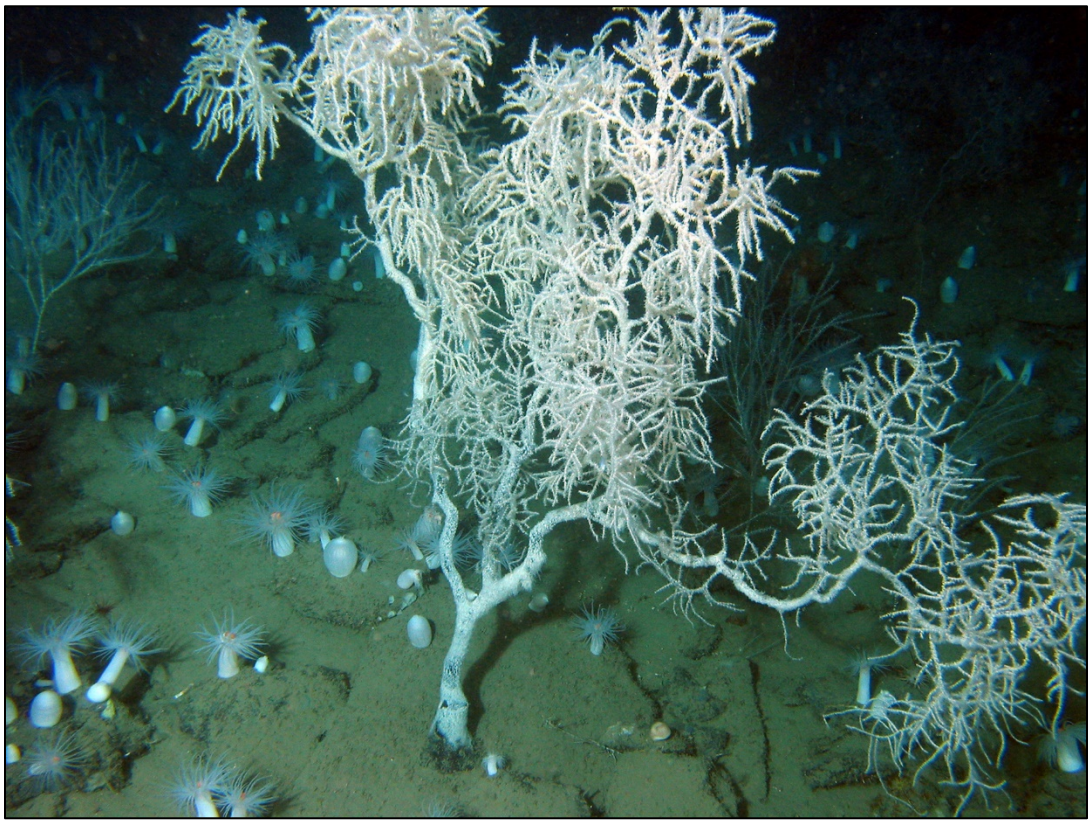

U.S. Department of the Interior
Bureau of Ocean Energy Management
Gulf of Mexico OCS Region

BOEM
Bureau of Ocean Energy Management

OCS Study
BOEM 2019-034

Multidisciplinary Assessment of Deepwater Coral Ecosystems: Tools to Detect Impacts of Sub-lethal Stress

Authors

Nancy G. Prouty
Christina A. Kellogg
Cheryle L. Morrison

Prepared under US Geological Survey Outer Continental Shelf Funding
by
US Geological Survey
12201 Sunrise Valley Dr.
Reston, VA 20192

Published by

U.S. Department of the Interior
Bureau of Ocean Energy Management
Gulf of Mexico OCS Region

New Orleans, LA
July 2019

DISCLAIMER

This study was supported by US Geological Survey Ecosystems Mission Area, Environments Program funding. This report has been technically reviewed by BOEM, and it has been approved for publication. The views and conclusions in this report do not necessarily represent BOEM, but do represent the views of the U.S. Geological Survey, nor does mention of trade names or commercial products constitute endorsement or recommendation for use

REPORT AVAILABILITY

To download a PDF file of this Gulf of Mexico OCS Region report, go to the U.S. Department of the Interior, Bureau of Ocean Energy Management, Environmental Studies Program Information System website and search on OCS Study BOEM 2019-034.

This report can be viewed at select Federal Depository Libraries. It can also be obtained from the National Technical Information Service; the contact information is below.

U.S. Department of Commerce
National Technical Information Service
5301 Shawnee Rd.
Springfield, Virginia 22312
Phone: (703) 605-6000, 1(800)553-6847
Fax: (703) 605-6900
Website: http://www.ntis.gov/

CITATION

Prouty NG, Kellogg CA, Morrison CL. 2019. Multidisciplinary assessment of deep-water coral ecosystems: Tools to detect impacts of sub-lethal stress. New Orleans (LA): US Department of the Interior, Bureau of Ocean Energy Management, Gulf of Mexico OCS Region. Study No.: OCS Study BOEM 2019-034.

ABOUT THE COVER

Cover photo of black coral (*Antipatharia*) provided by US Geological Survey DISCOVRE.

ACKNOWLEDGMENTS

The US Geological Survey Environments Program and Coastal and Marine Geology Program contributed to this document.

Contents

List of Figures

List of Tables

List of Abbreviations and Acronyms

Abbreviation	Meaning
ACL	average calculated length
ADCP	acoustic Doppler current profiler
AMS	accelerator mass spectrometry
ANOSIM	analysis of similarities
ATL	Atlantic
BOBO	bottom boundary
BOEM	US Department of Interior's Bureau of Ocean Energy Management
BSE	back-scattered electrons
BUSCO	Benchmarking Universal Single-Copy Orthologs
cDNA	complementary DNA
CDS	coding sequences
cds	coding regions
CPI	carbon preference index
CPS	counts per second
CRA	conventional radiocarbon age
CSIA	compound specific isotope analysis
DOI	US Department of the Interior
dTTP	deoxythymidine triphosphate
dUTP	deoxyuridine triphosphate
ESP	Environmental Studies Program
ESR	environmental stress response
GC	gas chromatograph
GO	gene ontology
Gulf	Gulf of Mexico

Abbreviation	Meaning
HMW	high molecular weight
HPLC	high performance liquid chromatograph
HSP	hear shock proteins
IEAE	International Atomic Energy Agency
KEGG	Kyoto Encyclopedia of Genes and Genome
KO	KEGG orthology
KOH	potassium hydroxide
LA-ICP-MS	Laser Ablation Inductively Coupled Mass Spectrometry
LCF	linear combination fitting
LLNL	Lawrence Livermore National Laboratory
MAR	Mississippi and Atchafalaya rivers
MARB	Mississippi and Atchafalaya River Basin
mRNA	messenger RNA
NCBI	National Center for Biotechnology Information
NCBI SRA	National Center for Biotechnology Information Sequence Read Archive
OCS	Outer Continental Shelf
OM	organic matter
OTUs	operational taxonomic units
PCR	polymerase chain reaction
POC	particulate organic carbon
poly-A	poly-adenylated
Q	quality
qPCR	quantitative PCR
QUAST	Quality Assessment Tool for Genome Assemblies
ROV	remotely-operated vehicle

Abbreviation	Meaning
rRNA	ribosomal RNA
SEDCI	Southeastern Deep Coral Initiative
SEM	scanning electron images
SIM	single ion monitoring mode
SSRL	Stanford synchrotron radiation lightsource
TLR	toll-like receptors
TNFR	tumor necrosis factor receptors
UNCW	University of North Carolina–Wilmington
USF	University of San Francisco
USGS	US Geological Survey
VK	Viosca Knoll
WFS	West Florida Shelf
WHOI	Woods Hole Oceanographic Institution
WSU	Washington State University
XANES	X-ray absorption near edge structure
XAS	X-ray absorption spectroscopy
XRF	X-ray fluorescence

List of Authors

Chapter Title	Authors	Affiliations
Chapter 2: Deep-Sea Coral Metagenomes	Christina A. Kellogg	U.S. Geological Survey, St. Petersburg Coastal and Marine Science Center
Chapter 3: De novo Assembly and Functional Annotation of the Transcriptome of the Deep-water Coral *Lophelia pertusa*	Cheryl L. Morrisons	U.S. Geological Survey, Leetown Science Center
	D. Katharine Coykendall	
	Lakyn Sanders	
Chapter 4: Uptake and Distribution of Organo-iodine in Deep-sea Corals	Nancy G. Prouty	U.S. Geological Survey, Pacific Coastal and Marine Science Center
	E. Brendan Roark	Department of Geography, Texas A&M University
	Lesley Mohon	Department of Geography, Texas A&M University
	Ching-Chih Chang	University of Arizona
Chapter 5: Impact of the *Deepwater Horizon* Spill on Food Supply to Deep-Sea Benthos Communities	Nancy G. Prouty	US Geological Survey
	Pamela Swarzenski-Campbell	
	Furu Mienis	Royal Netherlands Institute for Sea Research
	Gerard Duineveld	Royal Netherlands Institute for Sea Research
	Amanda Demopoulos	US Geological Survey
	Steve W. Ross	University of North Carolina-Wilmington
	Sandra Brooke	Florida State University

1 Introduction

As part of the National Ocean Policy, the Bureau of Ocean Energy Management (BOEM) has been involved with several major research programs examining the distribution and community ecology of deep-sea coral ecosystems, including two recent, large federal interdisciplinary studies focused on the Gulf of Mexico (Gulf; Chemo III and *Lophelia* II, see Boland et al. 2017 for overview). However, long-term changes and potential for recovery in these ecosystems following disturbances remains unresolved, as does knowledge about deep-sea coral response to the *Deepwater Horizon* oil spill. This comprehensive report addresses critical information needed for informed decision making: tools to detect impacts of sub-lethal stress and to quantify health and resilience factors in deep-sea coral ecosystems. Multidisciplinary in nature, report chapters include aspects of the geologic, biologic, and chemical components of these complex ecosystems. These data will be critical for National Environmental Policy Act documents for assessing the cumulative effects of the spill by providing time series and data trend information for identification of significant changes in the quality and productivity of these environments, and to identify the causes of these changes—in direct support of BOEM's mission to manage development of U.S. Outer Continental Shelf (OCS) energy and mineral resources in an environmentally and economically responsible way.

1.1 Study Area

Samples analyzed for this report were obtained from areas in the Gulf and one site in the western Atlantic (ATL) (Figure 1.1). For age analyses, black coral (*Leiopathes* sp.) specimens were collected east of the Mississippi Delta from the Gulf in the Viosca Knoll (VK) region, and the head of De Soto Canyon as described in Prouty et al. (2011). The head of De Soto Canyon is on the outer shelf zone with a relatively steep western wall and a much gentler eastern wall. An upwelling of deep nutrient-rich water occurs here, resulting in relatively high primary productivity. De Soto Canyon has been identified as the divide between the terrigenous Mississippi River muddy sediments to the west and the allochthonous carbonate sediments to the east (Bryant et al. 1991). Previous studies in the Viosca Knoll region of the northern Gulf highlight the Mississippi-Atchafalaya River (MAR) Basin as the major source of sediment and nutrients transported to the seafloor (Davies et al. 2010; Mienis et al. 2012; Prouty et al. 2014a, 2016). The large quantities of river-borne nutrients stimulate surface primary productivity in the Gulf, producing organic matter (OM) that flocculates and sinks to the seafloor. For example, Mienis et al. (2012) found peaks in near-seabed fluorescence corresponding to increases in pigments, organic carbon (C_{org}), total nitrogen (N_{tot}), and biogenic silica (SiO_2) in sediment trap samples. The Mississippi River discharges approximately 1.5×10^{12} g C yr^{-1} (Dubois et al., 2010), with enhanced weathering predicted from climate and land-use change (Beaulieu et al. 2012). The Loop Current System transports these large riverine plumes offshore (Schiller and Kourafalou 2014).

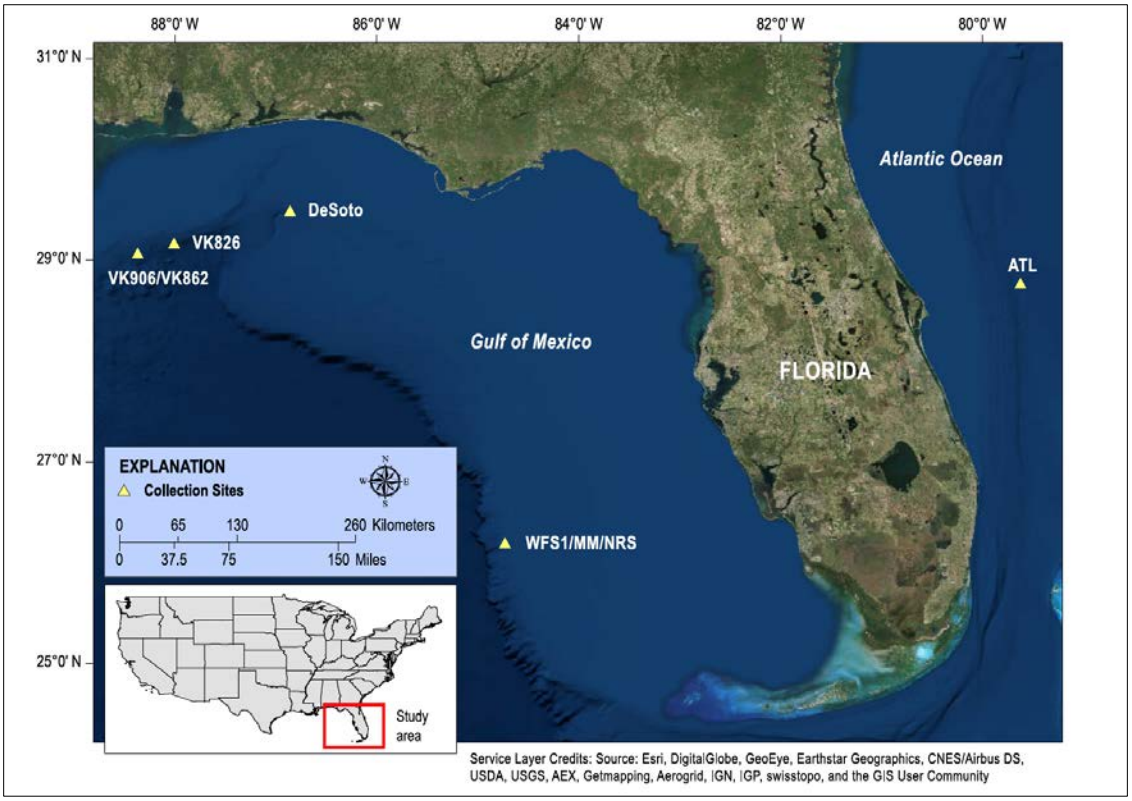

Figure 1.1 Study area map.

1.2 Background

The Gulf OCS is a geologically-complex region supporting extensive and valuable commercial and recreational fisheries as well as unique deep-sea communities, including chemosynthetic seeps and cold-water corals (Boland et al. 2017). The Gulf is also a natural hydrocarbon basin, with stores of oil and gas lying beneath the sea floor, along with salt deposits that may raise the sea bed to form banks or mounds. Natural, ephemeral seepage of hydrocarbons from the sea floor exposes biota to diffuse hydrocarbons and supports numerous chemosynthetic communities (Cordes et al. 2007). Once seepage of hydrocarbons and sulfide has subsided, authigenic carbonates created from the precipitation of carbonate associated with the activity of archaea and bacteria remain, and are often colonized by deep-water corals (Cordes et al. 2008; Brooks et al. 2016). Deep-water corals are long-lived and slow growing (Roark et al., 2009; Prouty et al., 2011), making them particularly vulnerable to anthropogenic disturbances and slow recovery rates (decades or longer; Montagna et al. 2013). Information on growth rates and life spans of deep-sea corals is important for understanding the vulnerability of these organisms to both natural and anthropogenic perturbations, as well as the likely duration of any observed adverse impacts. Demonstrated slow growth rates suggest that it may take centuries for certain deep-sea coral species to recover from negative impacts. One of the major challenges in using radiocarbon as a chronometer is uncertainty in the

differences between the radiocarbon content of the atmosphere and the deep ocean, referred to as the reservoir age. Therefore, developing chronologies independent of ^{14}C dating is an essential component in constraining reservoir ages. The development of iodine-based chronology is a promising geochronometer as well as an emerging tracer for continental material flux. Results presented in Chapter 4 demonstrate the usefulness of iodine as a biogeotracer with relevance to environmental science and geochronological studies as well as its uptake into the skeleton of the deep-sea black coral skeleton *Leiopathes* sp. collected from the Gulf. Additionally, little is known about the basic biology and ecology (including reproductive processes) of most deep-water corals (Waller 2005), hindering conservation and management decisions. The ecosystem services provided by these deep-sea biogenic communities are numerous, including nutrient cycling, providing a food source for higher trophic levels and creating habitat for commercially-important fishery species (Thurber et al. 2014).

The blowout of the Macondo well and the sinking of the *Deepwater Horizon* drilling platform was the largest accidental oil spill in U.S. history, resulting in approximately five million barrels of crude oil (McNutt et al. 2012a) spilled into the Gulf over an 87-day period beginning on April 20, 2010 and ending on July 16, 2010. A unique aspect of this spill was its depth at the Macondo wellhead site at 1,522 m. As a result of the wellhead's deep location, more oil and gas was released into the deep sea than any previous spill (Fisher et al. 2014a), including an estimated 2 million barrels of methane which remained in the deep sea (McNutt et al. 2012a). Another unique aspect was the response to the spill, and, specifically, the use of chemical dispersants (Corexit 9500 and 9527) to degrade and break down the oil. A total of approximately three million liters of Corexit was sprayed on the surface of the water or applied at depth at the Macondo site (Seidel et al. 2016). The dispersant allowed some of the oil to mix with sea water and remain suspended (Kujawinski et al. 2011), creating a 22-mile-long, 1.2-mile-wide plume of microscopic oil compounds at 1,100–1,300 m below the surface (Camilli et al. 2010; Reddy et al. 2012), contaminating and affecting deep-water habitats (Valentine et al. 2014; Beyer et al. 2016). The use of dispersant also contributed to the formation of large amounts of marine snow that settled with oil and clay minerals (oil snow) on the sea floor (Vonk et al. 2015; Daly et al. 2016; Passow 2016; van Eenennaam et al. 2016; Ziervogel et al. 2016).

The impact from the *Deepwater Horizon* event has been documented in several Gulf marine environments, including those listed below.

Environment	Reference
Microbes	Bik et al. 2012; Mason et al. 2012; Simister et al. 2016
Meiofauna	Montagna et al. 2013
Benthic foraminiferans	Schwing et al. 2015
Phytoplankton	van Eenennaam et al. 2016
Mesozooplankton	Carassou et al. 2014
Gelatinous zooplankton	Almeda et al. 2013
Marine-sourced organic matter (OM)	Prouty et al. 2016
Fishes	Whitehead et al. 2012; Dubansky et al. 2013; Murawski et al. 2014; Pilcher et al. 2014; Bayha et al. 2017; Jones et al. 2017

Environment	Reference
Fish larvae	Incardona et al. 2014; Mager et al. 2014; Adeyemo et al. 2015; Xu et al. 2016
Mesophotic	Silva et al. 2016
Cold-water corals	White et al. 2012; Hsing et al. 2013; Fisher et al. 2014a, 2014b

Although strides have been made to understand impacts since the *Deepwater Horizon* event (see Joye et al. 2016), the quantification of long-term ecosystem dynamics and projections about recovery of impacted populations remains incomplete. *Deepwater Horizon* oil may persist in sediments for decades if sequestered (Romero et al. 2017). The delivery of organic matter (OM) to the deep-sea is an important component of the oceanic carbon cycle and is crucial to sustaining the ecosystems that inhabit depths below the photic zone. Deep-sea corals therefore may be sensitive to changes in nutrient transport from surface waters to the seafloor. Differentiating the various sources of OM to the Gulf benthos is particularly complex given that the relative inputs of terrestrial and marine OM can vary both spatially and temporally. To investigate the impact of the *Deepwater Horizon* spill on quality and quantity of biomass delivered to the deep-sea, a suite of geochemical tracers (e.g., stable and radio-isotopes, lipid biomarkers, and compound specific isotopes) was measured from monthly sediment trap samples deployed near a high-density deep-coral site in the Viosca Knoll area of the north-central Gulf before the spill (October 2008 to September 2009) and after the spill (October 2010 to September 2011). Before the spill, marine-sourced OM dominated with a pronounced reduction in marine-sourced OM after the spill. The shift is characterized by a reduction in marine-sourced sterols and *n*-alkanes and a concomitant decrease in sediment trap organic carbon and pigment flux. Results from this study presented in Chapter 5 indicate a reduction in primary production and carbon export to the deep-sea. The data presented here fills a critical gap in our knowledge of biogeochemical processes and sub-acute impacts to the deep-sea that ensued after the 2010 *Deepwater Horizon* spill. Mortality is of limited use as a metric and provides no information on sub-lethal impacts. In an assessment of the environmental effects of the *Deepwater Horizon* oil spill, it was found that biomarkers for affected organisms were more informative regarding oiling stress compared to population and community indices (Beyer et al. 2016). Appropriate tools, such as biomarkers, that can be used to characterize coral health and identify their sensitivity and resiliency to disturbance are essential. These tools will provide monitoring metrics that can separate impacts due to oil and gas activities versus the natural range of variation and from other forms of disturbance, such as fishing activities, hurricanes and climate change.

1.3 Objectives

The overall objective of this project was to utilize samples in-hand from previous projects (e.g., *Lophelia II*) in the Gulf to develop assessment tools that may be utilized in future regional scenarios and elsewhere to predict and assess impacts to deep-water coral habitats. Specific objectives include:

- Characterization of taxonomic and functional genes in coral microbiomes (metagenomes) to develop indicators of coral health and/or to detect sub-lethal stress.
- Characterization of functional genes in corals (transcriptomes) to develop biomarkers of coral health and/or detection of sub-lethal stress.

- Obtaining better estimates of coral ages, and defining and tracing isotopic composition of petro-based carbon into the Gulf deep-sea coral food web.
- Tracking changes in nutrient dynamics (e.g., changes in quality, quantity, and source) and impact of the oil spill on biomass production.

1.4 Study Components and Principal Investigators

US Geological Survey (USGS) principal investigators worked with BOEM, the agency responsible for managing energy and mineral resource development on the OCS, to define the scope of the project. The USGS Ecosystems Mission Area, Environments Program, supported the project, along with the individual Science Centers of the principal investigators. Each USGS investigator involved with this study authored individual chapters of this report, based on their areas of expertise (Table 1.1).

Table 1.1. Individual Study Components and Lead Investigators

Chapter	Study Component	Author, Investigator, and Affiliation	Description
2	Coral metagenomes	Christina Kellogg, USGS St. Petersburg Coastal and Marine Science Center	Characterization of taxonomic and functional genes of microbiomes in Gulf *Lophelia pertusa*
3	Coral transcriptomes	Cheryl Morrison, USGS Leetown Science Center	Characterization of functional genes in Gulf *Lophelia pertusa*
4	Coral aging	Nancy Prouty, USGS Pacific Coastal and Marine Science Center	Development of iodine as a geochronometer
5	Nutrient dynamics	Nancy Prouty, USGS Pacific Coastal and Marine Science Center	*Deepwater Horizon* impact of OM flux to the deep sea

2 Deep-Sea Coral Metagenomes

2.1 Background

The Gulf OCS supports extensive and valuable commercial and recreational fisheries, and unique deep-sea communities, including corals and chemosynthetic seeps (Coleman et al. 2004; Cordes et al. 2007; Cordes et al. 2008). Deep-sea corals are long lived (Prouty et al. 2011) but their depth and distance from shore limits observations of impact and recovery in response to environmental change or anthropogenic impacts from oil and gas exploration or fishing gear (Fisher et al. 2014a). Mortality is of limited use as a metric and provides no information on sub-lethal impacts. To protect these corals, better assessment tools are needed to determine their environmental sensitivity to events like the *Deepwater Horizon* oil spill, plumes of drilling mud, or climate change. Coral samples collected during previous research efforts conducted in support of BOEM objectives (i.e., *Lophelia* I and *Lophelia* II; Demopoulos et al. 2017; Kellogg 2008) were available for expanded analysis to address these questions and to generate baseline assessments for development of diagnostic tools.

2.2 Introduction

Corals have a microbiome (a collection of microorganisms that is intimately associated with the host animal, and all their genetic capabilities) that is a fundamental part of their biology (Ainsworth and Gates 2016; Apprill 2017). Maintaining a balance between the host and various components of its microbiome is a critical part of coral health. Coral microbiomes can alter quickly (hours to days) in response to environmental stress or disease, and these shifts have been detected before visible changes in the host (Bourne et al. 2008; Littman et al. 2011; Pantos et al. 2003; Ziegler et al. 2016; Ziegler et al. 2017).

"Establishing microbial baselines that characterize the temporal and spatial microbial dynamics in coral reefs is urgently needed to underpin rapid and sensitive assessments of declining reef health and make predictions about the consequences of future environmental changes" (Glasl et al. 2018). This statement was about shallow-water tropical reefs but is equally true for deep-sea corals. Determining a baseline that encompasses both the microbial taxonomy ("who is there") and metabolic functionality ("what are they capable of doing") of these coral microbiomes will allow us to better predict what sorts of shifts might signal disease or sub-lethal impairment from environmental stress. Metagenomic analyses allow a broader view of available genetic information of the coral-associated microbiota (Wegley et al. 2007). Instead of focusing on a single gene within a pathway or identifying individual microbes by their 16S and 18S rRNA genes, the entirety of the genetic potential in the community can be observed (Delmont et al. 2011). Fragments of microbial genomes from the coral samples are sequenced and can be analyzed individually or pieced together to create longer contiguous sequences ("contigs"). These gene fragments include rRNA genes and genes that are part of larger biochemical pathways, allowing identification of both identity and potential functional roles within the coral-associated microbial community.

Research has determined that like shallow-water corals, the stony cold-water coral *Lophelia pertusa* maintains conserved bacterial symbionts in spite of its nearly global distribution (Kellogg et al. 2009; Neulinger et al. 2008). Previous work demonstrated that *Lophelia*-associated microbial communities are distinct from those of the surrounding seawater and sediments (Neulinger et al. 2008; Yakimov et al.

2006), and there is some evidence that long-term heat stress resulted in a detectable shift in the bacterial associates of *L. pertusa* in the Gulf (Kellogg et al. 2009). The objective of this work was to apply high-throughput sequencing to create: (1) a 16S rRNA amplicon dataset with deeper coverage than the previous clone library studies, from which conserved bacterial associates that might serve as microbial indicators could be identified (Kellogg et al. 2017), and (2) a shot-gun metagenome of the microbiome to reveal eukaryotic, archaeal, and viral components as well as functional genes indicative of dominant metabolic cycles in which the microbes are involved (Kellogg and Neulinger 2018). Both these datasets create new baselines against which future studies can compare to determine if microbial community shifts or indicator species are linked to specific stressors (e.g., oil, sediment, temperature). The characterization of taxonomic and functional genes from the *L. pertusa* microbiome is a critical first step towards the development of indicators of this coral's health state or the presence of sub-lethal stress.

2.3 Methods

2.3.1 Samples

All samples were collected during earlier field campaigns, so no new research cruises were associated with these samples. Both the amplicon dataset and the shot-gun metagenomic dataset were based on samples from *L. pertusa* colonies from three sites in the Gulf (Viosca Knoll [VK826 and VK906]; West Florida Shelf, [WFS1]) and one site in the western Atlantic (ATL) (Figure 1.1). All collections were made during either August or September of 2009 or 2010. However, different coral colonies were used for each dataset, as itemized in Table 2.1. The 2009 samples pre-date the *Deepwater Horizon* oil spill in the Gulf, which began in April 2010, and the 2010 samples were collected in September after the spill. All coral samples were preserved onboard ship using RNAlater® and frozen at -20 °C.

Table 2.1 Sample List for Amplicon (A) and Metagenomics (M) Datasets

Sample	Site	Location	Year	Depth (m)	Temp (°C)	Salinity	Latitude	Longitude	Dataset
ROV02Q1	VK826	Gulf	2010	490	8.2	35.0	29.170270	88.013202	A, M
ROV02Q2	VK826	Gulf	2010	490	8.2	35.0	29.169867	88.012117	A
ROV03Q2	VK826	Gulf	2010	489	8.6	35.0	29.169135	88.013418	M
ROV03Q3	VK826	Gulf	2010	487	8.6	35.0	29.169052	88.013330	A
ROV05Q1	VK906	Gulf	2010	405	9.8	35.2	29.073117	88.380533	M
ROV05Q2	VK906	Gulf	2010	403	9.6	35.1	29.073780	88.379637	A
ROV06Q1	VK906	Gulf	2010	410	11.0	35.3	29.072535	88.374222	M
ROV06Q3	VK906	Gulf	2010	413	11.0	35.3	29.071167	88.375190	A
3731K2	VK906	Gulf	2009	396	10.8	35.3	29.068545	88.377805	M
3731K3	VK906	Gulf	2009	397	10.7	35.3	29.068632	88.377852	A
ROV07Q1	WFS1	Gulf	2010	504	8.2	35.0	26.207422	84.727083	A
ROV07Q2	WFS1	Gulf	2010	518	8.2	35.0	26.206435	84.731165	M

Sample	Site	Location	Year	Depth (m)	Temp (°C)	Salinity	Latitude	Longitude	Dataset
ROV08Q3	WFS1	Gulf	2010	537	8.0	34.9	26.197992	84.732340	A
ROV08Q4	WFS1	Gulf	2010	543	8.0	34.4	26.197850	84.732617	M
ROV09Q1	WFS1	Gulf	2010	543	8.3	35.0	26.204765	84.731838	A
ROV09Q4	WFS1	Gulf	2010	522	8.3	35.0	26.204575	84.729930	M
3705K3	ATL	ATL	2009	751	7.5	35.0	28.775843	79.616130	A
3705K4	ATL	ATL	2009	745	7.5	34.9	28.775677	79.616043	M
3705K6	ATL	ATL	2009	743	7.5	35.0	28.775677	79.616043	A
3705K10	ATL	ATL	2009	743	7.5	35.0	28.775783	79.615905	A, M

2.3.2 DNA Extraction

Sterile pliers and hammer were used to break polyps off of the branch and crack the calyces open to get access to the coral tissue. Tissue was separated from the skeleton using sterile forceps and an airbrush with sterile phosphate buffered saline. The minimum volume of buffer necessary per sample (<500 μL) was used. This created a slurry of coral tissue.

For the amplicon dataset, please see the publication for detailed extraction methods (Kellogg et al., 2017). Briefly, approximately 50 mg aliquots of the coral tissue slurry described above was extracted using the MO BIO PowerPlant® DNA Isolation Kit with modifications to increase bacterial lysis (Baker and Kellogg 2014; Sunagawa et al. 2010). Three replicate extractions were done per sample and then the DNA combined at the end to ensure high enough concentration for sequencing.

For the metagenomics dataset, microbial DNA was extracted following a specialized protocol developed for this coral[1] . Briefly, DNA in the coral tissue slurry was sheared by repeated passage through a syringe and then centrifuged to remove larger chunks of tissue. A Percoll cushion was then used to separate the coral cells from the microbial cells based on size and density (Pertoft 2000). The microbial fraction was filtered onto a 0.22 micron Sterivex cartridge and the microbial assemblage DNA was extracted from that filter using the Qiagen DNeasy Blood and Tissue kit following the protocol for Gram-positive bacteria but with the reagent volumes doubled in the initial steps (see the online protocol for step by step directions).

2.3.3 Sequencing

The amplicon dataset was produced by using primers 563F/926R to target the V4-V5 variable region of the 16S rRNA gene (Claesson et al. 2010). Roche 454 pyrosequencing with GS FLX Titanium chemistry was performed by EnGenCore, LLC. Raw sequence data from all amplicon samples are available from

[1] Available online: https://coastal.er.usgs.gov/coral-microbes/discovre/lophelia-extraction.html

the National Center for Biotechnology Information (NCBI) data repository in the Sequence Read Archive (SRA) under Bioproject number PRJNA305617 and also online as a USGS data release (Kellogg and Goldsmith 2017).

The shot-gun metagenome dataset was produced by random shearing of the DNA, construction of a TruSeq library, and sequencing on an Illumina HiSeq2000 by Argonne National Laboratory. Raw sequence data from all metagenome samples are available from the NCBI SRA under Bioproject number PRJNA471489 and also online as a USGS data release (Kellogg and Goldsmith 2018).

2.3.4 Bioinformatics

Amplicon sequence data were analyzed via the QIIME platform (Caporaso et al. 2010) using an open-reference method with a 97% similarity threshold to select operational taxonomic units (OTUs) (Rideout et al. 2014) and the Greengenes database to assign taxonomy (DeSantis et al. 2006; McDonald et al. 2012). For full details, see Kellogg et al. (2017).

Metagenomic sequence data were analyzed under a contract by omics2view.consulting. There were originally 12 samples, but two had poor sequencing and were removed before initiating analysis, leaving 10 metagenomic files. Initial quality filtering was performed with Trimmomatic v0.35 to remove TruSeq library adapter fragments and remove low-quality reads. The filtered reads were pre-assembled using MEGAHIT v1.0.3–29 to generate contiguous sequences ("contigs"). The contigs were scaffolded using SSPACE standard v3.0 using default parameters. Ribosomal RNA (rRNA) genes were detected with rRNA_HMM of the RAMMCAP pipeline. Putative amino acid sequences (coding sequences, CDS) were identified with Prodigal v2.6.2 in metagenomics mode. A subset of CDS that were at least 80 amino acids long was generated (henceforth referred to as "filtered CDS"). Filtered CDS were classified by InterProScan v5, which also inferred affiliation of filtered CDS to Gene Ontology (GO) and various biochemical pathway classification systems. In addition, filtered CDS were annotated against KEGG orthology (KO) using the server GhostKOALA. VirSorter v1.0.3 was used to scan the filtered assembly for viral signatures. TAMER (Taxonomic Assignment of Metagenomic Reads) and BLASTN were used to query filtered contigs against taxonomic databases.

2.4 16S rRNA Amplicons

2.4.1 Results

These results have been published (Kellogg et al. 2017) and only the main points will be summarized here. Amplicon sequencing results were obtained from 12 individual *L. pertusa* samples (Table 2.1), with greater than 40,000 reads per sample. Principal coordinate analysis using weighted UniFrac distances (Lozupone and Knight 2005) to assess the beta diversity between samples showed a clear division between Gulf and Atlantic samples (Figure 2.1). A one-way Analysis of Similarities (ANOSIM) using the Gulf and Atlantic as factors confirmed that there was a significant difference between the samples when the data were square-root transformed ($R = 0.525$, $p = 0.032$) but not when the data were 4^{th}-root transformed ($R = 0.212$, $p = 0.141$). This indicates that the pattern seen in Figure 2.1 is being driven

primarily by differences in the abundances of dominant bacterial taxa rather than by differences in rare taxa numbers. This can be further visualized in Figure 2.2 comparing the relative abundance of the dominant families of bacteria between Gulf and Atlantic samples. The Atlantic samples have much higher relative abundance of Oceanospirillales. The Gulf samples have more Sphingomonadaceae and Pseudonocardiaceae. The biogeographic differentiation can also be visualized in terms of the relative contribution of total core microbiome (those bacterial sequences shared by all 12 corals), local core microbiome (those bacterial sequences shared within a geographic site) and individual variability (Figure 2.3). The Atlantic samples show much higher proportions of local core compared to the Gulf samples that are dominated by the total core. The total core consists of 15 OTUs (Figure 2.4) but is most heavily dominated by *Novosphingobium* and *Pseudonocardia*.

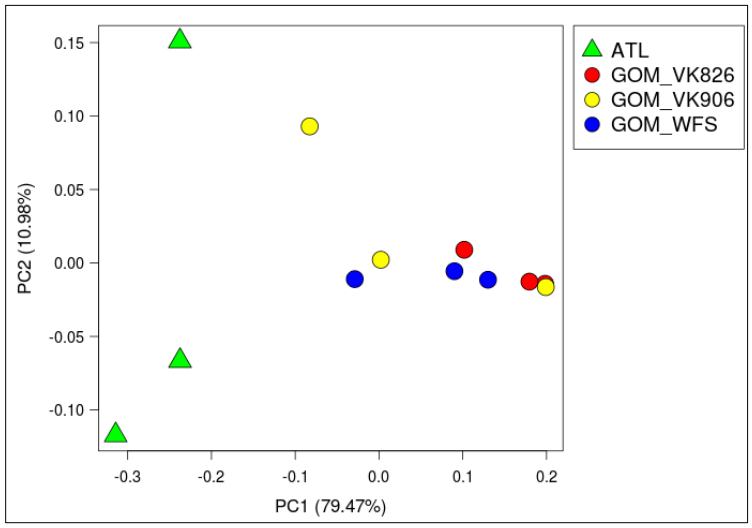

Figure 2.1 Principal coordinate analysis (PCoA) of weighted UniFrac distance of *L. pertusa*-associated bacterial communities.
Originally published in Kellogg et al. (2017).

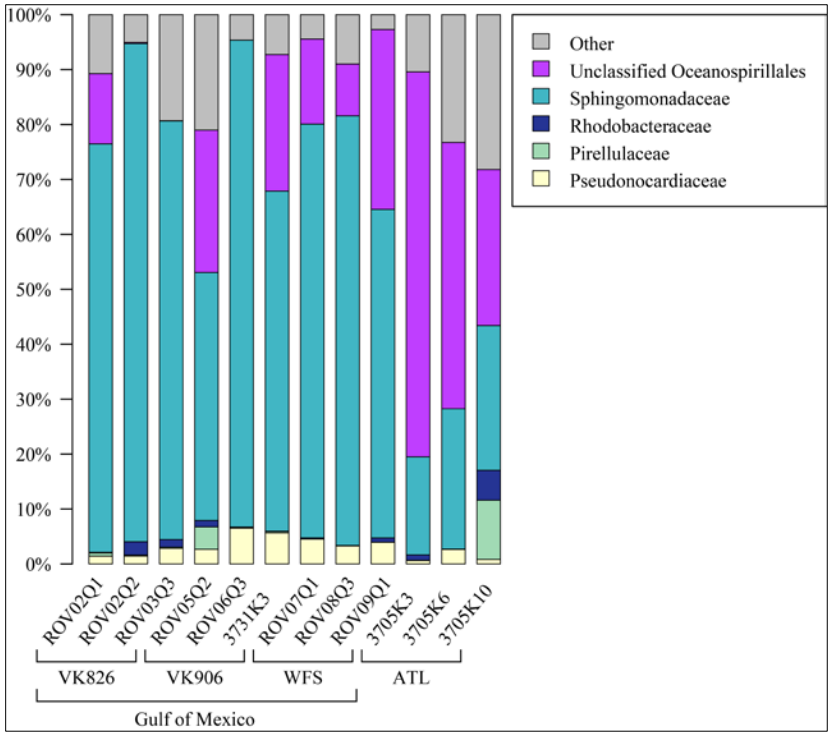

Figure 2.2. Relative abundance of families (or the lowest identifiable phylogenetic level) in *L. pertusa* samples.

Shown are bacterial groups that represent ≥ 1% of the total taxa. All remaining minor taxa are summarized as "Other". Originally published in Kellogg et al. (2017).

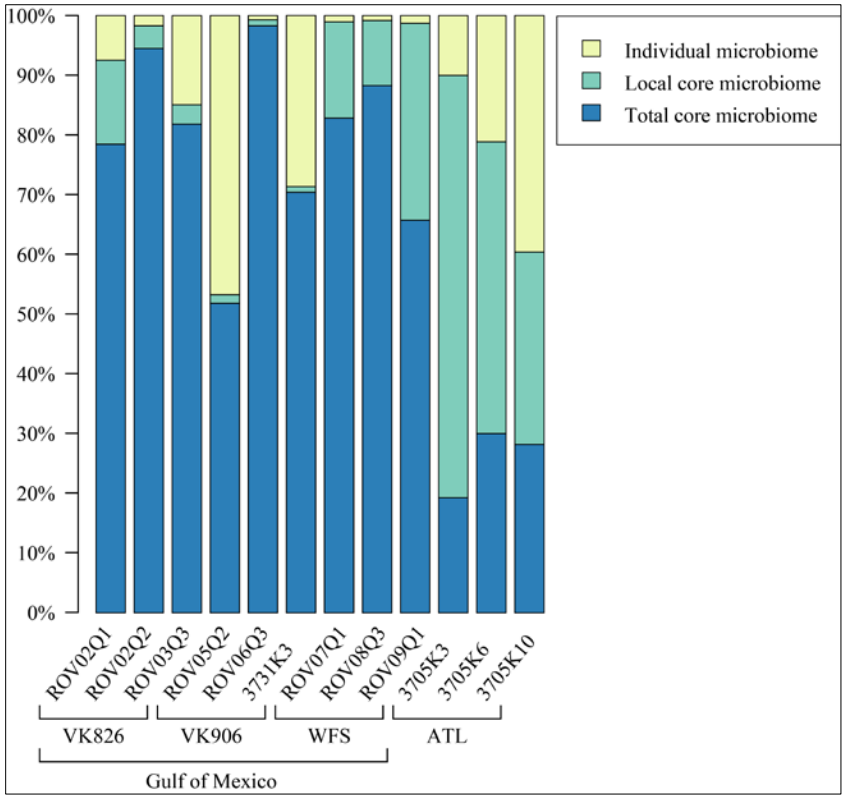

Figure 2.3. Relative abundance of total core (operational taxonomic units found in all samples), local core (OTUs found in all samples from one geographic site), and individually variable OTUs present in each coral colony.

Originally published in Kellogg et al. (2017).

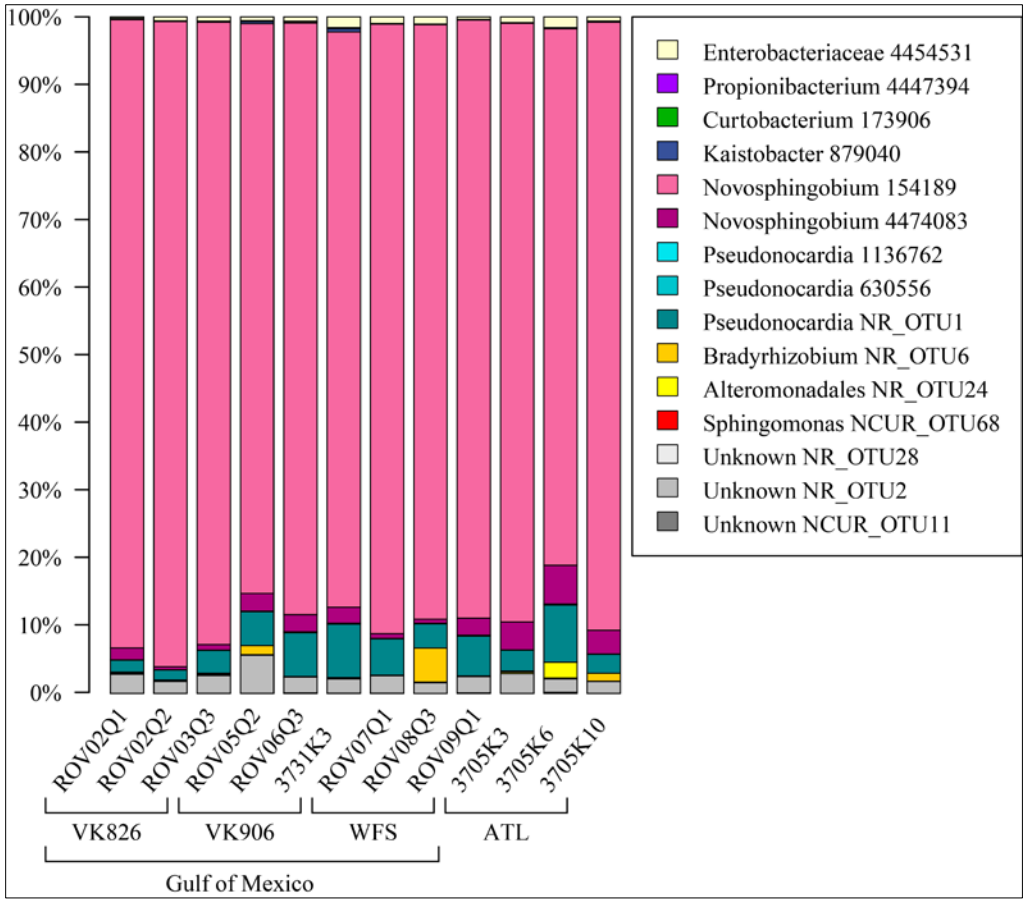

Figure 2.4 Conserved total core bacterial OTUs in *L. pertusa*.

Relative abundance of the 15 OTUs found to be conserved across all 12 coral samples. This equates to the blue "total core microbiome" bars in Figure 2.3. Originally published in Kellogg et al. (2017).

2.4.2 Discussion

Sequencing depth, the number of sequencing reads obtained per sample, is a critical factor in ecological studies and particularly necessary to identify rare but conserved bacterial symbionts (Ainsworth et al. 2015; Smith and Peay 2014). Though two other studies applied next-generation sequencing to study *L. pertusa*-associated bacterial communities, one was limited to less than 500 sequences per sample and the other to roughly 16,000 sequences per sample (Meistertzheim et al. 2016; van Bleijswijk et al. 2015). This work is the first to use high-throughput sequencing to describe western Atlantic *L. pertusa* bacterial communities and also to sequence to a depth of greater than 40,000 sequences per sample. This sequencing depth lends weight to the biogeographic pattern seen in the results that the Atlantic and Gulf samples were dominated by the same bacterial groups (Figure 2.2) but with significant differences in relative abundance between the two areas.

The Gulf samples contained a higher proportion of the total core, including *Novosphingobium* and *Pseudonocardia*, two genera that are known to degrade aromatic hydrocarbons. Recent papers on both shallow-water and deep-sea corals have noted the presence of oil-degrading bacteria in the coral microbiome and raised the question of whether this is an important function, either to provide a carbon source or detoxification (Al-Dahash and Mahmoud 2013; Röthig et al. 2017). Because the Gulf has many natural hydrocarbon seeps (MacDonald et al. 1990; Roberts et al. 2007), that may be a selective factor for *L. pertusa* in the Gulf to maintain a higher proportion of core bacteria capable of degrading these carbon sources. However, previous research did not find evidence of Gulf corals incorporating seep carbon, indicating that bacterial action is more likely to be detoxification over nutrition (Becker et al. 2009).

In addition to being hydrocarbon degraders, *Pseudonocardia* are also known to be antibiotic producers. This suggests another possible reason for their conservation in the *L. pertusa* core; protection of the coral from invading pathogens or to optimally structure the microbiome (Zhang et al. 2013).

Propionibacterium makes up a very small portion of the *L. pertusa* core; however, it has also been identified as a rare conserved symbiont in a number of shallow and mesophotic stony corals (Ainsworth et al. 2015; Hester et al. 2016). The core sequence (OTU 4447394) was 99% identical to *Propionibacterium* sequences derived from *L. pertusa* in Norway (Neulinger et al. 2008) and off Great Britain (van Bleijswijk et al. 2015), showing conservation of this sequence in datasets on both sides of the Atlantic. Further, although a Mediterranean study targeted a different variable region such that sequences could not be directly compared, screening of their *L. pertusa* microbiome libraries revealed the presence of *Propionibacterium* sequences (Meistertzheim et al. 2016).

In addition to producing a baseline description of the *L. pertusa* bacterial microbiome, a key goal of this work was to identify any consistently conserved bacterial groups for development as microbial indicators of coral health or stress. Because no datasets of equivalent sequencing depth currently exist for eastern Atlantic or Pacific *L. pertusa*, it is not possible to be certain that the identified core is maintained outside the western Atlantic. However, the consistent finding of *Propionibacterium* in the three existing high-throughput amplicon studies of *L. pertusa* as well as previous clone library studies, suggests that there are bacteria conserved by this coral regardless of ocean basin (Kellogg et al. 2017; Kellogg et al. 2009; Meistertzheim et al. 2016; Neulinger et al. 2008; van Bleijswijk et al. 2015).

2.5 Shot-gun Metagenomics

2.5.1 Results

Ten *L. pertusa* samples were successfully shot-gun sequenced to provide an assessment of the archaeal, fungal and viral members of the microbiome as well as the major functional capacities of the total microbiome (Table 2.1). These samples yielded between 2.4 million and greater than 68 million raw sequence reads per sample which were then filtered and joined into larger contigs, with gene coding sequences then identified and taxonomically assigned (Table 2.2). In all cases, 89–90% of the filtered coding sequences could not be taxonomically assigned (Figure 2.5, “unknown”). Of the assignable portion, the 10 individual samples were remarkably consistent, with Bacteria comprising 26.1 to 30.7%,

Archaea 0.5 to 0.6%, Viruses 0.2 to 2.9%, and Fungi 0.6 to 0.7% (Figure 2.5). The remaining portion of known filtered coding sequences were assigned to Eukaryota, most of which were coral sequences.

Table 2.2. *L. pertusa* Metagenome Sequence Statistics

Site	Sample	Raw Reads	Filtered Reads	Contig Counts	Gene Counts
VK826	ROV02Q1	47,539,638	32,045,754	22,163,728	5,174,770
VK826	ROV03Q2	22,208,204	15,078,273	10,368,021	2,412,916
VK906	ROV05Q1	15,750,928	10,646,444	7,302,435	1,715,646
VK906	ROV06Q1	23,197,772	15,657,150	11,131,656	2,466,041
VK906	3731K2	2,408,254	1,635,936	1,163,135	282,939
WFS1	ROV07Q2	26,937,222	18,076,499	12,694,012	3,355,631
WFS1	ROV08Q4	19,571,018	13,066,886	9,322,443	2,258,814
WFS1	ROV09Q4	68,074,764	45,976,300	33,031,980	7,440,087
ATL	3705K4	25,318,094	17,739,296	12,567,052	2,621,703
ATL	3705K10	23,918,238	16,367,611	11,559,964	2,718,869
Totals		274,924,132	186,290,149	131,304,426	30,447,416

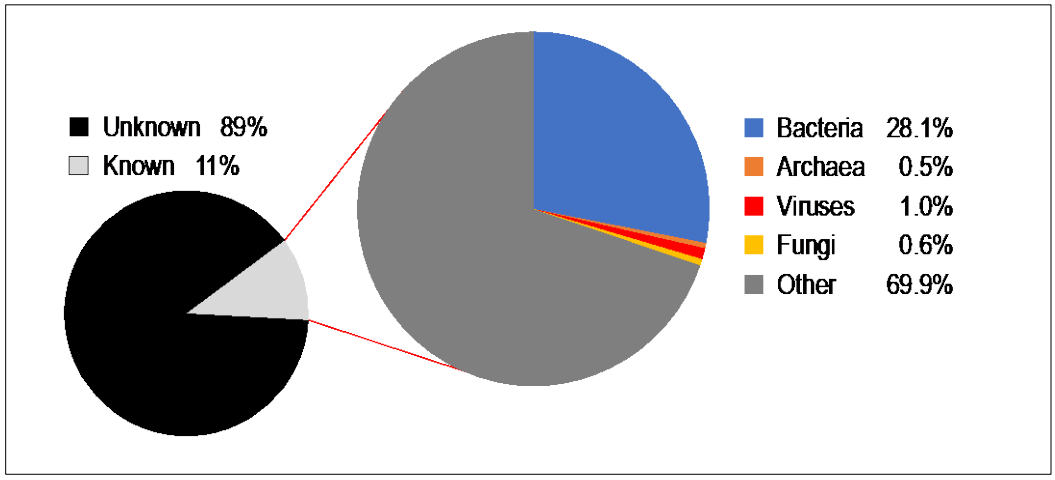

Figure 2.5. Average taxonomic assignments of filtered contigs from 10 *L. pertusa* metagenomes.

The archaeal fraction of the metagenomes was consistently dominated by Eurarchaeota (85–88%); the remainder was Thaumarchaeota (11–14%). Within these two archaeal phyla, 19 genera were identified (Table 2.3). The genus with the highest relative abundance was *Methanosarcina*, which comprised 40 to 45% of the archaeal fraction. The next highest was an unclassified Thaumarchaeota archaeon MY2, which ranged from 9 to 12% of the total archaea and consistently comprised the largest portion of

Thaumarchaota. The next most abundant genera included *Haloferax* (7 to 10%) and *Methanobrevibacter* (4 to 10%).

Table 2.3. Archaeal Genera Identified from *L. pertusa* Metagenomes

Euryarchaeota	
	Geoglobus
	Halopricum
	Halobiforma
	Halogeometricum
	Haloferax
	Haloplanus
	Haloquadratum
	Halorubrum
	Methanobacterium
	Methanobrevibacter
	Methanococcoides
	Methanococcus
	Methanohalophilus
	Methanosaeta
	Methanosarcina
	Natrialba
Thaumarchaeota	
	Cenarchaeum
	Candidatus *Nitrosoarchaeum*
	Candidatus *Nitrosopumilus*

Though the viral fraction of the *L. pertusa* metagenomes was small, it encompassed a lot of taxonomic variety (Table 2.4). Bacteriophages dominated the viral fraction, comprising 66 to 97% (median 88.5%). Potential hosts for the *Lophelia*-associated viruses include all members of the holobiont, for example, coral, fungi, protists, archaea, and bacteria.

Table 2.4. Viral Families Identified from *L. pertusa* Metagenomes

Virus Family	**Host**
dsDNA viruses	
Alloherpesviridae	Fish (coral?)
Baculoviridae	Crustaceans, insects
Iridoviridae	Molluscs, fish (coral?)
Fuselloviridae	Archaea
Mimiviridae	Protists
Nudiviridae	Crustaceans
Phycodnaviridae	Algae, protists
Poxviridae	Crustaceans, insects (coral?)
Podoviridae	Bacteria
Siphoviridae	Bacteria
ssDNA viruses	
Circoviridae	Fish (coral?)

Virus Family	Host
Microviridae	Bacteria (Mycoplasma?)
RNA viruses	
Retroviridae	Fish (coral?)

Fungi were primarily Ascomycota (0.7 to 0.8%), with smaller amounts of Basidiomycota (0.1 to 0.2%) and a handful of reads per sample listed as unclassified Microporidia. There was higher diversity of Ascomycota than Basidiomycota. Roughly one third (33 to 39%) of Ascomycota was class Saccharomycetes, the budding yeast. The remaining filamentous ascomycetes were mainly comprised of classes Dothideomycetes, Eurotiomycetes, Leotiomycetes, and Sordariomycetes. Basidiomycota sequences largely consisted of class Agaricomycetes, order Pucciniales (rusts), and family Ustilaginaceae (smuts).

In addition to being screened for ribosomal genes to identifying taxonomic groups, the filtered coding sequences were also searched for homology to known genes based on sequence similarity, genome annotation, and structure. The Gene Ontology (Ashburner et al. 2000; Gene Ontology Consortium 2017) is a bioinformatics initiative to unify the representation of gene functions and their relationship to each other, and can be used to classify sequences based on molecular function, cellular component, and larger biological processes. Figure 2.6 shows that there are not major differences between the Gulf sites and the Atlantic site in terms of domiant biological processes. It also highlights nitrogen compound metabolic processes as a specific area of activity. Sequences were also searched for matches to KEGG (Kyoto Encyclopedia of Genes and Genomes; Kanehisa et al. 2004) pathways, specifically investigating KEGG pathway 00624 (“Polycyclic aeromatic hydrocarbon degradation”) due to the presence of hydrocarbon-degrading bacteria in the core microbiome of *L. pertusa*, and KEGG pathway 00680 (“Methane metabolism”) due to the presence of methanogenic archaea. No matches were found for the hydrocarbon degradation pathway. However, six components of methane metabolism could be detected: S-(hydroxymethyl) gluathione dehydrogenase/alcohol dehydrogenase (K00121), glycine hydroxymethyltransferase (K00600), alanine-glyoxylate transaminase/serine-glyoxylate transaminase/serine-pyruvate transaminase (K00830), triose/dihydroxyacetone kinase/FAD-AMP lyase (K00863), acetyl-CoA synthetase (K01895), and trimethylamine monooxygenase (K18277).

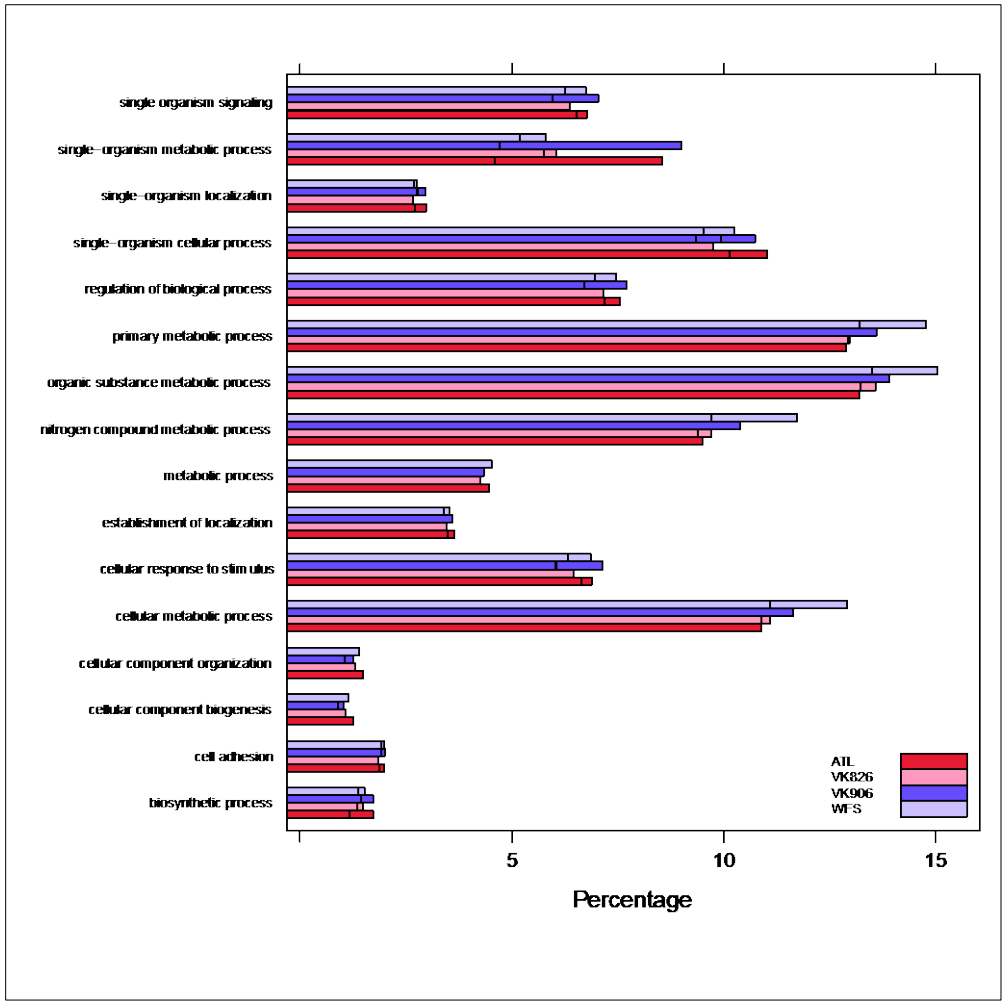

Figure 2.6. Gene Ontology categorization of biological processes based on *L. pertusa* metagenomes by site.

2.5.2 Discussion

It is not uncommon for metagenomics studies to have a large percentage of the sequences not be identifiable when compared against the taxonomic databases. The first coral metagenome, *Porites astreoides*, had 79% unknown sequences (Wegley et al. 2007). The large amount of unclassified reads in our dataset are likely from the host coral and due to the fact that a reference genome is not yet available for *L. pertusa*. As more organisms are fully sequenced and those sequences properly annotated, this unknown sequencing "dark matter" will be reduced. Further, in spite of efforts during extraction to separate coral and microbial cells using a density gradient, the majority of the classified reads were to Eukaryota, and most of them were coral. Fortunately, the depth of sequencing still provided enough non-

coral sequences to reveal new information about the microbial community associated with this cold-water coral.

Archaea have been detected in tropical stony corals, but typically with even representation of Euryarchaeota and Thaumarchaota (Kellogg, 2004) or with Euryarchaeota as minority (Wegley et al. 2004). The inverse was seen in *L. pertusa*, whose archaeal fraction was dominated by Euryarchaeota, particularly *Methanosarcina*. *Methanosarcina* and *Methanobrevibacter* are both anaerobic methane producers which explains the identification of six components of KEGG methane metabolism during functional analyses. *Methanosarcina* is particularly versatile at using multiple substrates to form methane, including acetate, methanol, monomethylamine, dimethylamine, trimethylamine, and carbon monoxide (Boone and Mah 2001).

Early attempts to detect Archaea associated with *L. pertusa* via amplification using targeted primers were not successful (Kellogg 2008; Yakimov et al. 2006). The first successful identification was as "by-catch" during a genomic analysis of Norwegian *L. pertusa*, and yielded *Cenarchaeum symbiosum*, *Nitrosopumilus maritimus*, and Candidatus *Nitrosoarchaeum* (Emblem et al. 2012), which collaborates this study's findings from western Atlantic samples (Table 2.3). An amplicon-based study of *L. pertusa* skeleton and mucus from off the United Kingdom detected some Thaumarchaeota, and Euryarchaeota classes Halobacteria and Thermoplasmata (van Bleijswijk et al. 2015). This study (Table 2.3) is the first to expand the detection of Euryarchaeota associated with *L. pertusa* and to highlight the apparent importance of Archaea to methane metabolism in the coral.

This study presents the first data to identify viral associates of a deep-sea or cold-water coral. Previous research on *L. pertusa* used microscopy to enumerate viral particles in the gastric fluid and mucus, finding 10^7 to 10^8 particles per milliliter (Weinbauer et al. 2012), which could explain the high diversity detected by the metagenomes even though the extraction protocol was not specifically targeted toward retaining viral particles. Bacteriophages were the dominant viral type found in *L. pertusa* which mirrors results from shallow-water corals (Hewson et al. 2012; Littman et al. 2011; Mahmoud and Jose 2017; Marhaver et al. 2008; Wegley et al. 2007). Viral families that target other members of the microbiome (archaea and protists) were also detected. Eukaryotic viruses detected may be targeting the coral host, or cryptic micro-associates such as crustaceans or molluscs. All of the viral families found associated with *L. pertusa* (Table 2.4), except for Alloherpesviridae, Fuselloviridae, and Nudiviridae, have previously been detected in tropical stony corals by metagenomics or viromics (Mahmoud and Jose 2017; Thurber et al. 2008; Wegley et al. 2007. Though it has been postulated that Phycodnaviridae infect *Symbiodinium* in tropical stony corals, there is also an alternative hypothesis: "that a major member of the coral virome is a unique mosaic physically reminiscent of the Phycodnaviridae and Iridoviridae, but more similar at the genomic level to Herpesviridae (Thurber and Correa 2011, p.109)." The absence of *Symbiodinium* in *L. pertusa* lends this hypothesis weight. Alternately, Phycodnaviridae could be infecting a protist in coral microbiomes. Thurber et al. (2008) also found that a herpes-like virus increased in abundance in corals under temperature, pH, and nutrient stress. This suggests that the sequences identified in *L. pertusa* as belonging to the Alloherpesviridae family might be targets for use as diagnostics.

Fungi have been previously isolated from *L. pertusa* via selective cultivation (Galkiewicz et al. 2012), but this is the first study to use molecular techniques to reveal additional fungal diversity. The metagenomic findings are corroborated by the previous culture-based work in that both isolated a larger diversity of Ascomycota than Basidiomycota from *L. pertusa* from these same geographic sites. Of the seven ascomycetes cultured by Galkiewicz et al. (2012), two were detected in the metagenomic sequences: *Nectria* and *Penicillium*. There was no overlap between the cultured Basidiomycota (*Kondoa*, *Rhodosporidium*, and *Sporidiobolus*) and the basidiomycetes detected by sequencing. Though endolithic fungi in shallow-water corals have been linked to nitrogen cycling (Wegley et al. 2007), *L. pertusa* skeleton was not included in these metagenomes. It is not clear that any specific fungi would be good candidates for development as diagnostic targets.

A recent study using isotope tracer evidence has shown the transfer of fixed nitrogen from unidentified microorganisms into *L. pertusa* tissue (Middelburg et al. 2015). The amplicon study of *L. pertusa* identified a number of bacterial taxa with the potential for nitrogen fixation and conversion of nitrogen compounds (Kellogg et al. 2017). This potential is further underscored by the high number of gene ontology matches to nitrogen compound metabolic processes found in the *L. pertusa* metagenomes (Figure 2.6) and suggests the importance of nitrogen cycling to the coral holobiont.

One of the targeted pathways searched in the KEGG database was hydrocarbon degradation, specifically to further investigate the question raised in section 2.4.2 as to whether the presence of hydrocarbon-degrading bacteria in the *L. pertusa* core indicated the importance of this activity either to provide the coral with new carbon sources or to detoxify the environment. No matches were detected, suggesting either this activity is minor in the microbiome or that it does not occur even though the potential exists. Conversely, the detection of methanogens as a majority of the *L. pertusa*-associated archaea was complemented by the detection of six areas in the KEGG pathway for methane metabolism.

2.6 Conclusion

Because of *L. pertusa*'s wide distribution, the information developed here may be applicable to other OCS areas. The following taxononomic groups or functional genes are proposed as potential targets for development of diagnostic indicators of *L. pertusa* health:

- This study identified 15 conserved bacterial sequences in western Atlantic *L. pertusa*. These bacteria, particularly dominant members like *Novosphingobium* and *Pseudonocardia*, and broadly geographically-conserved members like *Propionibacterium*, are presumed to be important to coral function due to their conservation.
- This study identified several archaeal groups previously unknown to be associated with *L. pertusa*, particularly *Methanosarcina* and *Methanobrevibacter*, indicating their importance to methane metabolism in the coral. Detected functional genes of methane metabolism included trimethylamine monooxygenase, triose/dihydroxyacetone kinase, and glycine hydroxymethyltransferase.
- This study identified a number of eukaryotic virus types associated with *L. pertusa*, including sequences from the family Alloherpesviridae. Previous work has found that herpes-like viral sequences increase in abundance in response to stressors including temperature, pH, and nutrients.

- Nitrogen cycling appears to be a key area of collaboration between the coral host and its microbiome. Known genes that could be considered for diagnostic targets include *nifH* (nitrogen fixation), *amoA* (ammonia oxidation), *nirS* and *nirK* (nitrite reduction).

3 De novo Assembly and Functional Annotation of the Transcriptome of the Deep-water Coral *Lophelia pertusa*

3.1 Background

An early organismal response to environmental stressors includes the alteration of gene expression. Metazoans possess many genes that participate in response to environmental stressors, collectively called the "chemical defensome" (Goldstone et al. 2006). Genes and proteins that afford protection to an organism from damage, or may allow for repairs after damage are included in the defensome, and the those involved specifically with defense or repair from chemicals comprise the chemical defensome (Goldstone et al. 2006; Shinzato et al. 2012). The following sets of genes are known to be involved in the chemical defensome: (a) stress-activated receptors, signal transduction proteins, and transcription factors; (b) efflux pumps; (c) oxidizing enzymes; (d) reducing and conjugating enzymes; and (e) antioxidant proteins (Goldstone et al, 2006). Using powerful molecular tools to detect chemical defensome genes, direct evidence of sub-lethal, chronic effects at the molecular and cellular level can be obtained, while also shedding light upon the actual mechanism by which organisms respond to environmental toxins. Through examination of transcriptomes, or the set of RNA transcripts present at a particular time within an organism, genes (or gene systems) that are potentially being regulated can be identified, including those involved in environmental stress response (ESR).

With increasing genomic resources specific to cnidarians and corals, researchers have been able to produce an in-depth characterization of genomic stress responses, and have been able to tease apart generic versus specific responses to stressors (Shinzato et al. 2012). For example, the *A. digitifera* genome was queried for chemical defense genes that have been identified in other cnidarians and metazoans. A comparable set of chemical defense genes was found, including some lineage-specific gene family expansions (Shinzato et al. 2012).

The most common stressors that have been examined by coral transcriptome profiling thus far are those involved with climate change, namely temperature and pH stressors. For example, in *A. millepora*, initial trancriptomic response to increased pCO_2 involves extensive disruption of gene expression, including disruption of metabolism and calcification genes (Moya et al. 2012; 2015). After longer exposures, gene expression changed, with fewer genes expressed. Both exposures produced an over-representation of heat shock proteins (HSP) and heat shock factors, such as HSP-70, which has been previously shown to be involved with acclimation to thermal stress (Moya et al. 2015). In longer exposures, the Bcl-2 family of genes was upregulated. This gene family includes genes that suppress apoptosis, with an end result of lessening programmed cell death. Along with elevated pCO_2, increased temperature elicits significant changes in gene expression profiles, and many of these changes involve specific genes or functional gene categories previously reported in thermal stress response (Barshis et al. 2013). Using an RNAseq approach on thermally sensitive compared against resilient individuals of *Acropora hyacinth*, a suite of genes involved in stress, including HSP-70 regulators of an apoptosis (cell death) cascade, plus immune response genes such as oncogenes, was identified in resilient *A. hyacinthus* that were upregulated under normal conditions (before heat stress), yet downregulated following exposures to heat (Barshis et al. 2013). It was concluded that the resilient *A. hyacinthus* individuals "front-loaded" expression of these

important stress-response genes involved in a frequently encountered environmental stressor, allowing for less physiological response necessary when the environmental stress was experienced. This suite of genes is a likely candidate for health and stress tolerance indicators. Together, studies of coral transcriptomes are allowing for mechanistic hypotheses about ways corals respond to environmental stressors (e.g., van de Water et al. 2015, 2018).

Baseline genomic references as well as experimental toxicological data from deep water coral species are scarce. A recent study of the effects of Corexit 9500A on respiratory epithelial cells of mammals and marine organisms found that exposure alters permeability by inhibition of junctional proteins and caspase-3 dependent death of epithelial cells, yet heme-oxygenase-1 protected the cells from oxidative stress (Li et al. 2015). Similarly, toxicity of both oil and dispersant to several cold-water coral species that occur in close proximity to the *Deepwater Horizon* site has been demonstrated (De Leo et al. 2015). The corals *Paramuricea* type B3, *Callogorgia delta*, and *Leiopathes glaberrima* were subjected to short-term (0–96 hours) exposures to bulk oil-water mixtures, water-accommodated oil fractions, and the dispersant Corexit 9500A® (Doughty et al. 2014). In this study, each coral species showed more severe health declines in response to dispersant and to oil and dispersant mixtures than to oil alone, and decline of coral health worsened with increased concentrations. In other words, the dispersant was more toxic to the corals than the oil. Considering the depth of the plume of oil and dispersant (3,000m) resulting from the *Deepwater Horizon* spill and the abundance of deep water wells in the Gulf, expanding the scientific knowledge of cold water coral's sensitivity to toxic, sub-lethal levels of contaminants is paramount.

The dominant framework-building cold-water coral, *Lophelia pertusa*, is common in the Gulf (Brooke and Shroeder 2007), and occurs within 40 kilometers of the Macondo wellhead (White et al. 2012). This coral is nearly cosmopolitan in distribution, occurring in all oceans except for polar seas (Cairns 2000), but is particularly abundant in the North Atlantic Ocean off the coasts of Europe (Roberts et al. 2009), and the southeastern USA. (Ross and Nizinski 2007; Messing et al. 2008; Brooke and Ross 2014). In recent years, research on *L. pertusa* and the habitat it creates has expanded due to growing recognition of its environmental importance and the potential for human impacts on these habitats (Roberts and Hirshfield 2004; Rogers 1999; Roberts et al. 2006, 2009; Brooke and Ross 2013).

The goal of this study is to develop a well-annotated transcriptome for *L. pertusa*. High quality *L. pertusa* samples were collected on a recent research cruise for expanded analysis to develop genomic resources that can be used for the development of assessment tools for coral health that will be available for future events in the Gulf and elsewhere. Using previously developed resources in shallow water corals and other cnidarians (mentioned above) as a reference, the annotated transcriptomes will be interrogated for genomic stress-response genes that will respond predictively to chemical stressors. Ultimately, fast and inexpensive quantitative PCR (qPCR) assays will be developed that target *L. pertusa* cellular stress response genes. A suite of biomarkers that reflect cold-water coral health will provide an inexpensive and effective method for monitoring the state of deep coral reefs exposed to oil spills or other environmental perturbations throughout the Gulf, and will provide insight into the mechanisms of coral response to environmental disturbances. A mechanistic understanding about the links between chemical and other stressors and cold-water coral health are critical for predicting future impacts.

3.2 Methods

3.2.1 Sampling, RNA Extraction, and Illumina Sequencing

The *Lophelia pertusa* tissue sample used to build the transcriptome was taken using Pelagic Research Services' remotely operated vehicle (ROV) *Odysseus* on a NOAA-led Southeastern Deep Coral Initiative (SEDCI) research cruise on NOAA's R/V *Nancy Foster* on August 10, 2017 from the Many Mounds site (26.34071˚ North Latitude, -84.76385˚ West Longitude, 476 m depth) located on the Western Florida Slope in the eastern Gulf (see Figure 1.1). Samples destined for RNA extraction were processed as soon as possible after ROV recovery (Treatment A). Several *L. pertusa* polyps were crushed with an isopropanol-cleaned mallet to allow penetration of liquid nitrogen preservative. A subset of *L. pertusa* samples were kept alive onboard throughout the cruise in a tank of recirculating seawater chilled to 4°C. After four days of acclimation, one to three polyps were sampled, crushed and stored as above (Treatment B- tank acclimated). We performed a heat shock experiment with a subset of the same corals from Treatment B. These were submerged in a bucket of seawater warmed to 22°C for approximately one hour, then sampled and stored as above (Treatment C- heat shock). Once on shore, samples were transferred to dry ice and shipped overnight to USGS-Leetown Science Center where they were stored at -80°C until RNA extraction.

Total RNA was extracted from *L. pertusa* tissue using the RNAzol® RT Column Kit (Molecular Research Center) following the manufacturers protocol. RNA quality was assessed by running samples on a Bioanalyzer RNA Nano chip (Agilent). RNA was quantified using a Qubit 2.0 fluorometer using an RNA high sensitivity assay kit (Thermo Fisher Scientific).

Messenger RNA (mRNA, aka transcripts) was isolated from the total RNA, converted to complementary DNA (cDNA), and ligated with indexes and primers using a TruSeq® Sample Preparation kit (Illumina®, 20020594) following the manufacturer's protocol. The mRNA was isolated from the total RNA via magnetic beads attached to the poly-adenylated (poly-A) tails of the transcripts, a near universal feature of mature eukaryotic mRNA. The isolated mRNA was fragmented and the first strand of cDNA was synthesized using random primers. When the second strand was synthesized, dUTP was used in place of dTTP, which prevents the extension of the synthesis during the PCR stage, thus favoring cDNA constructed from the first strand in the final library and preserving the information of the orientation of the read. Unique indexes for the Lpe_10_05 treatments (A, B, and C, as described above) were ligated using the TruSeq RNA Single Index Set A (catalog # 20020492). The final libraries were run on a Bioanalyzer 2100 expert DNA 1000 chip (Agilent) to assess fragment size and presence of self-ligated primer that would negatively affect the sequencing run. The libraries were quantified using both a Qubit 2.0 fluorometer with a DNA high sensitivity assay kit (Thermo Fisher Scientific) and via qPCR using the KAPA SYBR® FAST qPCR Master mix (KK4824; KapaBiosystems/Roche) and the "No Rox" protocol (KAPA Library Quantification Kit Illumina® Platforms Technical Data Sheet). Libraries, DNA standards, and DNA-free negative controls were run in triplicate on a Rotor-Gene (Qiagen) real-time PCR cycler. Standard curves and resultant calculated library concentrations were calculated with the Data Analysis Template provided by the manufacturer. The libraries were paired end sequenced on an Illumina® NextSeq 500 platform using 2 x 150 Mid-Output Kit (FC-404-2003). Both the libraries and the

PhiX control (Illumina®, FC-110-3002) were diluted to a final concentration of 1.8pM. The PhiX was pooled with the libraries at one percent of the total library loaded.

3.2.2 Bioinformatics

3.2.2.1 Read Processing

Concatenated text files that contain the nucleotide sequences along with each nucleotide's quality (Q) score as determined by the sequencing platform during post-sequencing analysis were used as input into downstream analyses. The Q scores are used as metrics for quality assessment and quality control for downstream analyses. The libraries' qualities were assessed with FastQC (Andrews, 2010), which reports the number of reads in each file, the Q score distribution across reads, GC content, and if any reads are over-represented in the data, suggesting contamination or a non-random capture of transcripts.

Shell scripts packaged together as BBTools (Bushnell et al. 2017) were used to process the reads for optimal assembly (e.g., adapter trimming, quality trimming, contamination filtering, and error corrections). Two different pipelines were used within BBTools that varied in the order of steps, whether reads were merged, and the level of normalization used. A more detailed account of the processing, including the commands used, can be found in the USGS data release. The merged reads from all three libraries in the first workflow were concatenated with the unmerged reads1 files (R1, left). The read 2 (R2, right) files per library were concatenated into a second file. These two files were the input from the "1st pass" workflow into the pipeline below. Because the reads remained unmerged in the 2nd processing workflow, the resultant files were the concatenated R1 files from each library and the concatenated R2 files from each library.

3.2.2.2 *De Novo* Transcriptome Assembly and Quality Control

Two assembly programs were used. First, the Trinity v2.2.0 (Grabherr et al. 2011) assembler was used through the open source web platform Galaxy (useGalaxy.org; Afgan et al. 2016). Trinity assemblies were run with the following settings: paired end data, with an orientation FR (Read1 is the forward direction of transcription, Read2 is the reverse direction), a group pairs distance of 500, a path reinforcement distance of 75, and a minimum contig (assembled, consensus transcript) length of 200. Second, we used SPAdes v 3.12.0 (Bankevich et al., 2012) using local computing resources and the same parameters. The SPAdes assemblies were run in read error correction and assembling mode and RNA-seq mode specifying the same read orientation as the Trinity assemblies.

Summary statistics and quality assessment metrics of the resultant four assemblies were calculated in QUAST (Quality Assessment Tool for Genome Assemblies) v 4.6.3 (Gurevich et al. 2013) through Galaxy. Results were reported for contigs > 500bp in length.

We used the quasi-mapping based mode of Salmon v 0.9.1 (Patro et al. 2017) to assess the quality of the assembly by mapping sequencing reads back to the assembly. The shuffle.sh script in BBTools was first used to randomize reads, using the entire set reads from each workflow, as opposed to those normalized to 30X (1st processing workflow) or 50X (2nd processing workflow). Finally, for reads from the first workflow, we only included those that were merged and specified them as single end reads in the Salmon input. We allowed Salmon to automatically detect the library type.

A method of assessing the completeness of transcriptome assemblies is to determine if single copy genes, common across many taxa, are present in the data. We used BUSCO (Benchmarking Universal Single-Copy Orthologs; Simão et al. 2015, Waterhouse et al. 2017) v 3.0.2 to look for single-copy orthologs (equivalent to the same genes but found in different species) that were in both our data as well as the BUSCO Metazoa dataset. BUSCO employs HMMER hidden Markov models to identify and classify gene sets in transcriptomic data and Augustus (Stanke et al. 2006) for de novo gene prediction.

3.2.2.3 Identification of protein coding genes

The following gene finding, blast, and annotation methods were executed through the bioinformatics platform Blast2Go Pro (Götz et al 2008) on the Trinity assembly from the 2nd processing workflow. To annotate putative genes in our data, an *ab initio*, eukaryotic gene prediction analysis was performed using WebAugustus (Hoff and Stanke 2013). Augustus trains its model using the closest species it can to the species being studied. Because none of the 81 species available were coral or cnidarian species, we chose the nematode, *Brugia malayi*, to train the model. Settings included: using both strands for gene searching, allowing for incomplete gene prediction at sequence boundaries (partial), imposing a minimum gene length of 20, and allowing for in-frame stop codons. The output is in tabular, gene finding file format and includes annotation of likely gene structures within the contigs (such as coding regions (cds), mRNA, start and stop codons, and introns) and is used to inform downstream annotation applications.

3.2.2.4 Functional Annotation

A blastx-fast search (query protein database using translated nucleotide sequences) using the public NCBI web service (Q Blast) via Blast2Go Pro was performed using the contigs from the Trinity assembly from the 2nd workflow. We used the NCBI nr database filtered with the metazoan taxonomy id as the subject for the query, using the default E-value cut-off of 1.0 E-3. Gene ontology (GO) terms were mapped to the resultant protein blast hits using the most recent (2018.04) extensively curated GO annotated proteins from the Gene Ontology Association and Unitprot's ID-mapping to assign functional labels. Next, annotation rules were applied to the found ontology terms that optimize specificity with reliability of the annotations via the application of an annotation score comprised of the sequence similarity of the blast hit, the evidence code of the source GO and the position of the GO term in the GO hierarchy. The GO was filtered by the stony coral (Scleractinia) taxonomy identification. Default values were used for other parameter values, including blast filters and all evidence codes.

3.3 Results

In this study, we produced a reference transcriptome for a Gulf sample of the deep-sea coral *Lophelia pertusa* (collected at 476 m depth) to gain an understanding of active genes and metabolic pathways that are used during homeostasis and under stress (in this case, heat shock).

The NextSeq run produced 55Gbp, above Illumina's benchmark (Table 3.1). The quality score per base with a Q score of 30 or greater was 78%, with 180,408,972 reads that passed filter, which is less than the upper limit, but still within the Illumina specification. Note that the pass filter reads reported from the NextSeq software is half the actual number of reads because it does not count read 1 and read 2 of the same fragment separately. The complete data set of trimmed reads was deposited in the NCBI Sequence Read Archive (SRA) with BioProject number PRJNA487533 and BioSample numbers (SAMN09904304 (Lpe10_05A, SRS3708499); SAMN09904305 (Lpe10_05B, SRS3708498), SAMN09904306 (Lpe10_05C, SRS3708496); and SAMN09904307 (undetermined reads; SRS3708497). This Transcriptome Shotgun Assembly project has been deposited at DDBJ/EMBL/GenBank under the accession GHDD00000000. The version described in this report is the first version, GHDD01000000.

Table 3.1. Illumina NextSeq sequencing statistics

LANE	READ	CLUSTER PF [a] (%)	%=Q30 [b]	YIELD (Gbp) [c]	ERROR RATE (%)	READS PF[a]
1	1	80.52 ±2.26	80.15	6.5	1.80 ±0.43	43,354,116
	2(I)		93.11	216.34 Mbp	0.00 ±0.00	
	3		76.32	6.49	2.14 ±0.47	
2	1	80.28 ±2.38	80.98	6.43	1.66 ±0.38	42,906,216
	2(I)		92.74	214.04 Mbp	0.00 ±0.00	
	3		76.55	6.43	1.88 ±0.40	
3	1	82.54 ±4.17	81.16	7.08	1.48 ±0.41	47,179,260
	2(I)		93.45	235.51 Mbp	0.00 ±0.00	
	3		76.52	7.07	1.81 ±0.44	
4	1	83.56 ±3.77	77.72	7.04	1.79 ±0.59	46,969,380
	2(I)	80.52 ±2.26	93.28	234.40 Mbp	0.00 ±0.00	
	3		74	7.03	2.07 ±0.62	
Total	1		78.15	54.97Gbp	1.83	180,408,972

Notes: The NextSeq is divided into four lanes and each library runs on all lanes. The libraries were run in paired-end mode, so that each read was sequenced in the forward (1) and reverse (3) direction. Read 2(I) is the library index and is included as a quality control check. [a]PF= reads that passed initial Illumina quality filter; [b]%=Q30 is a quality score representing base calling accuracy in which the probability of an incorrect base is 1 in 1,000; [c]Yield is reported in gigabase pairs or Mega base pairs in the case of the indexes.

Analysis of sequences in FastQC revealed that some sequences were over-represented in each raw fastq file. Most often these were primer adapters and/or indexes that were part of the library construction, which were subsequently removed from downstream analysis. Approximately forty sequences across all files contained other over-represented sequences (though not by more than 0.18%). The NCBI Nucleotide database was queried with these sequences using the blastn algorithm. Most had matches with 18S or 28S rRNA DNA fragments from species of coral, anemones, jellyfish, fungi, or plants. A subset had matches to undefined genomic regions but blasting those yielded 28S or 18S as top hits. Although the library construction method used is designed to isolate mRNA from non-polyadenylated RNA, due to the vast quantity of rRNA in a total RNA extraction (>90%, Conesa et al., 2016), some carryover is expected. These sequences were removed from further processing.

Two assemblies were performed on reads from each workflow using the de novo assemblers, Trinity and SPAdes, for a total of four assemblies. The number of unnormalized reads that made it through the first workflow was 213,217,177 reads, which after normalizing to 30X coverage reduced the number to 36,748,700 (Table 3.2). The number of unnormalized reads from the 2nd workflow was 289,309,276 and a normalization to 50X reduced the number to 67,459,930 reads, nearly double the reads that were input in the first workflows.

Table 3.2. Transcriptome Assembly Statistics

Assembly [a]	**Trinity 1**[b]	**Trinity 2**[b]	**Spades 1**[b]	**Spades 2**[b]
Input normalized reads	36,748,700	67,459,930	36,748,700	67,459,930
# contigs (≥ 0 bp)	460,583	446,415	49,754	123,834
# contigs (≥ 1000 bp)	62,749	46,918	32,840	29,382
# Total length (≥ 0 bp)	274,653,183	235,293,114	82,223,378	98,522,563
# Total length (≥ 1000 bp)	111,742,989	82,381,637	68,788,104	59,019,218
# contigs (≥ 1000 bp)	166,025	131,048	49,754	55,874
Largest contig	17,697	23,936	34,483	19,712
Total length	182,669,076	140,139,731	82,223,378	77,714,785
GC (%)	41.22	41.36	41.1	41.09
N50	1240	1176	1976	1707
# N's per 100 kbp	0	0	7.82	18.14
Annotated genes (Blast)	na	13,427	na	na
Annotated genes (GO)	na	7,551	na	na

Notes: [a] (# contigs ≥ 0 bp)=the number of contigs per assembly; (# contigs ≥1000 bp)=the number at least 1000 bps long; (# Total length ≥ 0 bp)=the total length of all the contigs; (# Total length ≥ 1000 bp)=contigs equal to or longer than 1000 bp. The remaining statistics are based on contigs of length 500 bp or greater. GC (%) is the percentage of the nucleotides guanine (G) and cytosine (C) in the contigs. See text for explanation of N50 assembly statistics. N's per 100 kbp=the number of unidentified bases (N) per kilo base pair per assembly. [b]Trinity and Spades assemblies each run with two workflows (1 and 2).

Assembly summary statistics obtained from QUAST are listed in Table 3.2. The number of contigs (>500 bp) in each assembly ranged from 49,754–166,025, with the Spades assemblies falling closer to the number of assembled genes found in other deep-sea corals (36,545–43,748; Yum et al., 2017). N50 represents the number of contigs it takes to reach 50% of the assembly if contigs were laid end to end. The N50 estimates from our assemblies ranged from 1,176–1,976 (Table 3.2), which was within the range reported for transcriptome assemblies of three deep-water corals from the Red Sea (1,396; 1,717; and 1,805 for *Eguchipsammia fistula*, *Dendrophyllia* sp.1, and *Rhizotrochus typus*, respectively; Yum et al., 2017). The unimodal distribution of GC% across the assembly (Figure 3.1) indicates that no significant prokaryotic contaminant is present. It is interesting to note that the GC content in our assemblies (41.09–41.36; Table 3.2) fell within the range of GC content recovered from other deep-sea coral transcriptomes (41.11–41.88; Yum et al. 2017).

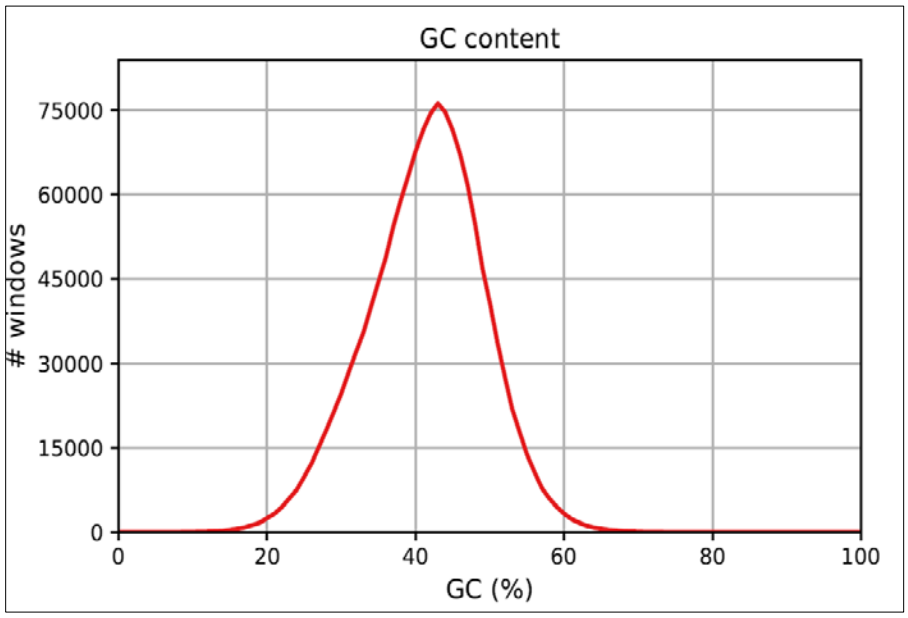

Figure 3.1 Distribution of GC content for assembled transcripts from the Trinity second pass workflow.

Notes: The y value is the number of non-overlapping 100 bp windows in which GC content equals X percent (x axis).

The percentage of mapped reads to each assembly was 78%–90% (Table 3.3), which lies within the range of mapping rate indicative of successful assemblies (Dobin et al. 2013). Closer examination of the mapping results suggests different qualities about each assembly. For instance, the two merged assemblies had higher numbers of assigned fragments and compatible fragment ratios of one. It follows that the best mapping rate was to the merged Trinity assembly (90.38 % mapping rate, Table 3.3). The second pass workflows produced a larger number of compatible fragments and assigned fragments, suggesting the 50X normalization may be superior to the 30X normalization used in the first pass workflow.

Table 3.3. Results of Read Mapping

Mapping statistic[a]	Trinity 1	Trinity 2	Merged Trinity	Spades 1	Spades 2	Merged Spades
Compatible frags	16,456,086	67,384,743	143,008,197	14,968,909	68,865,990	124,991,559
Assigned frags	20,676,691	122,253,867	143,008,197	18,699,591	119,571,224	124,991,559
Consistent	24,140,662	174,234,308	483,703,573	19,123,385	97,679,258	383,517,628
Inconsistent	50,136,190	200,053,319	0	38,572,367	98,892,841	0
Strand bias	0.52	0.33	0.48	0.36	0.42	0.56
Compatible frag ratio	0.80	0.55	1	0.80	0.56	1
Mapping rate (%)	75.20	84.51	90.38	68.01	82.66	78.99

Notes: Mapping performed using the Salmon software (Patro et al., 2017) on Trinity and Spades assemblies each run with two workflows (1 and 2). Listed for [a]Mapping statistic: Compatible frag= number of fragments compatible with the library type; assigned frag= total number of fragments that could be assigned to at least one transcript (including orphan mappings); consistent mappings= total number of consistent mappings, including those that may map in a library-compatible way to more than one transcript; accounts for multi-mapping; inconsistent mappings= number of inconsistent mappings; strand bias mapping= ratio describing how strand-specific the mappings were.

Of the 978 genes within the metazoan BUSCO set, 86 – 94% were recovered from our assemblies, suggesting that our assemblies were nearing completion at the gene level and disregarding alternative transcripts (Table 3.4). Three out of four of the assemblies had less than ~2% of BUSCOs missing. The Trinity assemblies had fewer complete single-copy genes identified and a higher percentage of duplicated genes than the Spades assemblies (Table 3.4, S and D, respectively).

Table 3.4. Benchmark Universal Single-copy Ortholog (BUSCO) Results

BUSCO	Trinity 1		Trinity 2		Spades 1		Spades 2	
	%	Total	%	Total	%	Total	%	Total
Complete (C)	93.7	917	92.4	904	85.6	837	89	871
Complete, single copy (S)	19.7	193	38.3	375	59.8	585	65.3	639
Complete, duplicated (D)	74	724	54.1	529	25.4	252	23.7	232
Fragmented (F)	4.6	45	5.7	56	5.2	51	8.8	86
Missing (M)	1.7	16	1.9	18	9.2	90	2.2	21

Notes: The percentage and total of each type BUSCO is reported for each assembly. (BUSCO; Simão et al., 2015).

Annotation of the Trinity second pass assembled contigs (131,048, Table 3.2) produced over 13,000 blast hits and over 7,000 annotations to GO terms (Figure 3.2). Gene ontology annotations fall into three main categories: biological processes (what is the gene doing), molecular processes (what is the likely pathway the gene is involved in), and cellular component (where are the genes being activated). The relative

conservation of genes between scleractinian corals and *L. pertusa* in the three GO categories are shown in Figure 3.3. Genes relating to cellular and metabolic processes were most conserved, while immune system processes and cell proliferation were more divergent among the biological process terms. Binding and catalytic activity were conserved molecular functions; translation regulator activity and protein tags were most divergent. Membrane, cell part, plus cell and membrane parts were conserved cellular components; synapse and nucleoid components were most divergent.

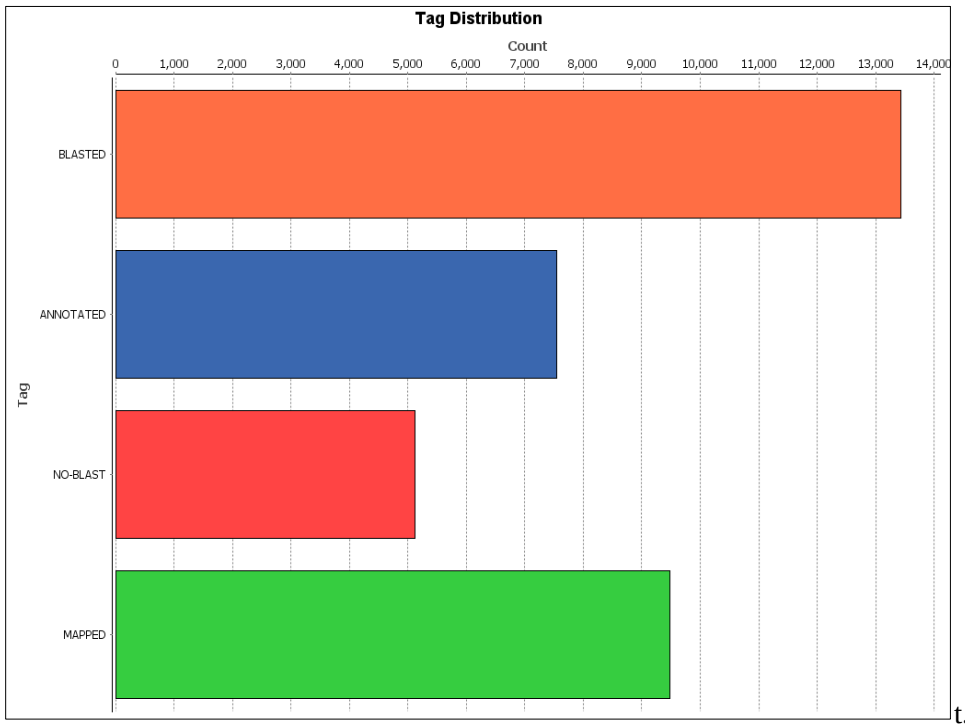

t.

Figure 3.2 Annotation results from the Trinity assembly second pass workflow.

Annotation results from the Trinity assembly second pass workflow, including: the number of contigs that produced a Blast hit against the Metazoa non-redundant database (BLASTED), the contigs that were annotated (ANNOTATED), the contigs that did not produce a significant Blast hit (NO-BLAST), and contigs associated with Gene Ontology terms (MAPPED).

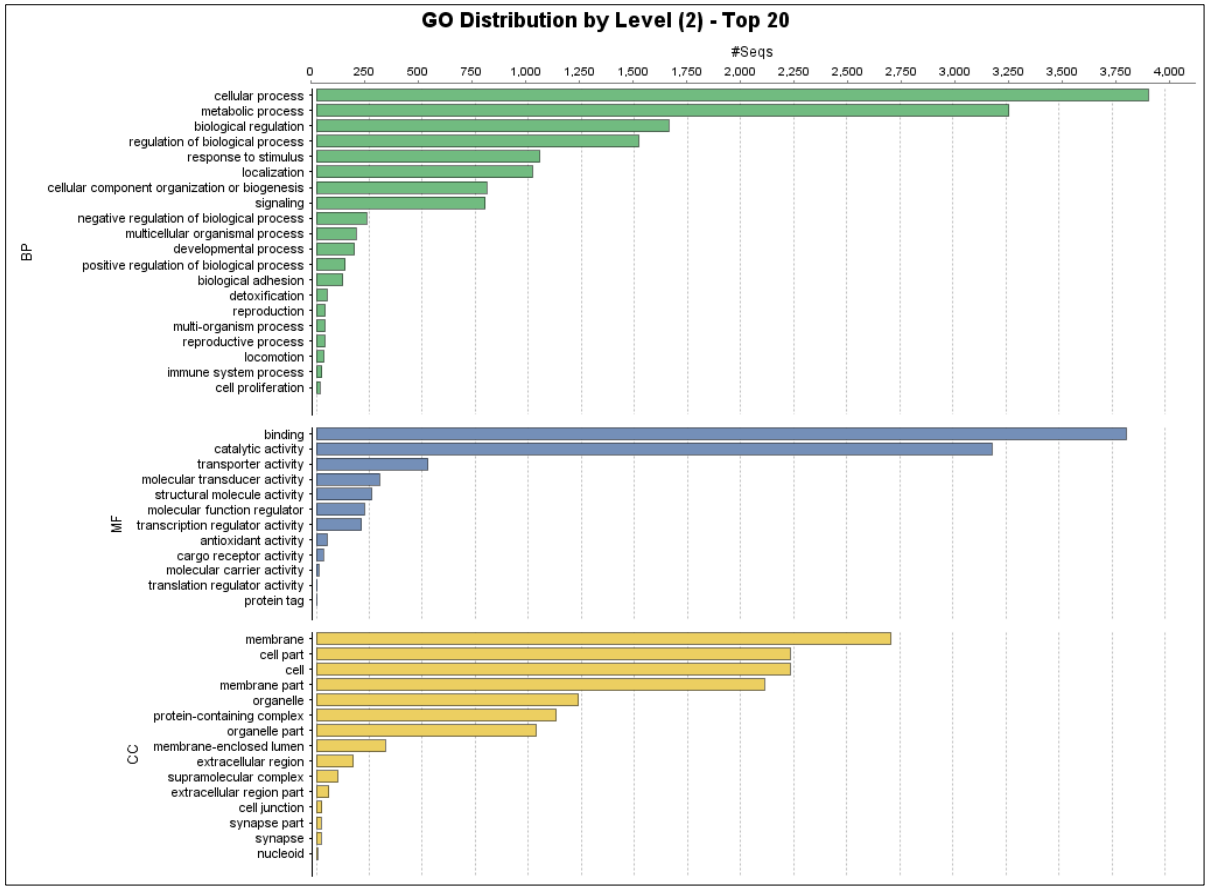

Figure 3.3. Relative conservation of homology between scleractinian coral and *L. pertusa* transcriptomes.

Shown by molecular function ontology terms and Gene Ontology categories: Biological Process (BP), Molecular Function (MF), and Cellular Component (CC).

Cnidarians made up the majority of species that the GO terms matched (Figure 3.4). The corals *Orbicella faveolata* and *Stylophora pistillata* produced the most matches for GO terms (Figure 3.4). Like *L. pertusa*, *O. faveolata* and *S. pistillata* belong to the Robust clade of corals. This result suggests higher similarity at the functional protein level between members of the Robust compared against Complex coral clades, as has been found in more comprehensive analysis of coral transcriptomes (Bhattacharya et al. 2016).

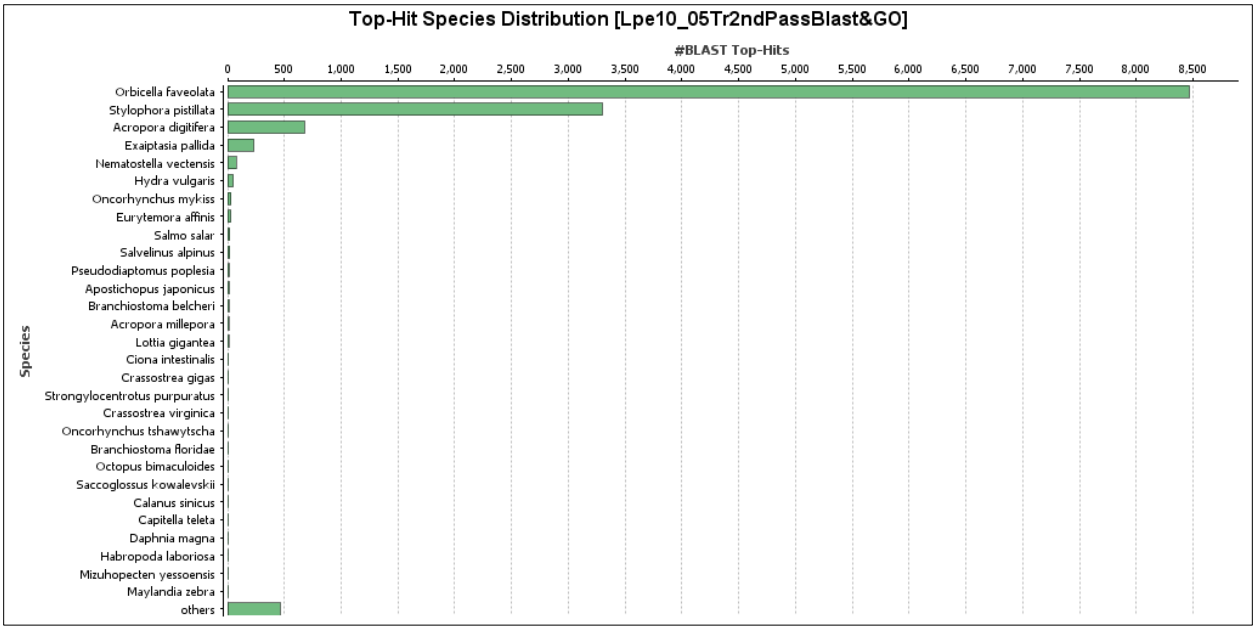

Figure 3.4. Species distribution of top hits of Gene Ontology terms.

We detected *L. pertusa* homologs for a range of genes potentially involved in stress-response that have been identified in other corals (Table 3.5). For example, chaperones such as several heat shock proteins (HSP) from families such as HSP90, HSP70, DNAJ, plus antioxidants such as peroxiredoxin, superoxide dismutase, and Maf family transcription factors are present at higher levels after heat stress in *Montipora aequituberculata* (van de Water et al. 2018). We identified many of the *L. pertusa* genes involved in immune response, such as Toll-like receptors (TLR) and tumor necrosis factor receptors (TNFR), plus kinases and proteins involved in the mitogen-activated protein kinases (MAPK) pathway that communicate a signal from cell surface receptors to DNA in the nucleus. Some of these genes, such as TNFR and the AP-1 transcription factor, are known to be a part of a coral "stress response module" that includes a large number of genes involved in general stress response (Rose et al. 2015).

Table 3.5. Putative Functions of Expressed Genes Involved in Stress and Immune Response Detected in *Lophelia pertusa* Transcriptome

Gene Name	Function	Reference
Antiviral response		
Interferon regulatory factor 1	Activated by TNF signaling. Induction of type I interferon leads to interferon type II IFNϒ expression	
Interferon regulatory factor 2	Inhibition of IRF1 function	Harada et al. 1989
DICER	Degradation of ds RNA viruses, suppression viral gene expression	Aliyari and Ding 2009

Gene Name	Function	Reference
Ubinuclein	Gene expression regulator- inhibits viral replication	Gruffat et al. 2011
ATRX	DNA structure modifying enzyme involved in repression of the lytic cycle following viral infection	Lukashchuk and Everett 2010
Complement System		
Ficolins	Activation complement system following MAMP binding	
C-type lectins	Activation complement system following MAMP binding	
Deleted in malignant brain tumor 1	Scavenger receptor- binds bacteria and virus	Leito et al. 2011; Madsen et al. 2010
Immune cell activation & phagocytosis		
Phosphatidylinositol-4-phosphate-3-kinase Ras-related C3 botulinum toxin substrate 2 Rho TRIO Wiskott-Aldrich Syndrome protein profilin	Actin re-organization during phagocytosis; cell migration	Bugyi and Carlier 2010; Flannagan et al. 2012; Schmidt and Debant 2014; Raftopoulou and Hall 2004
Hepatocyte growth factor-regulated tyrosine kinase substrate Charged mutlivesicular body protein 1	Phagosome trafficking and maturation, cell migration	
FYVE, RhoGEF and PH domain containing 5/6	Regulator of WASP-activating cdc42	Kurogane et al. 2012; Steensblock et al. 2014
Nitric oxide synthase	Oxidative burst, microbe elimination	
autophagy-related proteins 16, 1, 101	Autophagosome recruited by GIMAP6	Pascall et al. 2013; Weiss et al. 2013
Macrophage receptor MARCO	Scavenger receptor- binds bacteria and induces phagocytosis	Kraal et al. 2000

Gene Name	Function	Reference
Deleted in malignant brain tumor 1	Scavenger receptor- binds bacteria and viruses, induces phagocytosis	Madsen et al. 2010
Down syndrome cell adhesion molecule	Binds bacteria and viruses and parasites, induces phagocytosis	Ng et al. 2014
Vesicle-associated membrane portein-associated protein A	Secretion of DSCAM	
5-hydroxy tryptamine (serotonin) receptor 1, 2, 4, 5	Immune cell activation	Banganz and Blakely 2012
Calcineurin/protein phosphatase 3	Immune cell activation	Feske et al. 2003
Cytochrome P450 27C	Immune cell activation	Nagy et al. 2012
Aracidonate 5-Lipoxygenase	Produces leukotrienes- immune cell activation and chemotaxis	
Multidrug resistance associated protein neural cell adhesion molecule L1 Metalloproteinase	 Immune cell migration	 Van de Ven et al. 2008; Maddaluno et al. 2009
Ankyrin	Cell adhesion and migration (spectrin skeleton), promotes Rac1 signaling	Bourguignon et al. 2000
Other immune mechanisms		
Flavin-containing monooxygenase	Production of hydrogen peroxide	Siddens et al. 2014
Histones	Nucleosome formation and DNA binding- determines gene expression	
Immune response modulation		
Jagged	Ligand of Notch	Van de Water et al. 2017
Notch	Cooperates with TLR in pro-inflammatory cytokine production initially, but inhibits TLR-induced NF-κB activation at later phases	Hu et al, 2008; Zhang et al. 2012
Annexin	Modulator of immune responses	Gavins and Hickey 2012
Calcification		
Solute carrier family 26 member 6-like	Bicarbonate transport	Soleimani and Xu 2006
Carbonic anhydrase	Interconversion between carbon dioxide and water	Edge et al. 2005

Gene Name	Function	Reference
Chaperones		
Heat shock proteins DNAJ, HSP90, HSP70	Unfolded protein response; Induce immune response (TLR, cytokine)	Tsan and Gao 2009
Stress-induced Phosphoprotein 1	Enhance HSP function	Odunuga et al, 2004
Antioxidants		
Maf transcription factors	Regulation of antioxidant response	Motohashi et al. 2002
Peroxiredoxin 1	Reduce H2O2 and alkyl hydroperosides, Danger-associated molecular pattern, inflammatory response	Rhee et al. 2001; Riddell et al. 2010; Shichita et al. 2012
Peroxidase		
Superoxide dismutase		Cairo et al. 1995; Gasch et al. 2000
Gluthione		
Ferritin, Thioredoxin		Cairo et al. 1995; Gasch et al. 2000
TLR & TNFR signaling pathways		
Toll-like receptor (TLR) 4	Innate immune response (bacteria/viral); coral stress response module, shallow and deep corals	Kumar et al. 2009; Yum et al. 2017
Tumor Necrosis Factor Receptor (TNFR)	Initiate pro-inflammatory response, apoptosis induction	Newton and Dixit 2012 Taylor-Knowles et al. 2017;
TNFR-associated factors	Signal transduction from TLR/TNFR to MAPK pathways	Kumar et al. 2009
Mitogen & stress-activated protein kinases	Signal transduction (activated by TRAF)	
Dual-specificity phosphatase	Inhibition of MAPK activity	Arthur and Ley 2013
Apoptosis		
Phosphatidylserine-specifc receptor	Facilitates phagocytosis of apoptotic cells	Fadok et al. 2001
Apoptosis-inducing factor 3		
Epidermal Growth Factor (EGF)-like proteins	Bind apoptotic cells, eliminate dead cells	Ruiz-Ramos et al. 2017

Gene Name	Function	Reference
AP-1 transcription factor	Response to stimuli, including cytokines, growth factors, stress. Part of coral stress response module	Traylor-Knowles et al. 2012
Cytokine signaling & regulation		
Histamine receptors	Interleukin production	O'Mahony et al. 2011
NACHT, LRR, and PYD donmains-containing protein 3	Release interleukin upon intracellular MAMP binding. Expression induced by TLR signaling.	Qiao et al. 2012 Gross et al, 2011
Meprin-A	Release of interleuking cytokines	Herzog et al. 2009
Metalloprotease	Cytokine release	Worthington et al. 2012; McClellan et al. 2006

3.4 Discussion

In this study we have developed a *de novo* transcriptome assembly for the deep-sea coral *L. pertusa*. Metrics from one of the assemblies described here suggest that transcripts represent the majority of the protein-coding genes that have been identified. Within this set of annotated genes were *L. pertusa* homologs that correspond to many components of stress response and implement signaling cascades that lead to activation of genes that allow physiological response to environmental signals. This research provides a foundational step towards experimental studies to test the *L. pertusa* response to additional environmental stressors (such as oil and dispersant), allowing for a better understanding of specific physiological responses, as well as laying the groundwork for the development of biomarkers to track responses and ascertain overall coral health.

The full exploration of transcriptomic responses to environmental factors requires extensive laboratory manipulation and genomic tools, such as a fully sequenced genome (Orsini et al. 2016). For non-model organisms without fully sequenced genomes, assessing the completeness and quality of a *de novo* transcriptome assembly is challenging because we do not know what the ideal transcriptome would look like or how many genes it may contain. For corals, a good benchmark was provided by the recent study involving comparative genomics and transcriptomics of twenty scleractinian corals (Bhattacharya et al. 2016). The authors found an average of 21,657 protein sequences per coral transcriptome. Even though our BUSCO comparisons suggested a fairly complete set of complete orthologs in our transcriptome, the number of single-copy BUSCOs was lower, suggesting that unrecovered expressed genes exist for *L. pertusa*. Additionally, the number of GO annotated genes in our transcriptome (7,551) was about half the number found in three deep-sea corals from the Red Sea (13,795–17,689; Yum et al. 2017). The addition of longer read length sequences (Conesa et al. 2016) may improve our coverage of *L. pertusa* orthologs, and would likely improve completeness of the genes as well. Given that transcriptomes without comparative genomes often miss weakly expressed or underexpressed genes, deeper sequencing may result in a more complete set of *L. pertusa* genes.

Picking an optimal assembly was challenging because different assemblies performed better depending on the metric used. The different assemblies we performed each had strengths and weaknesses, but the merged assemblies had consistently higher mapping rates. The EvidentialGene assembly method (Gilbert et al. 2002) combines RNA assembly with genome-based modeling, using evidence from public gene expression and protein data sets to annotate new genes. Using the EvidentialGene assembly approach has improved many transcriptomes for model organisms as well as others with little genomic data available. Through the additional sequencing mentioned above, plus the more comprehensive bioinformatic treatment, we hope to create a complete and accurate gene and transcriptome repertoire.

Once a more comprehensive transcriptome is in hand, we will expand comparisons with well curated coral transcriptomic databases, such as the 20-coral comparative database. This will include comparisons with the 6,970 robust coral orthologs available (Bhattacharya et al. 2016).

3.5 Conclusions

In this study, we have developed a *de novo* transcriptome assembly for the deep-sea coral *L. pertusa*, including protein-coding genes putatively involved in both stress response as well as homeostasis.

- This study identified thousands of *L. pertusa* functional genes putatively involved in both stress response as well as homeostasis.
- Many of the genes are conserved across scleractinian corals and/or cnidarians.
- A suite of genes with expression patterns that correlate with stress response in other corals were identified.
- We plan to refine the *L. pertusa* transcriptome through additional sequencing and bioinformatics.
- The well annotated transcriptome can be queried in future RNA-seq experiments involving a variety of environmental stressors, including exposure to contaminants such as oil and dispersant.
- Genes that respond to contaminants will be targeted for custom codesets for gene expression analysis with the NanoString nCounter system that can be used for quantitative measurement of the expression of stress-related target genes.

4 Uptake and Distribution of Organo-iodine in Deep-sea Corals

4.1 Introduction

[2]The biogeochemical cycling and distribution of iodine and its isotopes in the environment is particularly relevant given iodine's biophilic nature and the propensity of its radionuclides to migrate and accumulate through biological systems. The stable iodine isotope occurs as ^{127}I and the long-lived ($t_{1/2}$=15.7 Ma) radioisotope is present as ^{129}I. Both are naturally occurring; however, human nuclear activity (e.g., bomb testing) has increased the marine $^{129}I/^{127}I$ ratio since the 1940s (Raisbeck and Yiou 1999). Concerted effort has focused on understanding concentration levels and the behavior of natural and anthropogenic iodine in the environment (see reviews by Fuge and Johnson 1986; Hou et al. 2009; Kaplan et al. 2014; Muramatsu and Hans Wedepohl 1998; Muramatsu et al. 2004). As an important tracer in geologic and biologic studies, iodine and its isotopes have been studied as a geochronometer (e.g., Santschi and Schwehr 2004), a water mass tracer (e.g., Guilderson et al. 2014; He et al. 2013), a proxy for organic carbon and sediment fluxes (e.g., Oktay et al. 2000; Santschi et al. 2007; Schwehr and Santschi 2003), an indicator of contaminants (e.g., Fuge and Johnson 2015; Hormann and Fischer 2017), and for monitoring nuclear activities (Fan et al. 2016; Lebel et al. 2016). More recently, marine archives of iodine variability over the last several decades have been developed from shallow, scleractinian coral records (Bautista et al. 2016; Biddulph et al. 2006; Chang et al. 2016), analogous to the application of radiocarbon (^{14}C) in shallow coral records to capture mixing of surface and subsurface water and CO_2 exchange (e.g., Druffel 2002; Guilderson et al. 2000). However, to date iodine uptake and distribution in long lived (> 4,000 years) deep-sea corals remains unexplored.

Iodine in proteinaceous corals was first observed by Goldberg (1978), noting that iodine accounted for 23% of the skeletal weight, contributing >94% of all halogens in the basal portion of the coral's skeleton. More recently, based on results from scanning electron images (SEM) and micro-Particle Induced X-ray Emission (μ-PIXE), Nowak et al. (2009) found elevated iodine concentrations associated with the carboxyamino acids and lipids and concentrated in narrow gluing zones between the rings. Over the lifespan of a deep-sea coral specimen from the Gulf, Prouty et al. (2010) found decreased iodine intensity in regions where the gluing zone was absent. The presence of iodine in the black coral microstructure therefore suggests a functional role given the corals' requirement to bind growth layers, consisting of protein and chitin (Goldberg 1978; Goldberg 1991).

The ocean is considered the main source of iodine with oceanic iodine typically trapped in soils, sediments, and biota (Hou et al. 2009) due to its biophilic nature (Elderfield and Truesdale 1980) (i.e., tendency to form covalent bonds in proteins and humic substances). For example, early studies showed particulate iodine below the euphotic zone linked to a biogenic origin (Wong et al. 1976). Macrophytic

[2] A version of this paper was published as: Prouty NG, Roark EB, Mohon L, Chang C-C. 2018. Uptake and distribution of organo-iodine in deep-sea corals. J Enviro Radioact. 187:122–132. DOI: 10.1016/j.jenvrad.2018.01.003

algae (e.g., brown algae) in particular bio-accumulates iodine at 30,000–150,000-fold relative to seawater (Leblanc et al. 2006), and iodine is concentrated in soils up to 1,000 times more than in the parent material (Muramatsu et al. 2004). Proteinaceous corals also appear to bioaccumulate iodine (Goldberg et al. 1994; Kaczorowska et al. 2003; Nowak et al., 2009), with Williams and Grottoli (2011) reporting iodine concentrations over 2×10^5 parts per million in black coral specimens collected from the western tropical Pacific. The biogeochemical cycle of iodine is complex given rapid chemical reactions that alter the speciation, fractionation, and accumulation in the terrestrial and marine environments. Understanding the bioavailability of iodine is therefore crucial in predicting its application as an oceanographic tracer and its behavior in the environment. Furthermore, the biological uptake and transfer of iodine is tightly linked to its speciation (e.g., Hou et al. 2009; Schlegel et al. 2006; Yamaguchi et al. 2006; Zhang and Hou 2013). Iodate is the dominant species in oceanic waters, but biological activity has been shown to reduce iodate (IO_3^-) to iodide (I^-) by bacteria (Farrenkopf et al. 1997; Tsunogai and Sase 1969) and phytoplankton (Chance et al. 2007; de laCuesta and Manley 2009). Similarly, the reduced form of iodine, iodide, accumulates in brown algae (e.g., Küpper et al., 2008). In comparison, in natural soils iodine is typically present as organo-iodine (Feiters et al. 2005; Schlegel et al. 2006; Shimamoto and Takahashi 2008).

Here we explore the utility of iodine and its uptake into the skeleton of the deep-sea black coral skeleton *Leiopathes* sp. collected from the Gulf. While the presence of inferred growth rings have been previously explored in a variety of different deep-sea coral species (Grigg 2002; Williams et al. 2006), this present study represents both a validation of annual growth layers as well as a mechanism to explain the formation of annual growth bands in deep-sea black corals. This novel approach combines the identification of growth bands captured in high-resolution SEM with synchronous peaks in iodine variability, and the identification of peak $^{129}I/^{127}I$ ratios in response to nuclear weapons testing. The methods and results presented here represent a unique approach to developing iodine-based deep-sea coral chronologies. Taken together, results presented here have wide application to the use of iodine as a biogeotracer with relevance to environmental science and geochronological studies.

4.2 Methods

4.2.1 Study Area and Sample Collection

Black coral (*Leiopathes* sp.) specimens were collected east of the Mississippi Delta from the Gulf in the Viosca Knoll (VK) region, and the head of De Soto Canyon as described in Prouty et al. (2011, 2014a). The occupied submersible, Johnson-Sea-Link (JSL, Harbor Branch Oceanographic Institute), was used to collect live black coral colonies from the VK sites at depths of 310–317 m and a bottom trawl (TOW) inadvertently collected specimens of living black coral from the head of De Soto Canyon at a depth of 304 m (Figure 4.1). The head of De Soto Canyon is on the outer shelf zone, with a relatively steep western wall and a much gentler eastern wall. An upwelling of deep nutrient-rich water occurs here, resulting in relatively high primary productivity. De Soto Canyon has been identified as the divide between the terrigenous Mississippi River muddy sediments to the west and the allochthonous carbonate sediments to the east (Bryant et al. 1991). Previous studies in the VK region of the northern Gulf highlight the MAR as the major source of sediment and nutrients transported to the seafloor (Davies et al. 2010; Mienis et al. 2012; Prouty et al. 2014a; 2016). Sediment trap data from the VK region consists of

fine-grained aggregates of riverine origin in combination with particles with high organic carbon content (Davies et al., 2010). The large quantities of nutrients and terrestrial OM stimulate surface primary productivity, producing OM that flocculates and sinks to the seafloor. For example, Mienis et al. (2012) found peaks in near-bed fluorescence corresponding to increases in pigments, C_{org}, total nitrogen (N_{tot}), and biogenic silica (SiO_2) in sediment trap samples. The Mississippi River discharges approximately 1.5×10^{12} g C yr^{-1} (Dubois et al. 2010), with enhanced continental weathering of soils predicted from climate and land-use change (Beaulieu et al. 2012). The Loop Current System contributes to the transport of these large riverine plumes offshore (Schiller and Kourafalou 2014).

Figure 4.1. Map of deep-sea black coral (*Leiopathes* sp.) collection sites in the Gulf.
Sites are located in two different regions on the upper De Soto Slope subprovince: the head of De Soto Canyon and Viosca Knoll to the east of the Mississippi River. Samples were collected at water depths of approximately 300 m.

4.2.2 Sample Preparation

Multiple (2–4) 0.5 cm thick cross-sectional disks were cut from the basal portion of the black coral (*Leiopathes* sp.) specimens using a diamond band saw. One cross-sectional disk was prepared for SEM analyses by polishing on one side using silicone carbide powder at 120, 400, 600, and 1000 grit size, then cleaned and dried for 24 hours before being epoxied using Epotech epoxy onto a glass slide for thin sectioning. The mounted disk was then cut to a thickness of 0.3–0.5 cm with an Isomet precision low-speed saw and the surface re-polished using a Hillquist grinder down to a thickness of 320–340 µm. The

final polishing steps were done using silicone carbide powder on glass lapping plates and a Buehler polishing wheel removing an additional ~70–90 µm for a final thickness of ~250 µm.

A second 0.5 cm thick cross-sectional disk adjacent to the SEM disk was used for radiocarbon and stable isotope analyses. After the diameter was measured at multiple points, the disk was separated into layers using the method developed by Williams et al. (2007). Briefly, the disks were placed in 4 g of potassium hydroxide (KOH) solution mixed with 50 mL of Milli-Q water in order to detach individual rings from the disk. Typically 4–7 rings at 1–2 mm thick were separated during this step. The thickness of each ring was measured at multiple points around the ring and then the rings were placed back in KOH solution for ~1 week after which individual layers ~10 µm thick were peeled from the ring using tweezers and a scalpel blade under a microscope. The separated layers were rinsed in Milli-Q water to remove the KOH solution and dried in air or in an oven at ~60°C. The radial distance of each layer was calculated by dividing the measured thickness of the ring by the number of layers separated from the ring. A subset of the layers were used for ^{14}C analyses as described in Prouty et al. (2011).

4.2.3 Analytical Techniques

4.2.3.1 Electron Microprobe and LA-ICP-MS Methods

Scanning electron microscope analyses were carried out using a Cameca SX50 electron microprobe at the Electron Microprobe Laboratory in the Department of Geology and Geophysics, Texas A&M University. The SEM analyses included both back scattered electrons (BSE) and x-ray elemental analyses of iodine on carbon coated thin sections. Images were acquired at an accelerating voltage of 15 kV and at a beam current of 1 nA along the radial transect of the specimen. X-ray elemental profiles of iodine along with BSE profiles were acquired along the radial transects of each specimen using a 1-µm diameter spot beam at an accelerating voltage of 15 kV and a beam current of 20 nA. The x-ray counts were acquired using wavelength-dispersive spectrometers (WDS). Iodine profiles were acquired using the I L alpha line on 2 PET (pentaerythritol) diffracting crystals. Starting from the center to the outer edge of each thin section, samples were measured beneath the fixed electron beam using a 1-µm spot measurement of shoulder-to-shoulder increments with 2-seconds of acquisition time at each point. BSE and iodine were measured from the center to the outer edge of each thin section.

Visual growth bands were identified and counted from the 900x magnification BSE-SEM images (Figure 4.2). Transects across the entire radius of the specimens were made using the 100-µm wide 900x BSE-SEM images stepped across the thin section with 10% overlap on each successive image. Three independent observers counted the number of growth bands in each of the 100-µm wide 900x SEM images across the entire radial transect of each specimen.

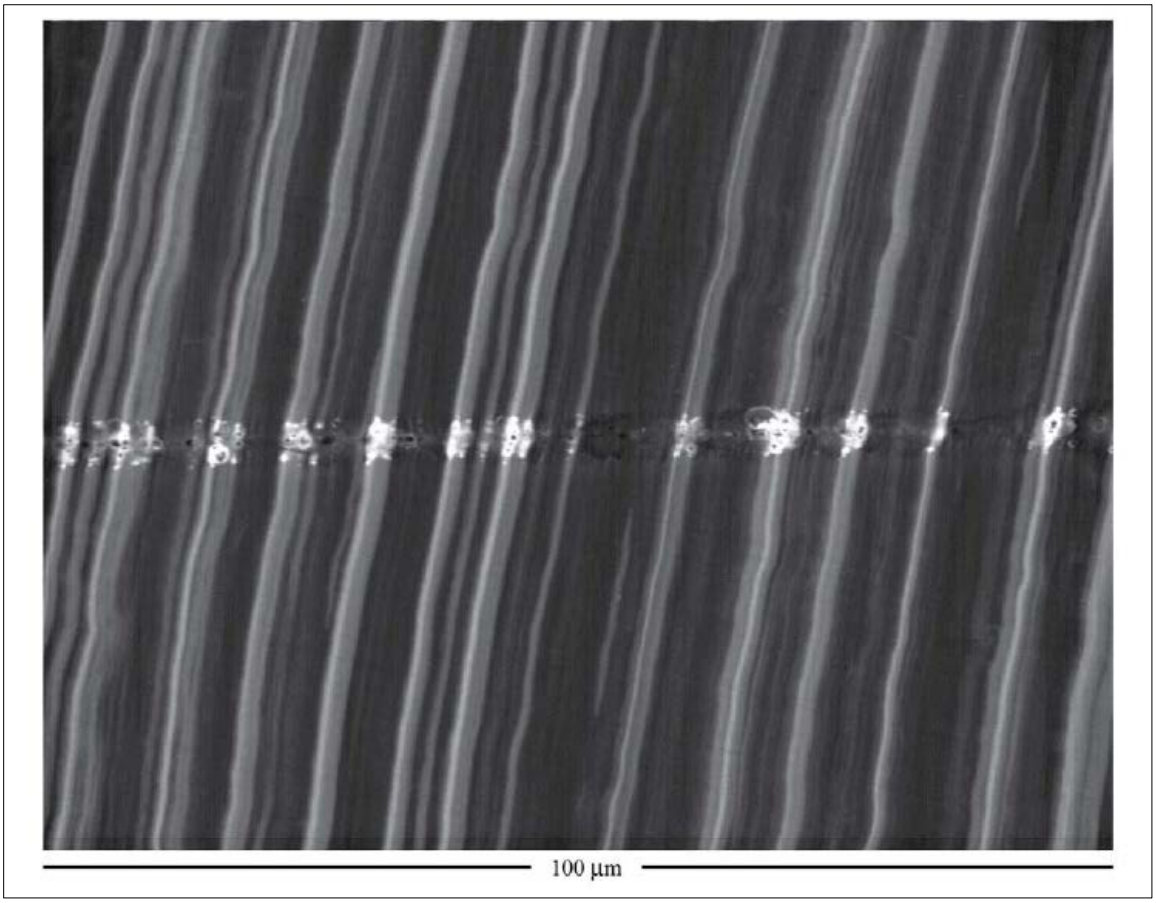

Figure 4.2. Scanning electron microscope image.

Scanning electron microscope image (100 µm width of view) along transverse cross section of deep-sea black coral at 900x magnification highlighting growth bands and showing 1 µm diameter electron beam spot for x-ray elemental analysis (see Figure 4.6).

Iodine counts were measured along the entire radial transects of the deep-sea coral specimens using a 1-µm diameter beam stepped shoulder to shoulder starting from the center and ending at the outer edge of the thin section. Iodine and BSE data points were removed when they corresponded to desiccation cracks. These gaps were not present when the corals were collected; they occurred as the specimen started to dry out and during the cutting and polishing phases of the thin section preparation. The desiccation cracks were identified in the iodine data by very low values. Once the gaps were removed from the iodine data, a new radial distance was calculated based on the assumption that each remaining data point represented 1 µm. To identify the iodine peaks, a set of criteria was used to minimize subjectivity of what constituted an iodine peak. A minimum threshold of 1,000 counts was used to identify and separate iodine peaks from the baseline noise for each specimen. After the potential peaks were identified, a second criteria to account for double peaks was used where double peaks within 4 µm or 2 µm were counted as one peak and counted to acquire the life spans for each coral.

In addition to x-ray elemental analysis, iodine variability over the coral lifespan was evaluated using Laser Ablation Inductively Coupled Mass Spectrometry (LA-ICP-MS) methods at the USGS LA-ICP-MS Facility in Denver, Colorado, following methods for quantitative trace element mapping (Koenig et al. 2009) and previously applied to deep-sea coral records (Prouty et al. 2014a). Iodine variability (counts per second [CPS]) was measured using a 193 nm wavelength laser connected to an Elan DRC-e quadrupole ICP-MS. The LA-ICP-MS was conducted using a modified procedure, with each time slice along the line scan treated as an individual measurement (Longerich et al. 1996). A pre-ablation cleaning scan was run prior to collecting data. To produce a rectangular elemental concentration map, a series of stacked radial lines (between 20 to 40) spaced ~40 µm apart were scanned at 20 µm sec^{-1} scan speed using a 35 µm spot size across the entire diameter of the specimen. The LA-ICP-MS quantification was conducted using a procedure where each time slice along the line scan was treated as an individual intensity (counts) measurement. Relative iodine variability is reported as CPS rather than concentration (e.g., ppm) given the lack of a suitable matrix-matched reference standard.

4.2.3.2 AMS Radiocarbon (Age Dating)

Individual layers (1-4 mg) were radiocarbon (^{14}C) dated by accelerator mass spectrometry (AMS) at the Central Accelerator Mass Spectrometry facility at Lawrence Livermore National Laboratory (CAMS-LLNL) following previously established radiocarbon (^{14}C) methods for proteinaceous deep-sea corals (Prouty et al. 2011; Roark et al. 2009). The carbon in the samples was converted to CO_2 via sealed-tube combustion, and upon cyrogenic purification the CO_2 was reduced to graphite in the presence of iron catalyst and a stoichiometric excess of hydrogen. Procedural blanks included either a coal or calcite blank. The $\Delta^{14}C$ values were age corrected to account for decay that took place between collection (or death) and the time of measurement using the following equation: $\Delta^{14}C$ =((Fm*age correction)-1)*1000 where age correction is defined as exp((1950- year of measurement)/8267). Radiocarbon results are reported as $\Delta^{14}C$ (‰) and conventional radiocarbon age (CRA) after applying a $\delta^{13}C$ correction (Stuiver and Polach 1977).

The radiocarbon ages were converted to calendar ages using the Calib 7.0 2013 program (Stuiver and Reimer 1993) and the Marine13 calibration curve (Hughen et al. 2004). Radiocarbon ages were corrected for the differences between the atmospheric radiocarbon content and the local radiocarbon content of the surface ocean, also known as a "reservoir age correction" (ΔR). These calibrations include the reservoir age correction (ΔR) for marine specimens to arrive at a calendar age. The Gulf had a ΔR of -30 ±26 ^{14}C years (Wagner et al. 2009). Both the reported radiocarbon and calibrated age uncertainties are reported at the 1-sigma level.

4.2.3.3 AMS: Iodine Isotope Analyses

The radioisotope of iodine, ^{129}I, was measured by AMS at the University of Arizona with an NEC 3 MV Pelletron accelerator following accepted methods (Biddulph 2004; Biddulph et al. 2006; Biddulph et al. 2000). Individual black coral growth layers (~ 1.9 to 14.1 mg) were chosen with coeval radiocarbon data. Sample pretreatment included either homogenizing skeletal material by freeze drying for 1 hour and placing the sample in a vacuum system and pumping out all the remaining water for ~2 hours, or

pretreating using an alkali fusion where the sample was soaked in NaOH, dried to completion on a hot plate, placed in a furnace at 200°C for one hour, and stayed in the furnace at 600°C for two hours (Nishizumi et al. 1983). The samples were then crushed and mixed with 10 mg silver powder and pressed in a cathode in preparation for AMS following the method in Biddulph et al. (2006) and Chang et al. (2016). AMS measurements were made in the +5 charge state at a terminal voltage of 2.50 MV with a transmission of 7.0%. Each sample was measured six times, and the weighted average of the measurements was calculated. Errors include statistical uncertainties and a random machine error of 4.3%. For the freeze dry method, silver powder served as a blank sample. For alkali fusion, two blank samples were treated using the exact reagents and chemical process as for the black coral samples. Counts from silver powder samples were subtracted from black coral counts before isotope ratios were calculated.

4.2.3.4 X-Ray Fluorescence (XRF) Mapping and X-Ray Absorption Near Edge Structure (XANES)

The spatial distribution of iodine and its speciation were determined using high-resolution (2-μm diameter beam) X-ray fluorescence (XRF) mapping and X-ray absorption spectroscopy (XAS) at the Stanford Synchrotron Radiation Lightsource (SSRL) hard X-ray microprobe. A Si(220) crystal set was used for energy selection, and X-ray fluorescence was measured using a single-element Vortex detector. X-ray fluorescence mapping was performed at 12,000 eV using a step size of 5 μm and a dwell time of 25 msec on beamline 2–3 on the coral thin sections. Using the fluorescence map as a guide, two points—one at the core of the coral sample (oldest portion), and another at the outer edge (youngest portion)—were chosen to examine the speciation of iodine using X-ray absorption near edge structure (XANES) spectroscopy at the K-edge (33**.**169 keV; beamline 11-2) (e.g., Feiters et al. 2005; Küpper et al. 2008; Reed et al. 2002; Shimamoto and Takahashi, 2008; Shimamoto et al. 2011). Five and six XANES spectra were collected at each point, respectively. Individual spectra were then averaged for each point as described in Prouty et al. (2014a) to improve the signal/noise ratio. Data reduction of the XAS spectra involved energy calibration, background subtraction, and normalization. Spectra were compared to the iodine (I_2) and iodide (I^-) standards and linear combination fitting of the first derivative was performed using the software ATHENA v 0.8.56 for semi-quantification of oxidation state and percent contribution from possible compounds (Ravel and Newville 2005). Reference spectra derived from similar beam line parameters from Feiters et al. (2005) were used for semi-quantification of oxidation state.

4.3 Results

4.3.1 Iodine Speciation and Isotope Analyses

Results from the *K*-edge XANES are shown for the coral skeleton material and reference standards of different valency of molecular iodine, sodium iodate ($NaIO_3$), and sodium iodide (NaI) (Figure 4.3). The adsorption edges of the reduced and oxygenated species of iodine are quite distinct at the *K*-edge. However, the spectrum for the black coral sample is relatively featureless, similar to the spectra of organo-iodine and molecular iodine (I_2) (Figure 4.3). These results indicate that identification between the

coral sample and the reduced and oxygenated species is relatively straightforward based on the XANES spectra. In comparison, distinguishing the coral sample from molecular iodine and organo-iodine is more difficult given similar adsorption edge positions. Therefore, calculating the first derivative of the XANES spectra improves XANES resolution by providing the position of the inflection point and hence the adsorption edge (e.g., Gaur et al., 2013). As seen in Figure 4.4, the adsorption edge between the coral sample and organo-iodine are similar (Figure 4.4a), whereas an offset between the coral sample and molecular iodine is observed in the first derivative plot (Figure 4.4b). As expected from the XANES spectra (Figure 4.3), the first derivative of iodide and iodate spectra show poor agreement with the coral sample. Linear combination fitting (LCF; Ravel and Newville 2005) was used to quantify the agreement between the various iodine species with the coral sample. With LCF, the X-ray absorption spectrum is modeled by least squares fitting using a linear combination of known species to fit an unknown spectrum and determine the proportions of the spectra for selected standards (e.g., Gaur et al. 2009). Subsequent results from LCF of the first derivative indicate that organo-iodine contributes 88% to the best fit, with a goodness-of fit parameter of 0.035 (Figure 4.4), expressed as the R-Factor and calculated as the mean square sum of the difference between the observed and reference spectra (Calvin 2013). Including the remaining species only improved the best fit by 8% and the R-Factor increased for molecular iodine, iodide and iodate to 0.091, 0.302, and 0.326, respectively, indicating reduced accuracy of each species to model the coral spectrum. Further LCF investigation of various organo-iodine species from Feiters et al. (2005), suggests that 1,2-diiodoethane (EtI_2) and iodoform (CHI_3) dominate the organo-iodine fraction (Table 4.1), with negligible contribution from the remaining organo-iodine species given a best fit improvement of less than 1% when additional spectra are incorporated into the LCF model.

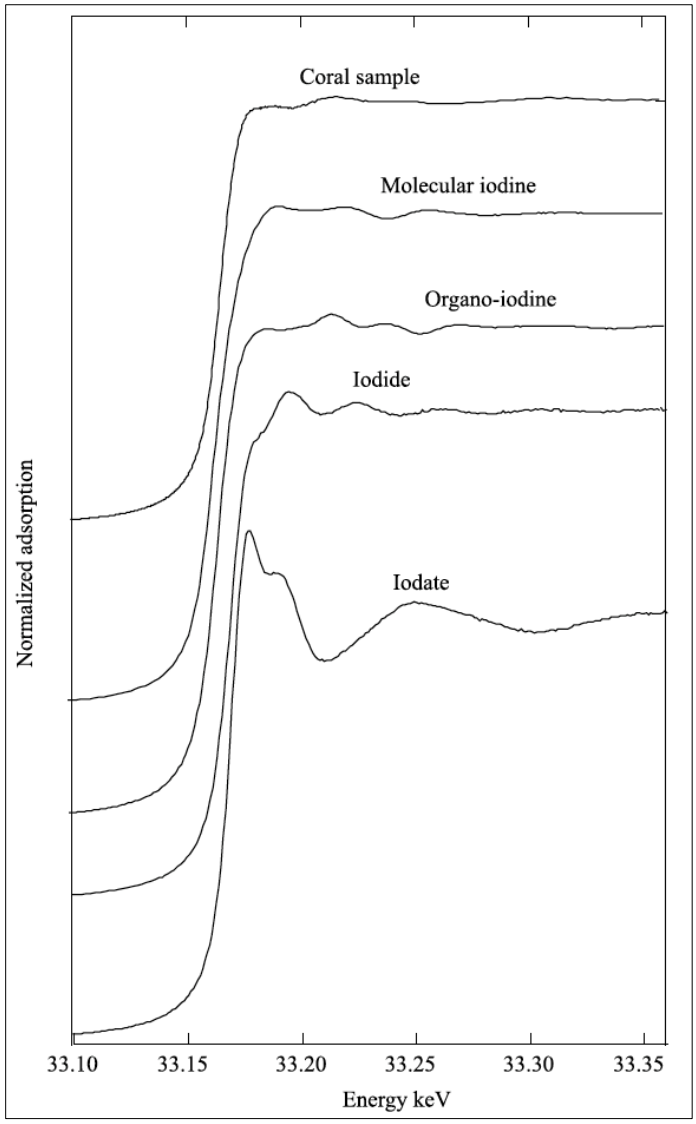

Figure 4.3. Iodine X-ray adsorption.

Iodine X-ray adsorption of a deep-sea black coral sample compared to different valencies of iodine, including inorganic iodine (iodide, NaI; iodate, $NaIO_3$; this study) and a representative organo-iodine and molecular iodine species (I_2; Feiters et al. 2005). Individual spectra are offset for presentation purposes.

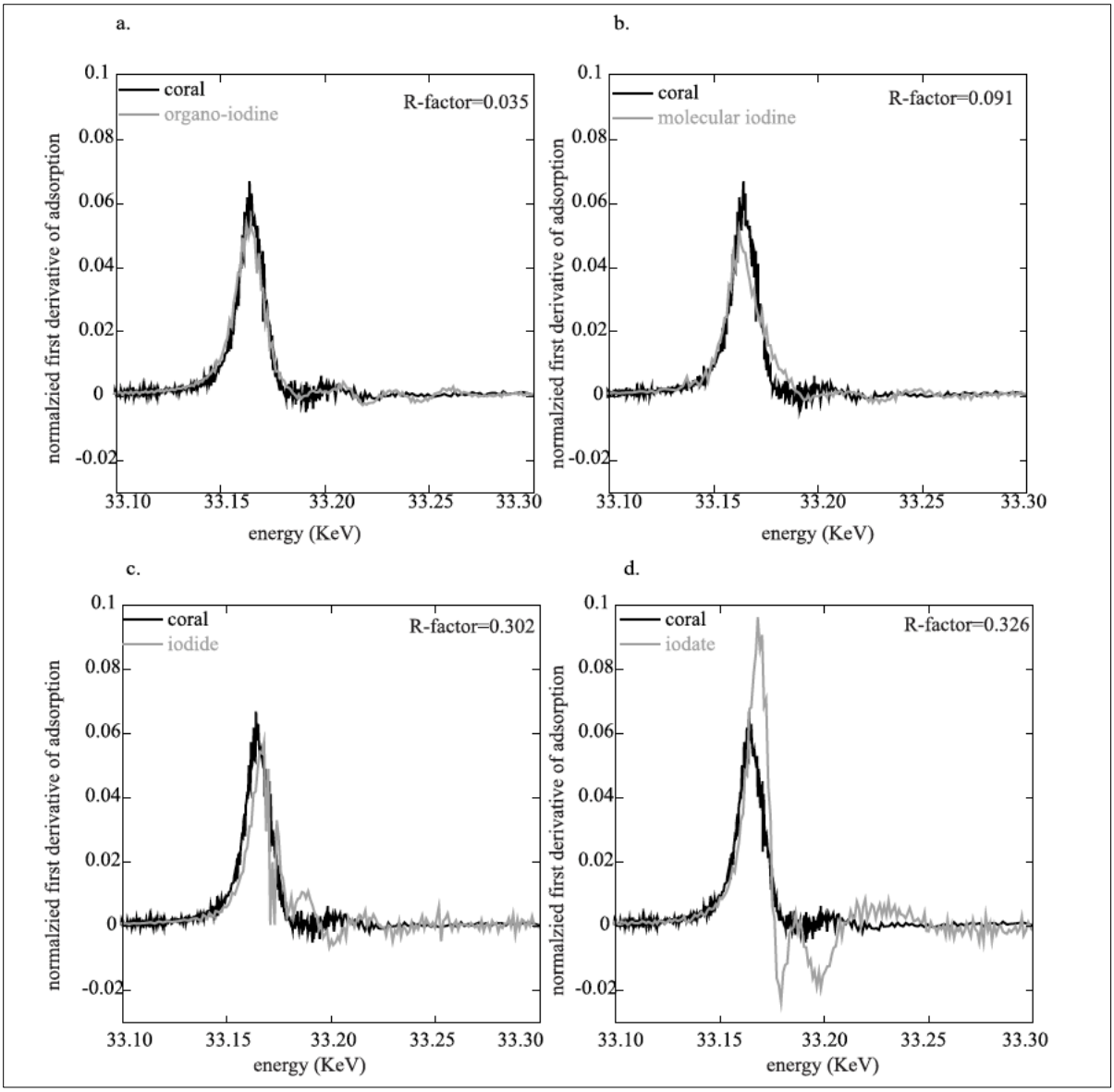

Figure 4.4. XANES spectra 1st derivative.

Comparison of the first derivative of the coral (black) and reference XANES spectra (grey) as shown in Figure 4.3 for a) organo-iodine, b) molecular iodine, c) iodide, and d) iodate. Results from the best fit for linear combination fitting are expressed as R-factors, as a measure of the agreement between the coral spectrum and the respective reference spectra.

Table 4.1 Results from Linear Combination Fitting of the First Derivative of the Coral and Organo-iodine Reference Spectra

Organo-iodine	R-Factor
1,2-diiodoethane	0.035
iodoform	0.039
3,5-diiodotyrosine	0.050
I_2 in tetrahydrofuran/acetonitrile	0.082
3-iodotyrosine	0.148

Note: The R-factor, a measure of the agreement between the coral and respective organo-iodine reference spectra from Feiters et al. (2005) is calculated as the mean square sum of the difference between the coral and reference spectra.

Eight individual growth layers were measured for iodine isotope analysis from the Gulf black coral samples, representing a radiocarbon age range of over 2,000 years BP to modern (Table 4.2). There was no statistical difference (Student t-Test; $p<0.05$) in the iodine isotope results between the two pretreatment methods described above. The $^{129}I/^{127}I$ ratios ranged from $0.30 \pm 0.3 \times 10^{-12}$ to $21.7 \pm 1.6 \times 10^{-12}$ (Table 4.2). Variability in the pre-bomb $^{129}/^{127}I$ ratios was 1.6, whereas the post-bomb variability was 4.1. The $^{129}I/^{127}I$ ratios were tightly coupled to the radiocarbon results (Figure 4.5a), with $^{129}I/^{127}I$ ratios increasing exponentially with $\Delta^{14}C$ values and inversely with radiocarbon age (Figure 4.5b). The oldest coral skeleton samples yielded $^{129}I/^{127}I$ ratios less than 0.5×10^{-12} whereas skeletal material from recent coral growth (i.e., Fm>1) resulted in $^{129}I/^{127}I$ ratios greater than 15×10^{-12} (Figure 4.5). In-between these end-member values was a pre-bomb sample with a $\Delta^{14}C$ value of -72.59 ‰ (Fm=0.93) and $^{129}I/^{127}I$ ratio of $7.8 \pm 0.4 \times 10^{-12}$ to $9.56 \pm 0.55 \times 10^{-12}$, reflecting an offset in the timing of the rise in $^{129}I/^{127}I$ ratios relative to $\Delta^{14}C$ values.

Table 4.2 Individual Results from Iodine Isotope ($^{129}I/^{127}I$; blank corrected) Analysis from Gulf Deep-sea Black Corals and Respective Radiocarbon Data, Including Fraction Modern (Fm), Radiocarbon ($\Delta^{14}C$; ‰), and Radiocarbon Age (years BP)

Sample ID	$^{129}I/^{127}I$ ($x10^{-12}$)[a]	$^{129}I/^{127}I$ ($x10^{-12}$)[b]	Fm	$\Delta^{14}C$ (‰)	^{14}C Age years BP
GOM-JSL09-3728-BC1-1.6	15.7 ± 0.4	21.7 ± 1.6	1.104	95.62	modern
GOM-TOW-BC2-1.1	18 ± 5	16.9 ± 1.4	1.055	47.26	modern
GOM-JSL05-4876-BC1-D3-1.3	19.3 ± 0.4	17.6 ± 0.6	1.082	75.04	modern
GOM-TOW-BC1-1	9.56 ± 0.55	7.8 ± 0.4	0.934	-72.59	550
GOM-TOW-BC1-184	0.33 ± 0.11	1.9 ± 0.9	0.903	-103.1	820
GOM-JSL05-4876-BC1-D3-7.17	0.37 ± 0.33	1.9 ± 0.8	n/a	n/a	1420[c]
GOM-JSL09-3728-BC1-3.2	0.37 ± 0.15	0.7 ± 0.4	0.822	-183.89	1570
GOM-JSL09-3728-BC1-7.1	0.46 ± 0.16	0.3 ± 0.3	0.772	-233.18	2070

Notes: [a] Samples freeze-dried and crushed [b] Samples soaked in NaOH. [c] Age determined based on established growth rates from Prouty et al. (2011).

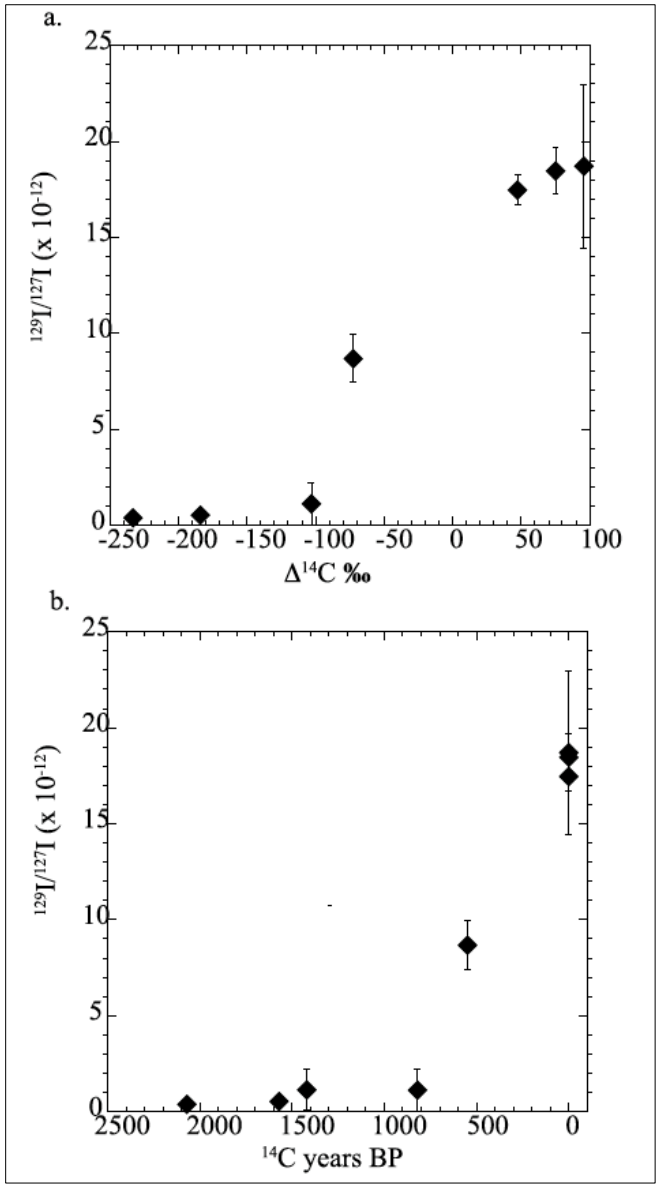

Figure 4.5. Radiocarbon and iodine isotopes.

a) Deep-sea coral radiocarbon isotope ($\Delta^{14}C$; per mil ‰) versus average iodine isotope ($^{129}I/^{127}I$) ratios, yielding a correlation coefficient (R^2) of 0.87. b) Time-series of deep-sea coral iodine isotope ($^{129}I/^{127}I$) ratios representing a radiocarbon age range of over 2,000 years BP to modern. The oldest coral skeleton samples yielded $^{129}I/^{127}I$ ratios less than 0.5×10^{-12} with $^{129}I/^{127}I$ ratios enriched in the modern samples. Error bars for $^{129}I/^{127}I$ ratios represent standard deviation (1σ) based on average of pair-wise measurements from two pretreatment methods.

4.3.2 Chronology: Elemental Band Counts (BSE/Iodine) and Visual Ring Counts

Visual ring counts were determined using the 900x magnification across radial transects of each black coral specimen from the VK region (GOM-JSL04-4734-BC1), and the head of De Soto Canyon (GOM-TOW-BC1) based on criteria described above. The lifespan for GOM-JSL04-4734-BC1 and GOM-TOW-BC1 was calculated at 785 ± 80 and 490 ± 50 years using 17 and 12 SEM images, respectively. The age estimates derived from counting individual iodine peaks yield the following lifespans: 695 ± 70 to 665 ± 65 years for the GOM-JSL04-4734-BC1 specimen, and 715 ± 70 to 630 ± 65 years for the GOM-TOW-BC1 specimen, with iodine peaks separated by 2 and 4 μm, respectively. The radiocarbon-derived ages reported in Prouty et al. (2011) were compared to the lifespans derived from the iodine peak and SEM-derived band counting (Table 4.3). The respective age errors for the different dating methods; the minimum difference between the radiocarbon-derived age and those reported here were 20 years and a maximum difference of 205 years for GOM-JSL04-4734-BC1. For GOM-TOW-BC1, the minimum difference was 10 years and a maximum difference of 195 years.

Table 4.3 Comparison of Lifespans (years)

Sample ID	Radiocarbon[1]	Iodine Peak Count		Visual
		4 μm	2 μm	Band Counts
GOM-JSL04-4734-BC1	620 ±40	665 ±65	695 ±70	785 ±80
GOM-TOW-BC1	670 ±35	630 ±65	715 ±70	490 ±50

Ages were derived from radiocarbon analysis, counting of iodine peaks separated by 2 and 4 μm, respectively, and SEM-derived visual band counts for the deep-sea coral specimens GOM-JSL04-4734-BC1 and GOM-TOW-BC1. [1] Radiocarbon ages reported in Prouty et al. (2011).

4.4 Discussion

4.4.1 Uptake of Organo-Iodine

In seawater, dissolved inorganic iodine is known to be present as iodide and iodate. However, little is known about the chemical state of bioaccumulated iodine. Speciation of iodine both in the environment and in the black coral skeletons is a critical element for understanding the uptake and pathway of iodine to the deep-sea food web. Previous work has established that deep-sea proteinaceous corals feed on recently exported particulate OM from the surface (Roark et al. 2009), as validated by preservation of the bomb-derived $\Delta^{14}C$ peak (Prouty et al. 2011; Roark et al. 2006; Sherwood et al. 2008). As a potential contributor to exported OM and food to the benthic community (Schoener and Rowe 1970), as well as a bio-accumulator of iodine (Küpper et al. 1998), uptake of algae may therefore be an important link in the transfer of iodine to the deep sea. Küpper et al. (2008) investigated the chemical identity of iodine in kelp using bulk X-ray absorption spectroscopy. They found K-edge XAS of freshly frozen *Laminaria digitata* (brown algae) in the reduced form, iodide. Iodide is also the preferred chemical species for uptake of several marine phytoplankton species, particularly under nitrate-replete conditions (de la Cuesta and Manley 2009). In contrast to these studies, results from the XANES on black coral samples from this study illustrate the dominance of organo-iodine.

Because of the strong biophilic nature of iodine, it is likely that some fraction will be bound to organic matter (Elderfield and Truesdale 1980), particularly proteins (e.g., Hou et al. 2000; Hu et al. 2005). This is not surprising given that the coupling of iodine and organic carbon cycles predict iodine will track the cycle of organic matter in surface environments (Santschi and Schwehr 2004), particularly in the soil-water system (Shimamoto et al. 2011). Warwick et al. (1993) suggest that the strong, covalent carbon-iodine bonds efficiently bind iodine onto natural organic matter, specifically humic material (Fuge 1996). This is consistent with micro-XRF analyses indicating higher iodine concentrations in areas rich in organic matter (Shimamoto et al. 2011). For example, peatlands and salt marsh vegetation sequester large amounts of iodine (Fuge and Johnson 1986; Keppler et al. 2003). The binding of iodine to organic matter therefore plays an important role in the transport and transfer of iodine in the environment.

As a result of those characteristics described above, variations in iodine concentration and iodine isotope variability have been used as indicators of Mississippi River hydrology (Oktay et al. 2001; Oktay et al. 2000; Santschi et al. 2007), and as a tracer for terrestrial organic carbon (Santschi and Schwehr 2004; Schwehr et al. 2005). For example, Santschi and Schwehr (2004) found that the majority of iodine is associated with high molecular weight (HMW) organic matter. According to sediment trap studies in the VK region, HMW organic matter (i.e., $>C_{21}$ n-alkanes) of terrestrial origin can contribute up to 52% of the organic matter to the VK region within a year (Prouty et al., 2016). Therefore, the most likely source and transport pathway of iodine to the deep-sea coral environment is associated with terrestrial organic carbon trapped in soils. This input of iodine serves to strengthen the “gluing zone” of the individual organic-rich growth layers in the deep-sea corals.

The delivery of carbon and sediment into the northern Gulf is intimately linked to the outflow from the Mississippi River (e.g., Bianchi et al. 2004; 2007) and transport offshore by the Loop Current System

(Schiller and Kourafalou 2014). The MARB drains approximately 41% of the contiguous United States, equivalent to more than 3,000,000 km^2 and transports approximately 210 million tons of sediment to the Gulf annually (Milliman and Meade 1983), with estimates of total organic carbon from 1,052 to 1,795 kg km^{-2} yr^{-1} (Turner et al. 2007). The weathering of organic-rich sediment could release 7.4×10^{12} g C yr^{-1} (Prouty et al. 2014a), consistent with a previous estimate of CO_2 flux from the Mississippi River tributaries of 7.8×10^{12} g C yr^{-1} (Dubois et al. 2010). Though long term trends are observed for MAR Basin sediment and nutrient export (Cai and Lohrenz 2010), the dominant temporal signature is seasonal, exhibiting a pattern of high flow during winter and spring, decreasing flow in mid-year and lowest flow in the summer and fall (Lohrenz et al. 1994). This temporal signature is also consistent with observations that iodine in suspended and sinking sediment is responding to higher river flow rates (Oktay et al. 2001). The high-resolution variability observed in the black coral iodine records are potentially recording seasonal inputs triggered by changes in hydrodynamic processes. Previous sediment trap studies at VK highlight the dominance of the MAR basin as the source of sediment and nutrient transport to the sea floor of this region (Davies et al. 2010; Mienis et al. 2012; Prouty et al. 2016). The sensitivity of deep-sea corals in the northern Gulf to changes at the land-sea interface has previously been demonstrated in deep-sea coral geochemical records (e.g., Williams et al. 2007). For example, coupled analysis of trace metals, bulk and compound specific nitrogen isotope variability in corals from the Gulf capture the onset of agro-industrialization and an increase in the intensity of land use change (e.g., tile drainage, fertilizer use, tillage, and irrigation) in the Mississippi River watershed over the last 200 years (Prouty et al. 2014a). Similarly, the most recent period of skeletal growth, representing the last 200 to 250 years, is characterized by elevated iodine levels (Figure 4.6). The coral skeleton iodine is presumably bound to terrestrial organic matter; this increase most likely reflects enhanced fluxes of nutrients linked to watershed land-use changes (McIsaac et al. 2001; Raymond et al. 2008). As a result, uptake of organo-iodine in deep-sea corals is potentially a sensitive recorder of continental material flux over decadal to millennial time-scales.

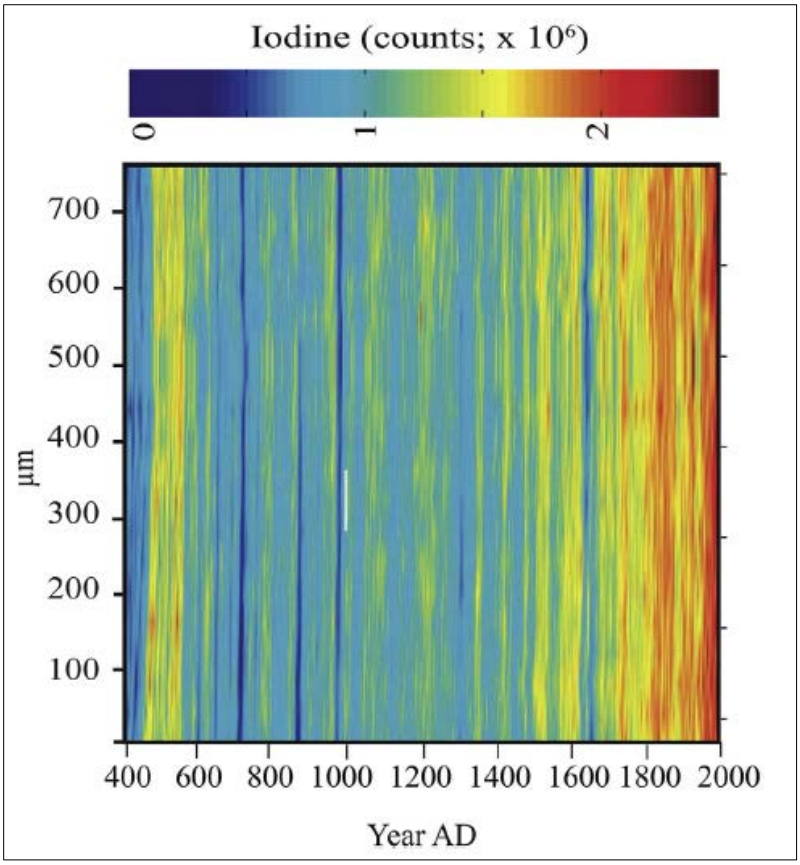

Figure 4.6. Iodine variability.

Iodine variability (counts per second; CPS) over the lifespan of the coral (GOM-TOW-BC2) as determined by Laser Ablation Inductively Coupled Mass Spectrometry. Black coral discs were ablated across the radial transect using a 35-µm spot size to scan 20 lines spaced 40 µm apart across the entire diameter (outer edge to center to outer edge) as described in Prouty et al. (2014a).

Freshwater input (i.e., continental runoff) into the Gulf is also a significant source of dissolved ^{129}I. For example, Schink et al. (1995) concluded that freshwater drainage into the Gulf accounts for ~4% of the total inventory of new ^{129}I (equivalent to ~12% in the upper 100 m), with a penetration depth of 470 m. Therefore, since the corals were collected at a depth of ~300 m, reduced coral $^{129}I/^{127}I$ ratios reflect a period of coral growth when surface water $^{129}I/^{127}I$ ratios mimic naturally occurring iodine ratios. For example, $^{129}I/^{127}I$ ratios were less than 0.5×10^{-12} in the oldest coral skeleton growth layers, similar to $^{129}I/^{127}I$ ratios measured in shallow coral (Porites sp.) samples dated before nuclear bomb-testing from the Pacific Ocean, South China Sea, and Papua New Guinea (Biddulph et al. 2006; Chang et al. 2016). The small range of $^{129}I/^{127}I$ variability observed in the older samples, and the consistent $^{129}I/^{127}I$ ratio over a time-span of ~1,200 years, supports earlier work suggesting that the long half-life of ^{129}I promotes homogeneity with respect to ocean mixing time (Fabryka-Martin et al. 1985). Analysis of the $^{129}I/^{127}I$ ratio from these older skeletal growth bands represents ^{129}I from natural sources, including atmospheric

spallation reactions involving cosmic rays and decay of ^{129}Xe, and spontaneous fission of natural uranium (see review by Hou et al. 2009).

In contrast, $^{129}I/^{127}I$ ratios from the youngest growth bands yielded samples enriched with "new" ^{129}I produced from a combination of weapons production, nuclear reactor production, and bomb testing (see review by Hou et al. 2009). It is estimated that approximately 90 kg of ^{129}I were released to the environment by atmospheric nuclear weapons tests in the 1950s and 1960s, increasing the $^{129}I/^{127}I$ ratio to $\sim 10^{-10}$ (Snyder et al. 2010). More recently, ^{129}I enrichment in the Northern Hemisphere is likely due to steadily increasing emissions by nuclear fuel reprocessing plants in Western Europe (Handl 1996; Moran et al. 1999; Raisbeck et al. 1995). The same deep-sea coral skeleton samples yielding enriched $^{129}I/^{127}I$ ratios were also characterized by post-bomb $\Delta^{14}C$ values ranging from 47 to 96‰. Deep-sea coral $\Delta^{14}C$ and $^{129}I/^{127}I$ values peak at 96‰ and $21.7 \pm 1.6 \times 10^{-12}$ respectively. The peak $^{129}I/^{127}I$ ratio is of similar magnitude ($\sim 20 \times 10^{-12}$) to the Solomon Islands shallow coral $^{129}I/^{127}I$ record, corresponding to the 1990s (Biddulph et al. 2006) and those from the South China Sea (Chang et al. 2016). Lower $^{129}I/^{127}I$ ratios in the deep-sea corals relative to potential parent material (e.g., soils) may be partly explained by geochemical iodine isotope fractionation related to mobility differences between the isotopes. Oktay et al. (2000) suggest fractionation occurs during organic carbon leaching from erodible soils in the Mississippi River Watershed. Therefore, the deep-sea black corals are recording surface waters recently enriched in ^{129}I relative to pre-nuclear values, in much the same manner marine archives capture enriched $\Delta^{14}C$ values in surface waters of the Gulf (Baker and Wilson 2001; Prouty et al. 2011; Wagner 2009). The chronologies based on the marine $\Delta^{14}C$ peak, referred to as bomb radiocarbon dating, has been widely used to date deep-sea corals (Roark et al. 2005; Sherwood et al. 2005), as well as validation of fish ages (Andrews et al. 2012). To date, this has not yet been applied to ^{129}I in deep-sea corals as an environmental tracer. Results from this study suggest that both high-frequency iodine variability associated with terrestrially-derived organic matter, and input of ^{129}I from nuclear testing, may provide an independent approach to age dating deep-sea corals. In particular, given the orders of magnitude of ^{129}I enrichment from anthropogenic activities, the $^{129}I/^{127}I$ ratio in deep-sea corals holds promise as an emerging geochronometer that in some cases is more robust than ^{14}C over the last 50 years.

4.4.2 Validation of Growth Bands

The iodine peaks along with the BSE measurements correlate very well with the growth bands seen in the SEM images (Figure 4.7). The visual ring counts seem to overestimate (GOM-JSL04-4734-BC1) or underestimate (GOM-TOW-BC1) the life spans for the Gulf specimens, whereas the life spans derived from the iodine data corresponded well with the radiocarbon results using both 2-µm and 4-µm thresholds (Table 4.3). The-2 µm threshold, however, had the best match in life spans with the visual growth band counts and ^{14}C ages. This suggests that iodine can be used as a dating method to determine the ages of deep-sea black coral (*Leiopathes* sp.) from the Gulf. Evidence for annual growth rings in deep-sea corals was initially suggested by Grigg (1974) and later by Sherwood et al. (2005) in *Muricea californica* and *M. fruticosa*, and *Primnoa resedaeformi.* Prouty et al. (2011) suggest annual ring formation based on agreement between visual growth ring counts and radiocarbon-derived ages, and Risk et al. (2009) found correspondence between visual ring-counts rings and calculated ages using bomb-radiocarbon age estimates. However, validation of the mechanism and causes of sclerochronological features remains

unresolved. This present study expands these observations by developing and demonstrating an independent age model based on iodine counts incorporated into the coral skeleton geochemistry, as well as proposing a mechanism to explain the formation of annual growth bands in response to seasonal riverine discharge. Developing chronologies independent of ^{14}C dating is an essential component in constraining reservoir ages and in using radiocarbon as a tracer of ocean circulation. These age estimates can be paired with ^{14}C measurements to better constrain reservoir ages and yield important information on ocean circulation and carbon exchange, as previously demonstrated with paired deep-sea coral ^{14}C and uranium-thorium (U-Th) measurements (Adkins et al. 2004; Robinson et al. 2005). For example, using coupled ^{14}C and U-Th measurements from black corals collected in the Tasman Sea, Komugabe et al. (2014) found significant changes in regional circulation of the southwest Pacific, possibly linked to changes in ventilation of surface waters. Therefore, the development of iodine-based chronology represents an important contribution to palaeoceanography by constraining reservoir ages.

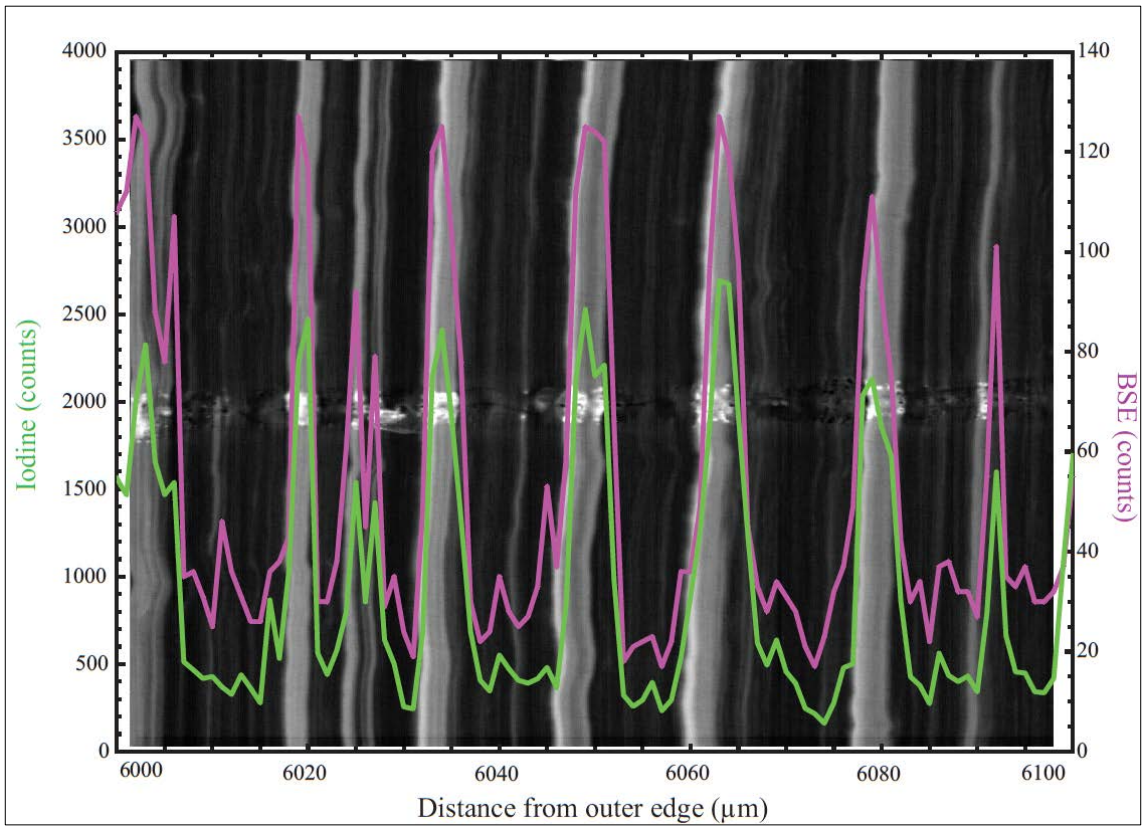

Figure 4.7. Iodine and backscatter electron data.

Iodine (green) and backscatter electron (BSE; purple) peaks derived from x-ray elemental analyses via electron microprobe overlain on SEM image (900x magnification) from specimen GOM-JSL04-4734-BC1 illustrating coherence between inferred visual growth bands and iodine counts.

4.5 Conclusion

Results presented here on deep-sea black coral iodine speciation and iodine isotope variability provide key information on iodine behavior in natural and anthropogenic environments and its geochemical transport pathways. The dominance of organo-iodine in the black coral skeleton suggests that binding of iodine to organic matter plays an important role in the transfer of iodine to deep-sea corals. The most plausible transport pathway is riverine delivery of terrestrial-derived organo-iodine, given iodine's biophilic nature and affinity to bind with humic substances. Therefore, in conjunction with leaching of iodine from soils and seasonal Mississippi River discharge, seasonal inputs of organo-iodine are available for coral uptake where it can accumulate in the narrow gluing zones between the skeletal growth rings of black corals. Whereas previous studies have suggested the presence of annual growth rings, this present study provides a mechanism to explain the formation of annual growth, leading to greater fidelity in the application of an independent age model. The development of an independent age model based on deep-sea coral skeleton iodine variability provides an opportunity to better constrain reservoir ages and yields important information on ocean circulation and carbon exchange. In addition, the sensitivity of the deep-sea corals to changes in $^{129}I/^{127}I$ ratios also holds promise as a tracer for water mass circulation and continental material flux. Taken together, the results presented here have wide application to the use of iodine and its isotopes as biogeotracers with relevance to environmental science and geochronological studies.

4.6 Acknowledgements

Funding was provided to N.G.P. from the US Geological Service Environments Program through the Outer Continental Shelf Study and Coastal and Marine Geology Program, and to E.B.R from the Norman Hackerman Advanced Research Program. Comments from P. Swarzenski (IEAE) greatly improved the text. We thank S.W. Ross (UNC-Wilmington) and K. Sulak (USGS) for providing access to and donating samples, and B. Kocar and R. Davis (SSRL) and J. Addison and A. Foster (USGS) for assistance with XANES data analysis, and M.C. Feiters (Radboud University) for sharing XANES spectra, and D. Biddulph and A. Jull (University of Arizona) for assistance with iodine isotope analysis, and A. Koenig (USGS) with LA-ICP-MS analysis. Any use of trade, product, or firm names is for descriptive purposes only and does not imply endorsement by the US. Government.

5 Impact of the *Deepwater Horizon* Oil Spill on Food Supply to Deep-sea Benthos Communities

5.1 Introduction

[3]Between 20 April and 15 July 2010, the *Deepwater Horizon* blowout event in the northern Gulf released an estimated 4.1–4.6 million barrels (~650,000 m^3) of oil (Kessler et al. 2011; Griffiths 2012; McNutt et al. 2012b) and up to 500,000 t of hydrocarbon gas (Joye et al. 2011). A 100-m thick deep-water plume of neutrally-buoyant water enriched with petroleum hydrocarbons from the *Deepwater Horizon* was also documented at 1,000 m depth in June 2010 (Camilli et al. 2010; Reddy et al. 2012). A majority of the oil and gas remained below the sea surface (Camilli et al. 2010; Reddy et al. 2012). But oil was detected at the surface, with the spatial extent of the spill controlled by circulation and wind-induced drift (Figure 5.1; Le Hénaff et al. 2012). Large marine snow formation may have potentially accelerated the rapid downward transport of oil-contaminated surface water to the pelagic ecosystems (e.g., Passow et al. 2012). *Deepwater Horizon* impact assessments of deep-sea benthic ecosystems observed localized responses (White et al. 2012; Hsing et al. 2013; Fisher et al. 2014a), including signs of coral stress (e.g., varying degrees of tissue loss, sclerite enlargement, excess mucous production), and reductions in benthic faunal abundance and diversity (Montagna et al. 2013; Fisher et al. 2014b). For example, at 11 km to the SW of the *Deepwater Horizon* spill, 86% of the coral colonies imaged in the area exhibited signs of impact (White et al. 2012). Other studies have documented the footprint of the *Deepwater Horizon* spill on deep-sea benthic communities (Montagna et al. 2013; Fisher et al. 2014b), trophic transfer of petro-carbon into the planktonic food web (Graham et al. 2010; Chanton et al. 2012; Cherrier et al. 2013; Prouty et al. 2014b) and intermediate trophic levels (Quintana-Rizzo et al. 2015), as well as potential recovery of deep-sea corals (Hsing et al. 2013). However, questions remain about how the 2010 *Deepwater Horizon* event impacted biomass production, specifically phytoplankton abundance and community structure (Abbriano et al. 2011). Based on positive chlorophyll anomalies detected in the northern Gulf in August 2010, Hu et al. (2011) suggested that the northern Gulf might have experienced a phytoplankton bloom after the *Deepwater Horizon* spill, although planktonic cycles are variable. This is consistent with observations of phytoplankton blooms after the IXTOC-1 oil spill in the southern Gulf in 1979 (Jernelov and Linden 1981), when phytoplankton thrived possibly due to a reduction in predation (e.g., Vargo et al. 1982; Sheng et al. 2011). Yet other studies have shown oil spills to hinder air-sea exchange and light penetration resulting in a decrease in photosynthesis (Nuzzi 1973; Dunstan et al. 1975; Miller et al. 1978).

[3] A version of this paper was published as Prouty NG, Swarzenski-Campbell P, Mienis F, Duineveld G, Demopoulos, A, et al.. 2016. Impact of *Deepwater Horizon* spill on food supply to deep-sea benthos communities. Estuar Coast Shelf Sci. 169:248–264. DOI:10.1016/j.ecss.2015.11.008.

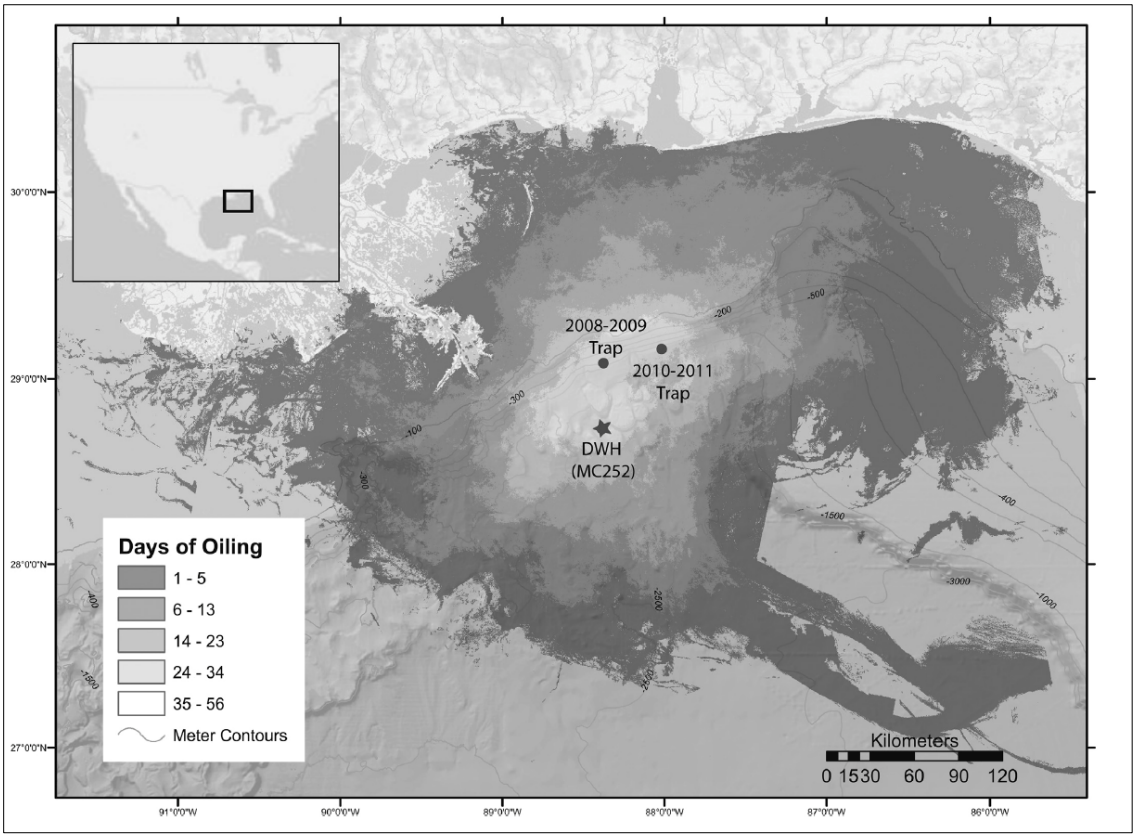

Figure 5.1. Map of Gulf sediment trap deployment locations.

Sediment trap deployments occurred in 2008–2009 and 2010–2011 at 476 m and 416 m, respectively. The *Deepwater Horizon* spill location at MC252 and the 100 m contour intervals are shown. Locations are superimposed on the number of days of oiling accessed from NOAA's Environmental Response Management Application (ERMA) for the *Deepwater Horizon* spill.

Most deep-sea corals are suspension feeders, feeding primarily on surface-derived organic carbon that is transported to depth (Druffel et al. 1995; Roark et al. 2009; Prouty et al. 2011). Deep-sea corals may be sensitive to changes in nutrient transport from surface waters to the seafloor and have the potential to record OM source through incorporation into skeletal structures (Williams et al. 2007; Williams and Grottoli 2010; Sherwood et al. 2011; Prouty et al. 2014a, 2014b). Differentiating the various sources of OM to the Gulf benthos is particularly complex given that relative inputs of terrestrial and marine OM can vary both spatially and temporally (e.g., Hedges and Parker 1976; Trefry et al. 1994; Bianchi et al. 1997; Goñi et al. 1998; Bianchi et al. 2002; Mead and Goñi 1996; Wysocki et al. 2006; Waterson and Canuel 2008; Sampere et al. 2011). This complexity is largely related to freshwater and sediment input from the Mississippi and Atchafalaya rivers (MAR) basin combined with seasonally high rates of primary productivity *(*>100 g C m^{-2} $year^{-1}$*)*. Because river discharge is tightly coupled to nutrient delivery into

surface waters of the Gulf (Figure 5.2b), periods of high riverine input deliver terrestrially-derived organic matter (OM) into the Gulf, stimulating primary productivity. Previous studies in the Viosca Knoll region of the northern Gulf highlight the MAR basin as the major source of sediment and nutrients transported to the seafloor (Davies et al. 2010; Mienis et al. 2012). The large quantities of nutrients and terrestrial OM stimulate surface primary productivity, producing OM that flocculates and sinks to the seafloor. For example, Mienis et al. (2012) found peaks in near-bed fluorescence corresponding to increases in pigments, C_{org}, total nitrogen (N_{tot}), and biogenic silica (SiO_2) in sediment trap samples, and Davies et al. (2010) described a 24 h diel vertical migration of zooplankton in the water column that may also form part of the coral diet. These data provide evidence that energy flux to the deep-sea in this region is tightly coupled to surface primary production. Percent organic carbon ($\%C_{org}$) has traditionally been used to evaluate marine biomass production, serving as an index of ocean productivity. However, in the Gulf the input of terrestrially-derived OM can potentially alter estimates of primary productivity and the autochthonous carbon flux if based on $\%C_{org}$ alone (Müller and Suess 1979; Stallard 1998). To investigate the impact of the *Deepwater Horizon* spill on quality and quantity of biomass particles and sediment reaching the deep-sea, a suite of geochemical tracers (e.g., stable and radio-isotopes, lipid biomarkers, and compound specific isotopes) was measured from monthly sediment traps deployed prior to and after the spill. Long-term measurements of seasonal deposition patterns, composition, and mass fluxes were also acquired through the deployment of benthic landers. By integrating biomarker data with other chemical and biological data, results presented here provide a unique perspective on the sub-acute impacts of the *Deepwater Horizon* spill to the Gulf deep-sea ecosystem.

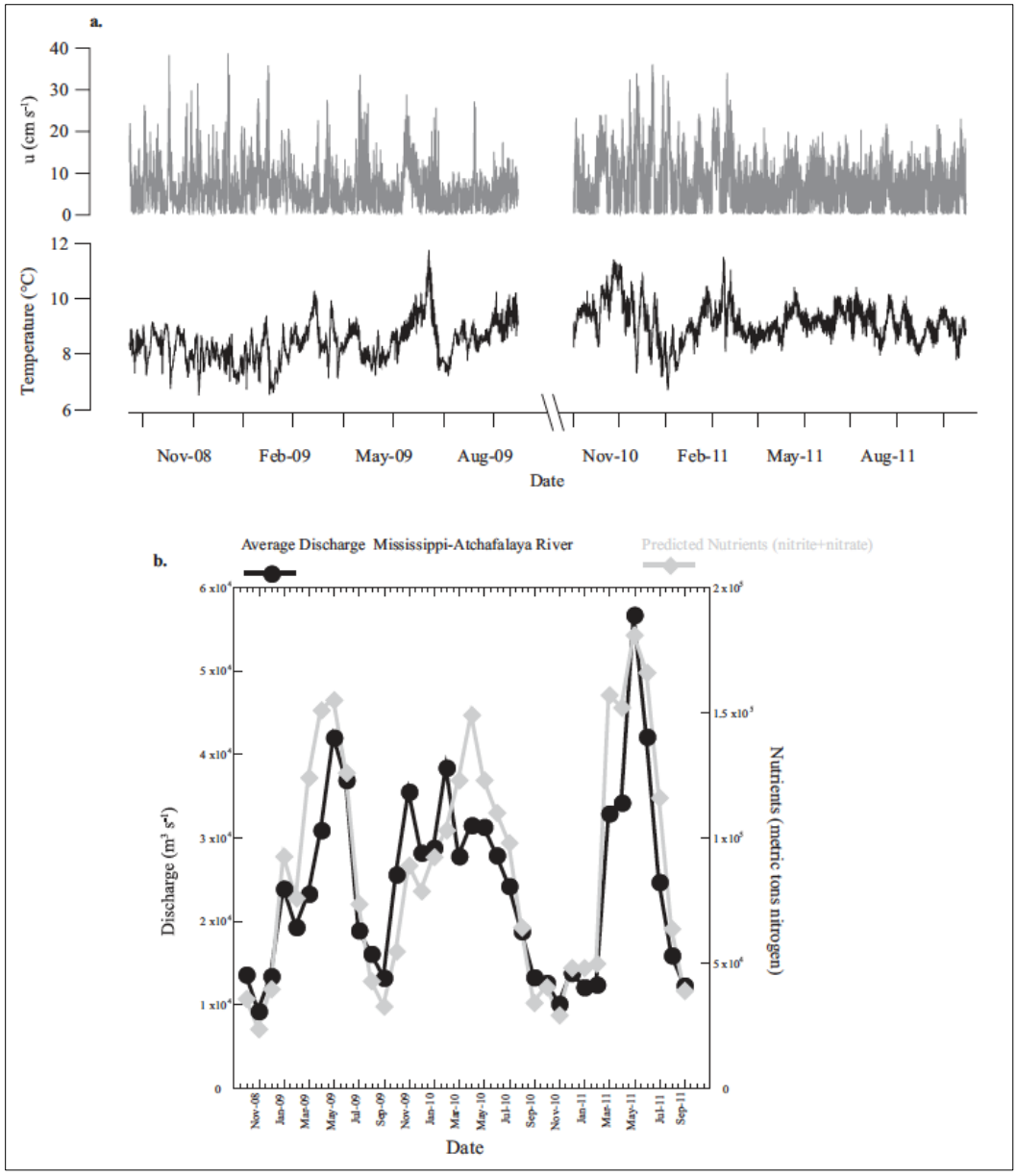

Figure 5.2. Lander time-series.

Time-series of lander current speed (*u* ; cm s^{-1} in the east-west direction) and temperature (°C) during the 2008–2009 and 2010–2011 deployments in the VK region. b. Monthly time-series of average discharge (m^3 s^{-1}) for the MAR and predicted nutrients (nitrite + nitrate, metric tons of nitrogen) from October 2008 through September 2011 (Aulenbach et al. 2007).

5.2 Methods

5.2.1 Study Site

In the Viosca Knoll region of the northern Gulf there is extensive development of the deep-sea coral *Lophelia pertusa* (Brooke and Schroeder 2007; Sulak et al. 2008; Lunden et al. 2013). The *L. pertusa* coral thickets mainly grow on top of authigenic carbonate deposits precipitated from microbial activity associated with hydrocarbon seepage (Schroeder 2002; Formolo et al. 2004; Roberts et al. 2009). The complex habitats created by *L. pertusa* are characterized by a high biodiversity of associated species. *L. pertusa* reefs provide habitat and other ecosystem services for a variety of invertebrates and fishes (Jensen and Frederiksen 1992; Reed et al. 2006; Dorschel et al. 2007; Henry and Roberts 2007; Sulak et al. 2007; Sulak et al. 2008; Buhl-Mortensen et al. 2010; Demopoulos et al. 2014). Previous studies in the Viosca Knoll region highlight the MAR basin as the major source of sediment and nutrients transported to the seafloor (Davies et al. 2010; Mienis et al. 2012). The large quantities of nutrients and terrestrial OM stimulate surface primary productivity, producing OM that flocculates and sinks to the seafloor. For example, Mienis et al. (2012) found peaks in near-bed fluorescence corresponding to increases in pigments, C_{org}, total nitrogen (N_{tot}), and biogenic silica (SiO_2) in sediment trap samples, and Davies et al. (2010) described a 24 h diel vertical migration of zooplankton in the water column that may also form part of the coral diet. These data provide evidence that energy flux to the deep-sea in this region is tightly coupled to surface primary production.

5.2.2 Benthic Landers

Two landers consisting of aluminum tripod frames were deployed in the Viosca Knoll region (OCS lease blocks VK826 and VK862/906) between 13-Oct-2008 to 01-Sep-2009 (VK826) and 01-Oct-2010 to 28-Sep-2011 (VK862/906) (Table 5.1). The location of the pre-spill lander (BOBO) was 29.336611º N, 88.055556 º W at 476 m water depth(see Davies et al. 2009; Mienis et al. 2012 for details), and the post-spill lander (UNCW) was deployed 35 km to the west-southwest at 29.111389 º N, 88.534167 º W at 416 m water depth. Both landers were positioned < 500 m from small coral mounds. The UNCW and BOBO landers were deployed approximately 35 km N and 54 km NE of the Macondo well, respectively. The post-spill lander was directly beneath the known *Deepwater Horizon* surface oil extent in the northern Gulf (Figure 5.1). Bottom hydrodynamic conditions (i.e., current velocity and acoustic backscatter) were characterized by either an acoustic Doppler current profiler (ADCP) or current meters mounted on the landers, as well as sensors to measure temperature and salinity. In addition, the BOBO lander was equipped with a combined fluorescence and optical backscatter sensor (Mienis et al. 2012). Each lander was equipped with a Technicap PPS 4/3 sediment trap with the aperture at 4 m (BOBO) and 2 m (UNCW) above bottom, rotating at a 27 days interval. Sediment trap samples were preserved in pH buffered $HgCl_2$ solution in seawater collected from the deployment sites following Bonnin et al. (2002) to effectively minimize microbial activity, and kept at 4° C until geochemical analyses. Sediment trap samples were sieved with a 1 mm sieve to isolate zooplankton for identification. At the Netherlands Institute of Sea Research (NIOZ), samples were split with a rotor splitter and rinsed with demineralized water to remove salts and $HgCl_2$. Samples were freeze-dried, total matter was weighed, and mass fluxes were calculated.

Table 5.1 Deployment Details for the Landers

Trap ID	Seafloor (m)	Trap Depth (m)	Lat (N)	Long (W)	Deployment	Recovery
BOBO	480	476	29.336611	88.055556	13-Oct-08	01-Sep-09
UNC-W	420	416	29.111389	88.534167	01-Oct-10	28-Sep-11

Landers were equipped with monthly (27 day period) rotating sediment traps deployed in the VK region from 13-Oct-2008 to 01-Sept-2009 (VK826) and 01-Oct-2010 to 28-Sept-2011 (VK862/906)

5.2.3 Bulk Sediment Composition

Grain size analysis of the dry sieved samples was performed with a particle size analyzer (Coulter LS I3 320). Before grain size analysis, samples were decalcified with 6 M HCl (Mienis et al. 2012). Concentrations of chlorophyll *a* and its derivatives were determined using a reverse-phase high performance liquid chromatograph (HPLC) at NIOZ according to methods described in Witbaard et al. (2000). Carbon and nitrogen isotopes ($\delta^{13}C$ and $\delta^{15}N$), N_{tot} and C_{org}, and C/N ratios of bulk sediment were determined at University of Bremen using a CHN-O-Rapid element analyzer and elemental analyzer-isotope ratio mass spectrometer (EA-IRMS) on 3.5-5 mg and 10 mg of sample, respectively. Sulfur isotopes ($\delta^{34}S$) were determined on 8–10 mg of sediment trap material by an elemental analyzer and analyzed with a continuous flow isotope ratio mass spectrometer at the Stable Isotope Core Laboratory (Washington State University). Radiocarbon ($\Delta^{14}C$) was measured at Lawrence Livermore National Laboratory (LLNL) Center for Accelerator Mass Spectrometry (CAMS) where ~50 mg of acidified sediment was converted to CO_2 and graphitized for accelerator mass spectrometry (AMS) (Vogel et al. 1987). The activity of ^{210}Pb was determined by alpha spectrometry from ^{210}Po using a Canberra alpha detector.

5.2.4 Molecular and Compound Specific Isotope Sediment Composition

Homogenized samples were weighed directly into pre-cleaned Mars X (CEM, Corp.) microwave digestion system vessels in preparation for molecular biomarker analysis. Subsamples (~2 g) of the 2010-2011 samples were used to determine water content and organic content by a UIC Coulometrics CM5012 CO_2 coulometer via combustion at the USGS Laboratories in Santa Cruz, California. Internal and surrogate standards (deuterated PAHs (acenaphthene, phenanthrene, chrysene, and pyrene), 5-α-androstane, and 5-α-androstan-3-β-ol) were added to samplesbefore extraction. Samples were extracted with a hexane:acetone (1:1) solvent mixture followed by a second extraction in dichloromethane:methanol (2:1) solvent mixture. After evaporation of extracts to 5 ml volume utilizing TurboVap Evaporation Concentrator (Zymark, Corp.), samples were loaded onto liquid chromatography columns for compound class separation. Each column was layered with 2.5 g of 5% deactivated alumina, 2.5 g of 62 silica gel and 5.0 g of 923 silica gel. Two separate fractions were collected and analyzed: F1-saturate (100% hexane eluent) and F3- polar (50% ethyl acetate: 50% hexane) and reduced in volume to

1.0 ml. The polar fraction (F3) was further derivatized with BSTFA (N,O-bis(trimethylsilyl) trifluoroacetamide) containing 2% TMCS (trimethylchlorosilane) and acetonitrile. All fractions were analyzed by splitless injection onto an Agilent 6890 gas chromatograph interfaced to an HP 5973 mass spectrometer (GC-MS) at the USGS Organic Geochemistry Laboratories in Santa Cruz, California. The gas chromatograph oven program had an initial temperature of 90 °C which was held for 4.0 min then ramped at 5 °C min^{-1} to a final temperature of 310 °C which was held at this final temperature for 10 min. The capillary column (DB-5MS: 30 m length, 0.25 mm id with a 25 µm phase thickness) was directly interfaced to the ion source of the mass spectrometer. Compound identifications were made by comparison with known standards and/or published reference spectra. Lipid biomarkers (sterol and *n*-alkane) concentrations are reported normalized to organic content of dry sediment (µg g^{-1} C). Select biomarker ratios (Appendix 5.1 and 5.2) were calculated from GC-MS single ion monitoring mode (SIM) chromatograms of m/z (mass of ion divided by charge) 191 (triterpanes/hopanes) and 217 (steranes) using peak height or area (Figure 5.3). Biomarker values were used to correlate the trap samples, along with a sub-sample of Macondo 252 well oil in order to group them according to their probable source locations (Peters et al. 2008).

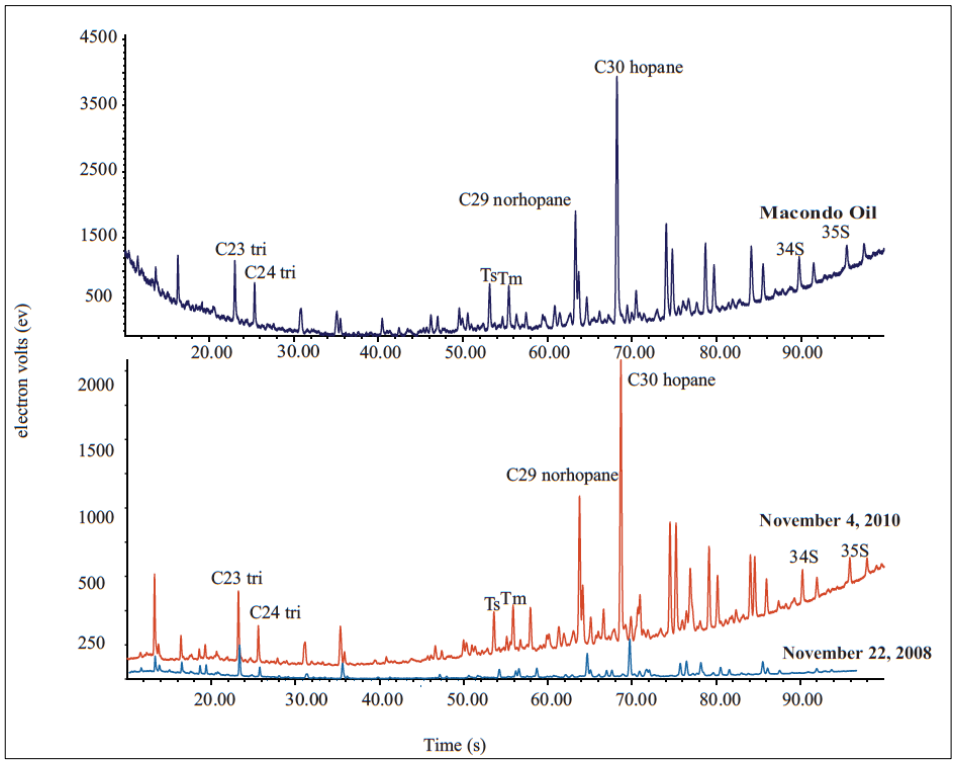

Figure 5.3. Chromatogram.

Selected ion monitoring (SIM) chromatograms of m/z 191 of Macondo 252-1 well oil (upper panel) and sediment trap samples from November 2011 and November 2008 for triterpene/hopane distribution (lower panel). Hopanoid peaks are integrated for parameter ratios used in hierarchical cluster analysis and are identified in Appendix 5.1 and 2.2.

Major OM sources to the sterol and *n*-alkane molecular signatures were investigated by calculating relative proportions of marine, terrestrial higher plants, and anthropogenic/petroleum contributions. Following designations from Pisani et al. (2013), relative contributions from natural (autochthonous versus allochthonous) and anthropogenic OM sources were calculated for both sediment trap deployments. Terrestrial OM composition of sediments were quantified using concentrations of odd numbered *n*-alkanes in the C_{21} to C_{31} range as well as the sterols campesterol, stigmasterol, and β-sitosterol. Marine components were determined using the sterols cholesterol and brassicasterol concentrations, as well as odd and even numbered *n*-alkanes in the C_{15} to C_{19} range. The anthropogenic components were determined using the sterol composition of coprostanol, epicoprostanol, and coprostanone, and the isoprenoid hydrocarbons pristane and phytane. Although high pristane concentrations in sediment can be derived from zooplankton, the pristine/phytane ratios observed in this study are indicative of a petrogenic, anthropogenic source (Blumer et al., 1963).

The following indices were used to further characterize and source the OM. The Carbon Preference Index (CPI) for *n*-alkanes was calculated as:

$$CPI=0.5 * [(nC_{25} + nC_{27} + nC_{29} + nC_{31} + nC_{33}) /(nC_{24} + nC_{26} + nC_{28}+ nC_{30})] + [(nC_{25} + nC_{27} + nC_{29} + nC_{31} + nC_{33})/ (nC_{26} + nC_{28} + nC_{30}+ nC_{32})]$$

The CPI describes the molecular distribution of odd number *n*-alkanes relative to even number *n* – alkanes, and can be used as an indication of source (Bray and Evans 1961). For example, compounds originating from land plant material show a predominance of odd-numbered carbon chains (Hedges and Parker 1976).

The *n*-alkane average chain length (ACL) was calculated according to the following equation:

$$ACL=[25(nC_{25})+27(nC_{27})+29(nC_{29})+31(nC_{31})+33(nC_{33})]/ nC_{25}+nC_{27}+nC_{29}+nC_{31}+nC_{33}$$

The ACL describes the average number of carbon atoms per molecule based on the abundance of odd-carbon-numbered higher plant *n*-alkanes (Poynter and Eglinton 1990), with changes in ACL values linked to differences in vegetation type (i.e., grasslands versus forests).

The Alkane Proxy (P_{aq}) was calculated as:

$$P_{aq}=(nC_{23}+nC_{25})/(nC_{23}+nC_{25}+nC_{29}+nC_{31})$$

As a proxy for aquatic macrophytes compared with terrestrial plant input (Ficken et al. 2000), the P_{aq} expresses the relative proportion of mid-chain length to long-chain length *n*-alkanes.

Compound specific carbon isotopic composition of sterols and *n*-alkanes in the sediment traps was determined by GC-combustion isotope ratio mass spectrometry (GC-C-IRMS) at the Stable Isotope Facility at the University of California, Davis. Extracted lipid biomarkers (sterols and *n*-alkanes) were analyzed using a Thermo GC/C-IRMS system composed of a Trace GC Ultra gas chromatograph coupled

to a Delta V Advantage isotope ratio mass spectrometer through a GC/C-III interface with compound identification support for the compound specific carbon isotope laboratory provided by a Varian CP3800 gas chromatograph coupled to a Saturn 2200 ion trap MS/MS. The CSIA of the sterol fraction was performed under the following GC conditions with a silica capillary column (DB-5; 30 m): the initial oven temperature was 60 °C, ramped at 15 °C to 200 °C, 2nd ramp at 5 °C to a final temperature of 300 °C and held for 25 min. Samples were analyzed at 3 and 4 μL injection volume for sterols and *n*-alkanes, respectively. The sterol $\delta^{13}C$ values were corrected for added derivative carbons using a functional relationship estimation by maximum likelihood equation from Ripley and Thompson (1987).

5.3 Results

5.3.1 Hydrodynamics and Flux

Records of both temperature and current speed were similar between the two lander deployments (Figure 5.2a), despite some distance between the sites and different deployment periods (2008–2009 and 2010–2011). Temperatures varied between 6.5 and 11.7 °C with peak current speeds up to 38 cm s^{-1} (Figure 5.2a). Grain size during both years was dominated by silt fraction (7-30 μm). Mass fluxes were highest in the late fall-early winter of 2010 with the largest peak during December (14.3 g m^{-2} day^{-1}) and tapered off for the rest of the year (monthly average flux of 3.7 ± 1.9 g m^{-2} day^{-1}) (Figure 5.4a). Mass fluxes for 2008–2009 were less variable with a monthly average of 2.8 ± 1.3 g m^{-2} day^{-1} (Table 5.2a). Both years yielded an inverse relation between mass flux and ^{210}Pb, r=-0.62 and -0.81 for 2008–2009 and 2010–2011 respectively (Table 5.3a and 5.3b). Increased pigment flux corresponded to periods of elevated fluorescence during the 2008-2009 deployment (Mienis et al. 2012). Pigment flux from the 2010–2011-deployment year was less variable and did not display the level of enrichment observed in the 2008–2009-deployment year when pigment fluxes exceeded 150 mg m^{-2} day^{-1} (Figure 5.4f, Table 5.2a and 5.2b); fluorescence data were not available for the 2010–2011-deployment year.

Table 5.2a Mass Fluxes and Bulk Geochemical Measurements for the 2008–2009 Sediment Trap Samples

Date	**J mass*** g m^{-2} day^{-1}	J pigments mg m^{-2} day^{-1}	**C_{org}*** %	N_{tot} %	^{210}Pb Bq g^{-1}	**C/N*** molar	**$\delta^{13}C$*** ‰	**$\delta^{15}N$*** ‰	**$CaCO_3$*** %	**$\Delta^{14}C$*** ‰	±	^{14}C age ‰	±	**$\delta^{34}S$*** ‰	±
10/26/08	4.5	12.40	3.44	0.28	1191	10.41	-21.12	4.17	26.63	-99.9	2.8	785	25	6.50	0.79
11/22/08	3.6	31.80	3.61	0.33	1239	9.42	-21.46	4.51	16.39	n/a	n/a	n/a	n/a	6.87	0.02
12/19/08	3.7	30.90	3.24	0.27	1090	10.41	-21.49	3.79	17.90	-12.9	2.9	40	25	6.73	1.04
1/15/09	1.1	2.90	4.53	0.43	1531	9.11	-20.95	4.38	22.21	-56.4	2.7	405	25	9.80	1.42
2/11/09	1.2	2.30	3.93	0.34	1289	9.99	-21.13	3.82	24.39	n/a	n/d	n/a	n/a	9.21	0.72
3/10/09	2.9	9.40	3.89	0.28	1127	11.73	-21.31	2.98	33.51	-137.3	2.5	1125	25	8.44	1.43
4/6/09	3.1	169.00	5.12	0.47	1030	9.37	-20.44	4.26	25.53	-66.4	3.6	490	35	9.02	0.26
5/3/09	1.7	14.00	4.18	0.39	1243	9.09	-20.88	4.05	21.42	n/a	n/a	n/a	n/a	9.34	1.76
5/30/09	3.2	38.60	4.59	0.40	1138	9.92	n/d	n/d	15.67	-71.8	3.8	535	35	9.86	1.07
6/26/09	4.8	42.20	3.80	0.39	1100	8.39	-21.45	7.01	28.28	-90.2	2.6	695	25	5.45	0.88
7/23/09	2.5	148.80	6.71	0.69	967	8.33	-21.46	3.18	20.62	-32.8	3.4	205	30	6.26	0.72
8/19/09	1.1	1.90	6.32	0.60	1408	9.07	-21.35	3.94	16.45	n/a	n/a	n/a	n/a	10.01	2.22
Average	2.8	42.02	4.45	0.41	1196	9.60	-21.19	4.19	22.42	-71.0	3.0	535	28	8.12	1.03
SD	1.3	56.58	1.10	0.13	159	0.96	0.33	1.05	5.49	39.0	0.5	340	5	1.64	0.61

Variables that are statistically different (Student's t-Test; P≤ 0.05) between the 2008–2009 and 2010–2011 deployments are indicated in bold and with an asterisk (*).

Table 5.2b Mass Fluxes and Bulk Geochemical Measurements for the 2010–2011 Sediment Trap Samples

Date	**J mass*** g m^{-2} day^{-1}	J pigments mg m^{-2} day^{-1}	**C_{org}*** %	N_{tot} %	^{210}Pb Bq g^{-1}	**C/N*** molar	**$\delta^{13}C$*** ‰	**$\delta^{15}N$*** ‰	**$CaCO_3$*** %	**$\Delta^{14}C$*** ‰	±	^{14}C age ‰	±	**$\delta^{34}S$*** ‰	±
11/4/10	9.7	15.02	2.22	0.28	979	9.25	-21.56	4.91	34.23	-151.3	2.7	1255	30	0.01	0.36
12/4/10	14.3	20.21	2.13	0.27	937	9.23	-21.57	4.77	36.60	-148.9	2.5	1235	25	3.20	0.46
1/3/11	3.2	10.29	2.36	0.31	1144	8.92	-21.99	4.61	35.09	-127.5	2.5	1035	25	3.84	1.34
2/2/11	7.6	18.51	2.15	0.28	882	8.84	-21.91	4.71	33.33	-145.0	2.7	1195	30	1.58	0.04
3/4/11	4.8	46.72	2.99	0.42	1048	8.28	-21.30	5.38	29.55	-73.5	3.0	550	30	-1.42	0.04
4/3/11	3.2	25.46	3.05	0.40	1130	8.90	-21.75	5.14	28.13	-86.6	2.6	665	25	-3.85	0.03
5/3/11	2.5	7.68	2.82	0.36	1252	9.17	-22.09	4.77	31.25	-106.1	2.6	840	25	-0.97	0.92
6/2/11	2.7	38.71	3.41	0.49	1161	8.12	-22.44	5.63	30.97	-78.2	2.7	590	25	-0.72	0.77
7/2/11	1.5	8.24	3.91	0.56	1345	8.06	-22.69	6.14	29.11	-61.8	3.0	450	30	-0.59	0.50
8/1/11	1.9	14.70	3.41	0.47	1152	8.48	-22.57	6.25	28.21	-76.0	2.7	575	25	-0.31	1.12
8/31/11	4.5	55.31	2.82	0.37	1146	8.91	-22.25	5.95	28.37	-96.7	2.6	755	25	0.57	0.19
9/30/11	4.3	19.24	2.55	0.32	1107	9.35	-22.20	5.47	25.53	-119.0	3.0	955	30	4.27	1.08
Average	5.0	23.34	2.82	0.38	1107	8.79	-22.03	5.31	30.86	-105.9	2.7	842	27	0.47	0.57
SD	3.8	15.51	0.57	0.09	130	0.45	0.43	0.58	3.34	31.9	0.2	288	3	2.38	0.46

Variables that are statistically different (Student's t-Test; P≤ 0.05) between the 2008–2009 and 2010–2011 deployments are indicated in bold and with an asterisk (*).

Table 5.3a Pearson Product-Moment Correlation Coefficients (r; p ≤ 0.05) in the 2008–2009 Monthly Sediment Trap Samples

	$\%C_{org}$	$\%N_{tot}$	^{210}Pb	C/N	$\delta^{13}C$	$\delta^{15}N$	% $CaCO_3$
$\%N_{tot}$	0.97						
^{210}Pb	-0.04	-0.06					
C/N	-0.53	-0.70	-0.05				
$\delta^{13}C$	0.07	0.02	0.10	-0.02			
$\delta^{15}N$	-0.28	-0.12	0.03	-0.49	-0.06		
% $CaCO_3$	-0.28	-0.31	-0.21	0.37	0.23	0.10	
J mass	-0.48	-0.42	-0.62	0.15	-0.26	0.46	0.23
J pigment	-0.29	0.54	-0.70	-0.38	0.31	-0.06	0.01

Table 5.3b Pearson Product-Moment Correlation Coefficients (r; p ≤ 0.05) in the 2010–2011 Monthly Sediment Trap Samples

	$\%C_{org}$	$\%N_{tot}$	^{210}Pb	C/N	$\delta^{13}C$	$\delta^{15}N$	% $CaCO_3$
$\%N_{tot}$	0.99						
^{210}Pb	0.79	0.74					
C/N	-0.80	-0.87	-0.42				
$\delta^{13}C$	-0.65	-0.62	-0.68	0.41			
$\delta^{15}N$	0.80	0.79	0.54	-0.60	-0.67		
% $CaCO_3$	-0.60	-0.53	-0.49	0.24	0.44	-0.71	
J mass	-0.74	-0.70	-0.81	0.52	0.63	-0.52	0.66
J pigment	0.10	0.12	-0.15	-0.26	0.19	0.31	-0.29

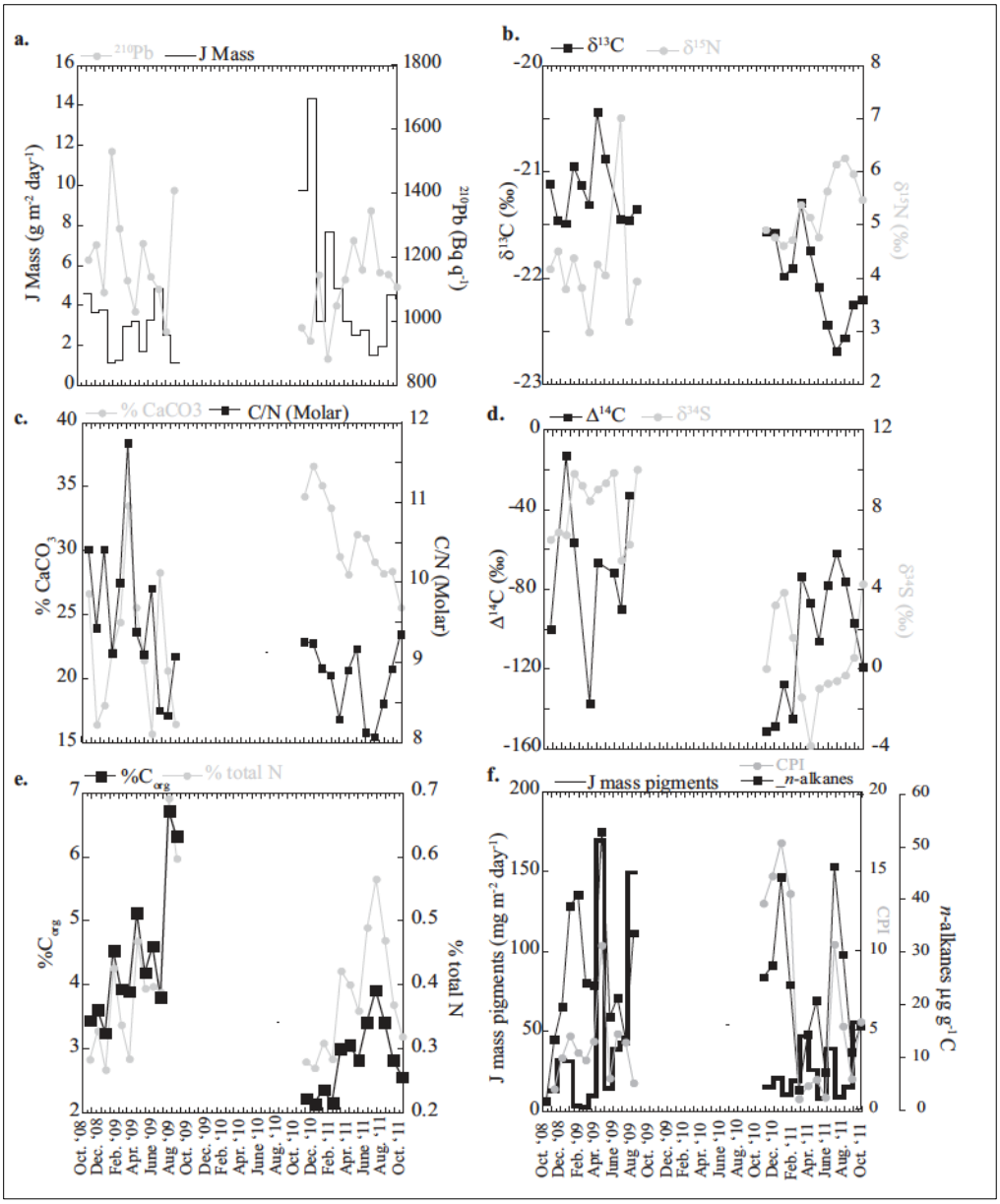

Figure 5.4. Sediment trap time-series.

Time-series for bulk sediment measurements derived from monthly sediment trap samples deployed in the VK region from 2008–2009 and 2010–2011 of a. 210Pb (Bq q^{-1}) and mass flux (g m^{-2} day^{-1}), b. stable ($\delta^{13}C$) carbon and nitrogen ($\delta^{15}N$) isotopes (‰), c. %CaCO3 and C/N (molar) ratios, d. radiocarbon ($\Delta^{14}C$) and stable sulfur ($\delta^{34}S$) isotopes (‰), e. % organic carbon (Corg) and % total nitrogen (Ntot), f. total n-alkane concentration (□g g^{-1} C), Carbon Preference Index (CPI), and pigment mass flux (□g m^{-2} day^{-1}).

5.3.2 Bulk Elemental and Stable Isotopic Composition

Calcium carbonate ($CaCO_3$) dominated the inorganic composition of the sediment trap material with average $\%CaCO_3$ values between 22.42 ± 5.49 % and 30.86 ± 3.34 % in 2008–2009 and 2010–2011, respectively (Table 5.2a,b; Figure 5.4c). Overall $\%CaCO_3$ values were greater in 2010–2011 compared with 2008–2009. Peak $\%CaCO_3$ values were attained in April 2009 and December 2010, with the latter concomitant with an increase in mass flux (Figure 5.4a and Figure 5.4b). By March 2011 $\%CaCO_3$ fell to values close to the maxima measured in 2008–2009.

Peaks in $\%C_{org}$ occurred in July for both deployment years; however, the peak $\%C_{org}$ value in 2008–2009 (6.7%) was two times higher than the peak value observed in 2010–2011 (3.9%) (Figure 5.4e). In 2008–2009, the average $\%C_{org}$ value (4.45 ± 1.10%) was significantly greater (Student t-Test; $P \leq 0.05$) than the average value (2.82 ± 0.57 %) in 2010–2011. Percent C_{org} was tightly coupled to $\%N_{tot}$ (r=0.97 to 0.99, Table 5.3a and 5.3b) with a positive $\%C_{org}$ intercept at zero $\%N_{tot}$ of 1% in 2008–2009 and 0.5% in 2010–2011. The low inorganic nitrogen composition of the sediment trap samples suggests that C/N ratios are primarily recording inputs from organic sources. Though $\%N_{tot}$ also peaked in July for both years, overall $\%N_{tot}$ was statistically similar (Student t-Test; $P > 0.05$), averaging 0.41 ± 0.13 % (2008–2009) and 0.38 ± 0.09 % (2010–2011, Figure 5.4e, Table 5.2a and 5.2b). Both $\%C_{org}$ and N_{tot} were inversely related to mass flux (Table 5.3a and 5.3b). In 2010–2011 both $\%C_{org}$ and $\%N_{tot}$ were correlated to ^{210}Pb (r=0.79 and r=0.74, respectively). The C/N ratios from both years ranged from 8.1 to 11.7, enriched in carbon relative to the canonical Redfield ratio of 6.7 (Redfield et al. 1963). The lowest C/N ratio occurred in July 2011 (Figure 5.4b) while C/N ratios peaked in March 2009. The C/N ratios were statistically different (Student t-Test; $P \leq 0.05$), with C/N ratios lower in 2010–2011 compared to the 2008–2009 deployment; although $\%N_{tot}$ was not different between years, there was significantly (Student's t-Test; $P \leq 0.05$) less C_{org} per mol of N in the post-*Deepwater Horizon* samples.

Stable carbon isotope ($\delta^{13}C$) values closely matched those of marine phytoplankton (-22‰ to -21‰) and were within the reported range for Gulf marine-derived $\delta^{13}C$ organic matter (e.g., Rosenheim et al. 2016). Overall $\delta^{13}C$ values in 2010–2011 were more negative relative to 2008–2009 (Figure 5.4b). July 2011 marked the period of greatest $\delta^{13}C$ reduction while the corresponding $\delta^{15}N$ signal was higher (Figure 5.4b). Average $\delta^{15}N$ values equaled 4.19 ± 1.05 ‰ and 5.31 ± 0.58‰ in 2008–2009 and 2010–2011, respectively. Neither isotope showed a linear relationship to $\%N_{tot}$ or $\%C_{org}$ in 2008-2009; however, $\delta^{13}C$ and $\delta^{15}N$ were correlated to both $\%N_{tot}$ and $\%C_{org}$ in 2010-2011 with $\delta^{13}C$ negatively related and $\delta^{15}N$ positively related to $\%N_{tot}$ and $\%C_{org}$, respectively (Table 5.3a,b).

Average sediment trap radiocarbon ($\Delta^{14}C$) values ranged from -71.0 ± 39.0 ‰ to -105 ± 31.9 ‰ (Figure 5.4d), equivalent to ^{14}C ages of 535 ± 340 and 842 ± 288 years BP in 2008–2009 and 2010–2011, respectively (Table 5.2a,b). Radiocarbon isotope values were depleted in the 2010-2011 samples relative to the 2008–2009 samples (Student's t-Test; $P \leq 0.05$). A statistically significant difference was also observed in the sulfur isotopes ($\delta^{34}S$) (Table 5.2a,b; Student t-Test; $P \leq 0.05$). Average $\delta^{34}S$ values decreased from 8.12 ± 1.64 ‰ in 2008-2009 to 0.47 ± 2.38 ‰ in 2010-2011 (Figure 5.4d).

5.3.3 Molecular Biomarker Composition

The total concentrations of *n*-alkanes for both the 2008–2009 and 2010–2011 sediment trap samples represent a resolved *n*-alkane range from C_{14} to C_{33}, as well as detectable amounts of the isoprenoid hydrocarbons pristane (pr) and phytane (ph) (and petroleum source biomarkers including *hopanes* and steranes). Individual *n*-alkane concentrations ranged from < 2 μg g^{-1} to > 60 μg g^{-1} dry weight normalized to OC (μg g^{-1} C) (Figure 5.5a). Total *n*-alkane concentrations were similar between 2008–2009 and 2010–2011; annual average values were 24.8 ± 14.1 and 22.2 ± 13.2 μg g^{-1} C, respectively (Table 5.4a and 5.4b). However, the lower molecular weight (LMW, $<C_{21}$) *n*-alkanes dominated the 2008–2009 sediment trap samples, contributing up to 76% of the bulk composition (Figure 5.5b), whereas in the 2010–2011 sediment trap samples the relative contribution from marine sources decreased to 48%. This shift in 2010–2011 was characterized by increased concentrations in C_{29} and C_{31} *n*-alkanes and a corresponding reduction in *n*-alkanes $<C_{21}$ (Figure 5.5a). Specifically, there was a statistically significant (Student t-Test; $P \leq 0.05$) reduction in the marine-sourced *n*-alkanes (e.g., C_{17}- C_{19}) after the 2010 *Deepwater Horizon* event (Figure 5.5a; Table 5.4b). The most abundant compound, defined as the carbon number maximum (C_{max}), was *n*-C_{19} in the 2008–2009 sample, whereas in 2010–2011 the C_{max} was *n*-C_{21} but varied throughout the year with C_{29} dominating during the late fall/winter of 2010-2011 (Table 5.4a,b). Overall, there was a strong odd-to-even predominance, with a CPI consistently > 1.0 (Table 5.4a and 5.4b). The CPI from both years ranged from 0.7 to 16.8, with the fall/winter of 2010–2011 characterized by greater or higher CPI values (Figure 5.4f). The 2010–2011 samples showed a greater variability in CPI values relative to 2008–2009 (Figure 5.4f). The ACL, an indicator of vegetation type, showed a similar pattern, yielding a correlation (r) of 0.70 between ACL and CPI. The ACL values were higher in the 2010–2011 sediment trap samples, with the highest values in the late fall/early winter of 2010–2011. The P_{aq}, a parameter used to distinguish between macrophytes and higher plant waxes (Ficken et al. 2000), averaged between 0.52 ± 0.22 and 0.87 ± 0.16 in the 2008–2009 and 2010–2011 sediment traps, respectively.

Table 5.4a Concentration of Total (Σ) and Select *N*-Alkane Concentrations (μG G^{-1} C), and Parameters, Including Carbon Preference Index (CPI), Average Chain Length (ACL), and the Alkane Proxy (P_{aq}), and Annual Average and Standard Deviation (SD) for the 2008–2009 Sediment Trap Samples

Date	C_{max}	Σ *n*-alkanes	CPI	ACL*	P_{aq}	*n*-C_{17}*	*n*-C_{18}*	*n*-C_{19}*	Terrestrial	Marine*	Anthropogenic*
10/26/08	C15	1.5	n/d	n/d	0.3	0.00	0.00	n/d	n/d	1.5	n/d
11/22/08	C19	13.1	1.3	25.9	0.3	2.16	1.87	3.0	3.0	7.0	4.2
12/19/08	C19	19.3	3.2	27.3	0.4	1.42	2.43	4.7	4.8	8.5	4.2
1/15/09	C19	38.3	4.6	27.2	0.2	2.73	4.98	8.7	9.2	17.3	7.0
2/11/09	C19	40.4	3.6	27.0	0.5	3.09	4.97	9.4	10.0	17.5	n/d
3/10/09	C19	23.8	3.1	27.3	0.9	1.43	2.72	4.9	6.3	9.7	n/d
4/6/09	C19	23.3	4.3	27.0	0.7	2.92	2.53	4.8	5.3	10.9	4.5
5/3/09	C19	52.4	10.3	27.7	0.7	3.66	6.17	10.2	13.4	21.9	9.1
5/30/09	C19	17.4	2.0	26.9	0.6	2.26	2.44	3.8	2.8	9.5	4.3
6/26/09	C19	21.1	4.7	27.2	0.6	2.73	2.45	3.4	4.6	10.5	n/d
7/23/09	C19	13.2	4.2	28.5	0.7	1.60	2.00	2.8	5.5	10.3	3.9
8/19/09	C19	33.2	1.7	27.6	0.3	2.38	4.81	8.1	6.8	16.5	6.2
Average		24.8	3.9	27.2	0.5	2.2	3.1	5.8	6.5	11.8	5.4
SD		14.1	2.4	0.6	0.2	1.0	1.7	2.8	3.2	5.6	1.8

Major OM sources were calculated for terrestrial (odd numbered n-alkanes in the C21 to C31 range), marine (odd and even numbered n-alkanes in the C15 to C19 range), and anthropogenic (sum of the isoprenoid hydrocarbons pristane and phytane) contributions. Variables that are statistically different (Student's t-Test; P≤ 0.05) between the 2008–2009 and 2010–2011 deployments are indicated in bold and with an asterisk (*). n/d=below detection limit.

Table 5.4b Concentration of Total (Σ) and Select *n*-alkane Concentrations (μg g^{-1} C), and Parameters, Including Carbon Preference Index (CPI), Average Chain Length (ACL), and the Alkane Proxy (P_{aq}), and Annual Average and Standard Deviation (SD) for the 2010–2011 Sediment Trap Samples

Date	C_{max}	Σ *n*-alkanes	CPI	ACL*	P_{aq}	*n*-C_{17}*	*n*-C_{18}*	*n*-C_{19}*	Terrestrial	Marine*	Anthropogenic*
11/4/10	C29	24.9	13.0	29.4	n/d	0.16	1.20	1.2	12.6	3.6	2.3
12/4/10	C29	27.1	14.7	29.5	n/d	0.66	1.09	1.4	11.5	3.1	1.6
1/3/11	C21	43.7	16.8	29.3	0.6	1.89	1.67	2.7	21.4	7.2	2.8
2/2/11	C29	23.5	13.6	29.0	0.6	0.82	0.65	1.1	12.9	3.3	3.8
3/4/11	C21	3.6	0.7	29.0	0.7	0.41	0.19	0.5	1.3	1.2	0.7
4/3/11	C21	14.2	1.5	26.4	0.6	1.01	1.17	1.7	5.9	4.5	2.8
5/3/11	C21	20.6	1.9	27.7	0.7	0.98	1.30	2.0	9.4	5.7	2.0
6/2/11	C21	7.0	0.7	28.1	0.4	0.76	0.26	0.4	2.7	1.9	0.5
7/2/11	C21	45.8	10.4	28.2	0.7	1.09	1.58	2.9	22.3	5.5	2.2
8/1/11	C21	29.2	5.2	27.5	0.6	1.14	1.39	2.2	13.1	6.3	2.6
8/31/11	C20	10.8	1.9	27.0	0.2	1.08	0.85	1.2	3.7	3.6	1.1
9/30/11	C20	15.7	5.5	28.8	0.5	1.16	1.20	1.4	7.5	4.0	2.6
Average		22.2	7.1	28.3	0.6	0.9	1.0	1.6	10.3	4.1	2.1
SD		13.2	6.1	1.0	0.2	0.4	0.5	0.8	6.7	1.8	1.0

Major OM sources were calculated for terrestrial (odd numbered n-alkanes in the C21 to C31 range), marine (odd and even numbered n-alkanes in the C15 to C19 range), and anthropogenic (sum of the isoprenoid hydrocarbons pristane and phytane) contributions. Variables that are statistically different (Student's t-Test; P≤ 0.05) between the 2008–2009 and 2010–2011 deployments are indicated in bold and with an asterisk (*). n/d=below detection limit.

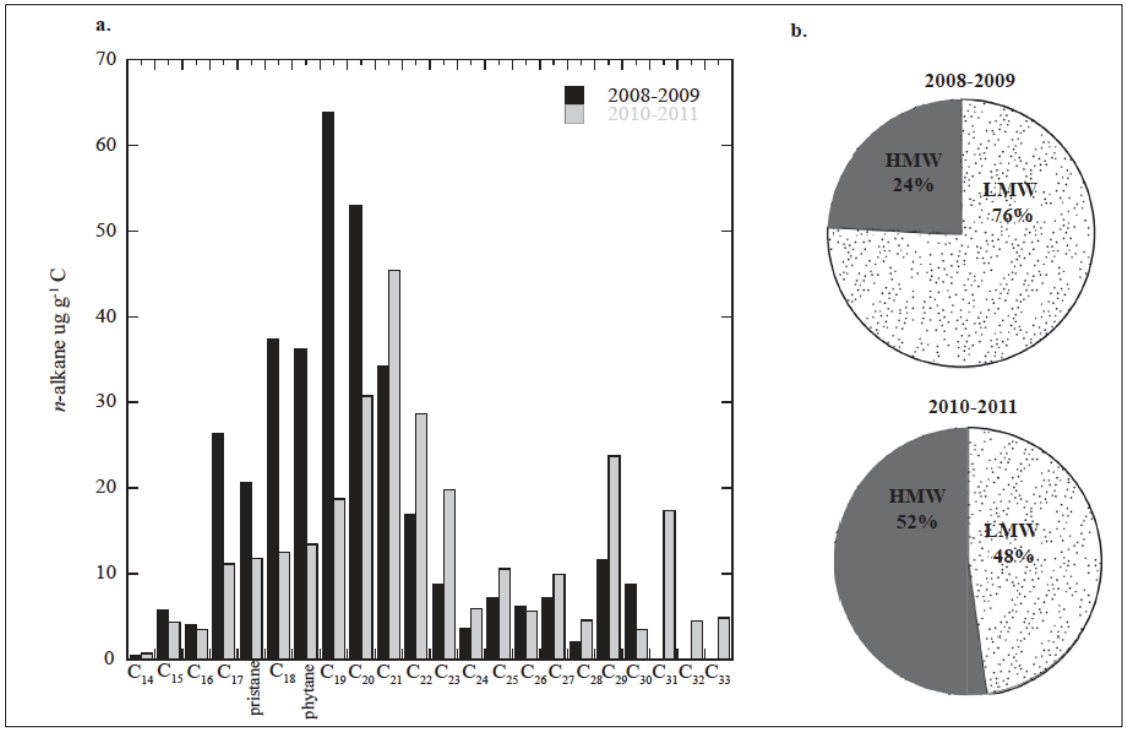

Figure 5.5. Biomarker histogram.

Histogram of total resolved *n*-alkane concentration from C_{14} to C_{33}, and the isoprenoid hydrocarbons pristane (pr) and phytane (ph) (μg g^{-1} C) from the 2008-2009 (grey bars) and 2010–2011 (black bars) sediment traps. b. relative contribution (%) from lower molecular weight (LMW, <C_{21}) and higher molecular weight (HMW, > C_{21}) *n*-alkanes from the 2008–2009 and 2010–2011 sediment traps.

Annual average total sterol concentrations ranged from 3,440 ± 2,230 to 1,980 ± 1,110 μg g^{-1} C in 2008–2009 and 2010–2010 respectively (Table 5.5a,b). The sterol cholesterol explained between 35 to 54% of the total sterol composition in 2008–2009 and 2010–2011, respectively. In comparison, the smallest contribution was calculated for the anthropogenic-sourced sterols, specifically coprostanol (5β-cholestan-3β-ol) and epicoprostanol (5β-cholestan-3α-ol) during both years. Coprostanol and epicoprostanol are produced by the microbial reduction of cholesterol and also through the intestinal microflora of higher animals, including marine mammals and birds, but are frequently used as sewage tracers correlated with anthropogenic inputs (Takada et. al. 1994; Wade et al. 1988). The relative sterol contribution showed a consistent trend with the following enrichment to the total sterol composition: C_{27} >C_{28}>C_{29}. Overall, total sterol concentrations were greater in 2008–2009 compared to 2010–2011 (Table 5.5a and 5.5b). This shift is, in large part, due to a statistically significant reduction in the following sterol concentrations after the *Deepwater Horizon* spill: 22-dehydrocholesterol, cholesterol, brassicasterol and β-sitosterol, whereas a statistically significant (Student t-Test; $P \leq 0.05$) increase occurred in the anthropogenic-sourced ketone and sterols, coprostanone, and coprostanol (Table 5.5b).

Table 5.5a Concentration of Total and Individual Sterols (μg g^{-1} C), C_{27}:C_{29} Ratios, Major OM Sources, and Annual Average and Standard Deviation (SD) for the 2008–2009 Sediment Trap Samples

Date	**Coprostanol***	Epicoprostanol	**Coprostanone***	**22-dehydrocholesterol***	**Cholesterol***	Cholestanol	Brassicasterol	Campesterol	Stigmasterol	**β-sitosterol***	Stigmastanol	**Σ-sterols***
			C_{27}	C_{27}	C_{27}	C_{27}	C_{28}	C_{28}	C_{29}	C_{29}		
	Anthropogenic	Anthropogenic	Anthropogenic		Marine		Marine	Terrestrial	terrestrial	Terrestrial		
10/26/08	1	1	12	65	452	24	96	27	25	57	19	779
11/22/08	3	5	38	24	2266	134	378	263	115	237	111	3574
12/19/08	3	4	26	171	828	79	250	278	86	176	88	1989
1/15/09	5	8	86	576	5467	314	615	315	210	545	134	8273
2/11/09	11	11	128	613	3482	285	762	234	272	544	210	6552
3/10/09	1	2	33	279	1843	100	195	159	68	103	43	2825
4/6/09	1	1	14	65	377	23	84	47	24	62	19	716
5/3/09	3	3	54	287	1688	157	359	498	134	316	125	3623
5/30/09	3	1	43	234	1713	141	254	210	102	296	77	3074
6/26/09	7	8	28	194	933	125	218	188	99	232	80	2113
7/23/09	2	3	5	73	1306	101	125	742	52	318	113	2839
8/19/09	3	5	88	605	2056	273	449	844	153	304	122	4902
Average	4	4	46	266	1868	146	315	317	112	266	95	3438
SD	3	3	37	218	1424	97	210	255	73	161	54	2225
% contribution	<1	<1	1	8	54	4	9	9	3	8	3	

Date	C_{27}: C_{29}	Terrestrial	**Marine***	**Anthropogenic***
10/26/08	6	110	548	14
11/22/08	7	615	2644	46
12/19/08	4	540	1078	34
1/15/09	8	1070	6082	99
2/11/09	5	1050	4244	150
3/10/09	12	330	2038	36
4/6/09	5	132	461	16
5/3/09	4	948	2046	60
5/30/09	5	609	1966	47
6/26/09	3	520	1151	43
7/23/09	4	1662	2167	31
8/19/09	6	1301	2505	96
Average	6	740	2244	56
SD	3	474	1588	40

Major OM sources were calculated from sterol data for terrestrial (campesterol, stigmasterol, and β-sitosterol), marine (cholesterol and brassicasterol), and anthropogenic (coprostanol, epicoprostanol, and coprostanone) contributions. Variables that are statistically different (Student's t-Test; P≤ 0.05) between the 2008–2009 and 2010–2011 deployments are indicated in bold and with an asterisk (*).

Table 5.5b Concentration of Total and Individual Sterols (μg g^{-1} C), C_{27}:C_{29} Ratios, Major OM Sources, and Annual Average and Standard Deviation (SD) for the 2010–2011 Sediment Trap Samples

Date	**Coprostanol***	Epicoprostanol	**Coprostanone***	**22-dehydrocholesterol***	**Cholesterol***	Cholestanol	Brassicasterol	Campesterol	Stigmasterol	**β-sitosterol***	Stigmastanol	**Σ-sterols***
			C_{27}	C_{27}	C_{27}	C_{27}	C_{28}	C_{28}	C_{29}	C_{29}		
	Anthropogenic	Anthropogenic	Anthropogenic		Marine		Marine	Terrestrial	Terrestrial	Terrestrial		
11/4/10	15	0	23	39	125	44	66	54	28	58	40	490
12/4/10	6	0	40	0	82	34	80	21	40	73	47	423
1/3/11	14	11	144	47	278	104	245	96	92	205	76	1311
2/2/11	6	9	38	78	183	65	130	54	28	123	52	765
3/4/11	19	26	148	60	555	229	260	298	82	153	84	1915
4/3/11	16	25	13	140	337	135	270	667	111	185	101	2000
5/3/11	10	32	155	245	160	77	58	905	75	141	87	1944
6/2/11	197	0	301	157	1704	905	275	142	94	131	74	3981
7/2/11	38	5	336	96	1003	318	306	89	130	198	109	2629
8/1/11	146	0	238	64	995	685	234	338	112	179	119	3107
8/31/11	71	0	266	53	1887	0	195	278	57	178	105	3089
9/30/11	10	0	48	188	1043	104	200	184	84	124	91	2076
Average	46	9	146	97	696	225	193	260	78	146	82	1977
SD	63	12	116	71	626	284	88	271	33	47	26	1108
% contribution	2	<1	7	5	35	11	10	13	4	7	4	

Date	C_{27}: C_{29}	Terrestrial	**Marine***	**Anthropogenic***
11/4/10	2	392	522	169
12/4/10	1	205	313	53
1/3/11	1	534	815	193
2/2/11	2	139	190	38
3/4/11	3	962	607	54
4/3/11	2	1121	217	197
5/3/11	2	367	1979	499
6/2/11	8	135	166	47
7/2/11	3	417	1309	379
8/1/11	4	628	1228	384
8/31/11	8	512	2082	337
9/30/11	6	392	1243	59
Average	3	484	889	201
SD	3	304	677	162

Major OM sources were calculated from sterol data for terrestrial (campesterol, stigmasterol, and β-sitosterol), marine (cholesterol and brassicasterol), and anthropogenic (coprostanol, epicoprostanol, and coprostanone) contributions. Variables that are statistically different (Student's t-Test; P≤ 0.05) between the 2008–2009 and 2010–2011 deployments are indicated in bold and with an asterisk (*).

5.3.3.1 Molecular Biomarker Sources

Marine (e.g., autochthonous) sources of OM dominated the sediment traps in both years, contributing on average between 72% in 2008–2009 and 52% in 2010–2011 to the total (i.e., sterols and *n*-alkanes) biomarker composition (Figure 5.6). In comparison, inputs of OM from vascular plant sourced biomarkers contributed 26% and 36% in 2008–2009 and 2010–2011, respectively. The lowest relative contribution was from anthropogenic/petroleum sources, contributing between 2% in 2008–2009 and 12% in 2010–2011. A shift in the relative contribution from the different OM sources was observed between the two years. Specifically, there was a shift away from marine-dominated OM sources in 2010–2011, and a relative increase in the contribution in OM derived from terrestrial plants and anthropogenic and/or petroleum sources (Figure 5.6).

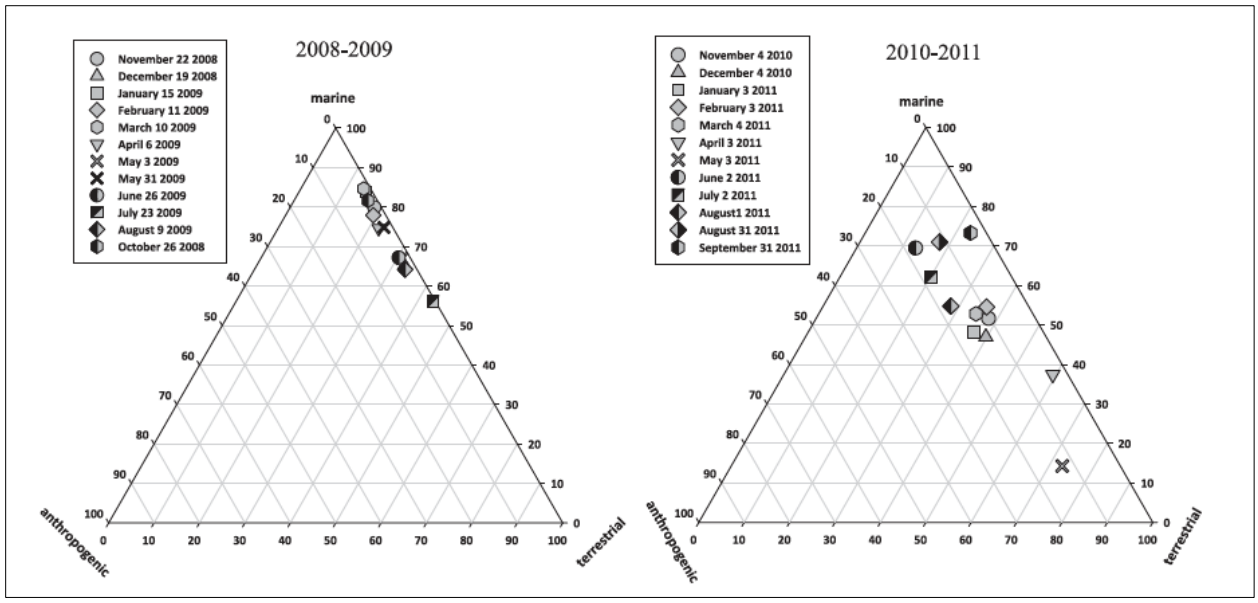

Figure 5.6. OM sources to sediment traps.

Ternary plots of distribution of major OM sources (terrestrial, marine, and anthropogenic) for the monthly sediment trap samples from 2008–2009 and 2010–2011. Terrestrial OM composition of the sediment was quantified using concentration of odd numbered *n*-alkanes in the C_{21} to C_{31} range and the sterol concentration of campesterol, stigmasterol, and β-sitosterol. The marine component was determined using the sterol concentration of cholesterol and brassicasterol and the odd and even numbered *n*-alkanes in the C_{15} to C_{19} range. The anthropogenic component was determined using the sterol composition of coprostanol, epicoprostanol, and coprostanone, and isoprenoid hydrocarbon (pristane and phytane) concentrations.

The pattern described above was also evident when the sterol and *n*-alkane compositions were investigated independently. There was a reduction in total sterol concentrations in 2010–2011 relative to the 2008–2009 samples, with the reduction explained by a significant decrease in marine-sourced sterols (Student t-Test; P=0.01). In contrast, anthropogenic-sourced sterols increased during June through August

of 2011, with a statistically significant (Student t-Test; $P \leq 0.05$) increase relative to the 2008–2009 sediment trap samples (Table 5.5a and 5.5b). Whereas total *n*-alkane concentrations did not change between the two years, there was a significant decrease (Student t-Test; $P \leq 0.05$) in marine-sourced *n*-alkanes in the 2010–2011 samples, equivalent to a relative decrease of 30%. The reduction in both marine-sourced sterols and *n*-alkanes after the spill also corresponded to a decrease in sediment trap derived % C_{org}, as well as a decrease in surface % particulate organic carbon (POC) based on satellite-derived estimates (Hu et al. 2011) (Figure 5.7).

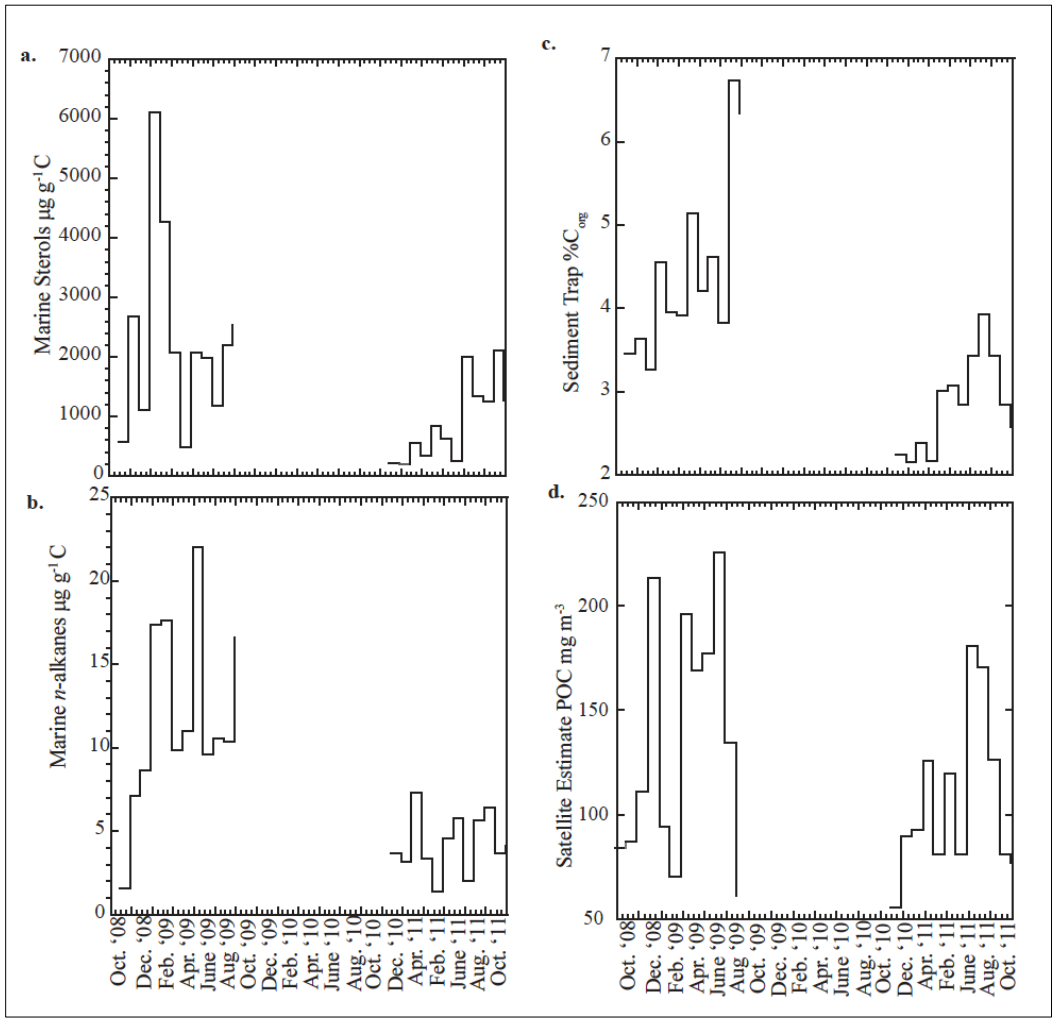

Figure 5.7. Time-series of biomarkers.

Time-series of marine-sourced a. sterol and b. *n*-alkane concentrations (µg g^{-1} C) where marine sourced OM is defined as *n*-C_{15} to *n*-C_{19} and as brassicasterol (C_{28}) and cholesterol (C_{27}), c. sediment trap % organic carbon (C_{org}), and d. satellite estimate of surface (1 optical depth, ~10-20 m) POC (mg m^{-3}) stationed at 28.943 to 29.280°N; 87.730 to 87.393°W (*data from Monthly MAMO_POC_4km.CR product*).

In addition to the biogenic biomarker composition, the sediment trap samples from both years contain a petrogenic component, characterized by select hopanes and steranes (Appendix 5.1 and 5.2). The abundance of hopanes was higher in the 2010–2011 sediment trap sample relative to the 2008–2009 sediment trap samples. Both years share some similar structure with the Macondo well MC252 oil chromatogram (Figure 5.3). However, hierarchical cluster analyses (HCA) of hopanoid source parameters (Hostettler et al. 2004) resulted in a separation of the sediment trap samples into two groups (Figure 5.8). Group 1 is characterized by samples from late winter/fall 2010–2011 through June 2011 with the exception of May 2011. In comparison, Group 2 is characterized by the 2008–2009 samples as well as the July and May 2011 samples.

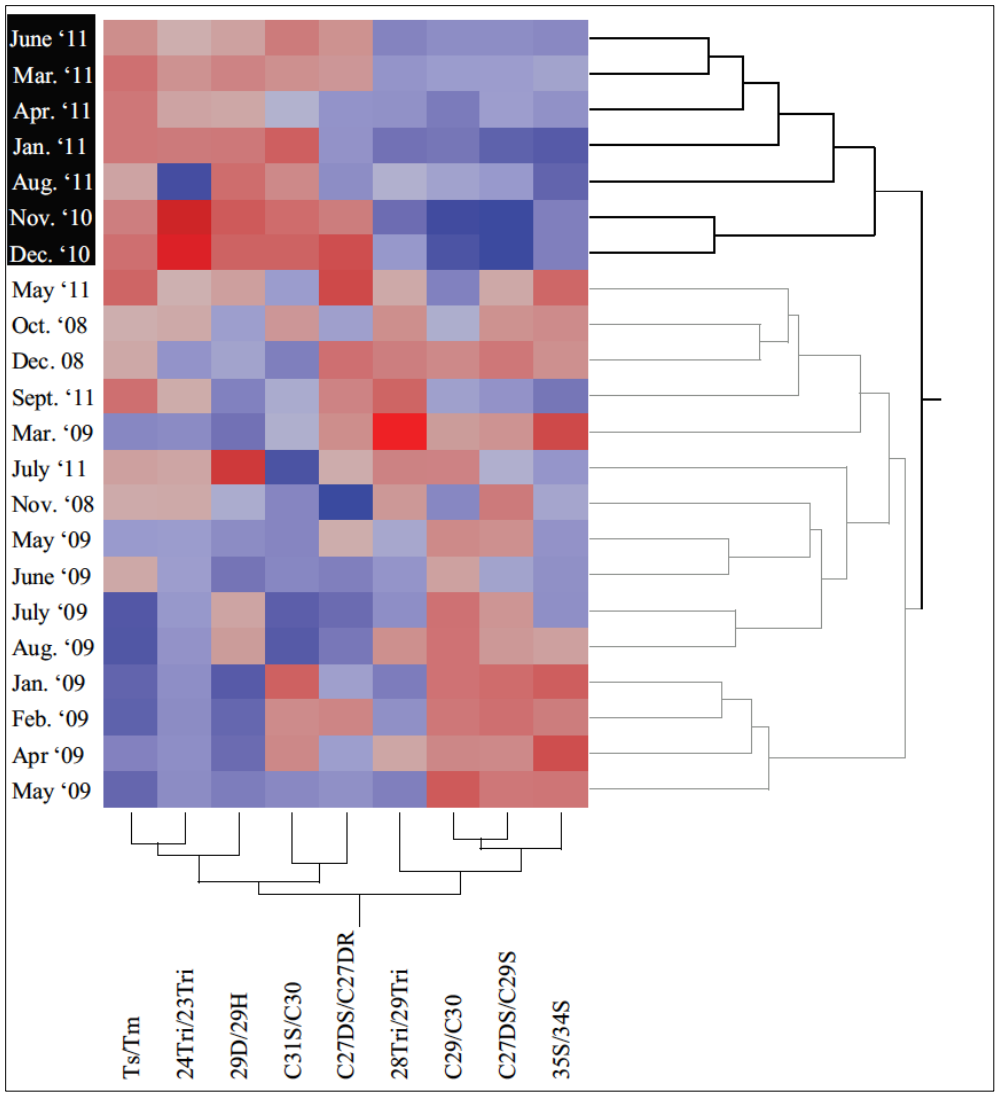

Figure 5.8. Hierarchical cluster.

Two-way hierarchical cluster diagram of 22 sediment trap samples from Viosca Knoll. The sediment trap data cluster into two groups according to differences in the biomarker ratios of hopanes and steranes as defined in Appendix 5.2. Group 1 is characterized by samples from late winter/fall 2010–2011 through June 2011 with the exception of May 2011 and group 2 is characterized by the 2008–2009 samples as well as the July and May 2011 samples.

5.3.3.2 Compound Specific Isotope Analysis

The $\delta^{13}C$ composition of the detected *n*-alkanes in the sediment trap samples was between -44.0 to -25.7‰, with an average isotope value from both years of -32.3 ± 3.3‰ (Table 5.6a,b). The full *n*-alkane range for CSIA could not be reported because most samples were too dilute for successful isotopic analyses given the low biomarker concentrations. Evaluation of the $\delta^{13}C$ signature of the C_{max} for each year was -34.0‰ for *n*-C_{19} and -31.4‰ for *n*-C_{21} in the 2008–2009 and 2010–2011 samples, respectively. The range of $\delta^{13}C$ values for individual *n*-alkanes <C_{21} is within the range for algal lipids (Volkman 2006), whereas the average $\delta^{13}C$ value of the odd numbered *n*-alkanes in the C_{21} to C_{31} range (-32.8 ± 2.3‰) is consistent with terrestrial C_3 plants using a Calvin-Benson cycle for photosynthetic carbon fixation (e.g., Deines 1980). Compound specific isotope analyses for the sterols identified (cholesterol, brassicasterol, β-sitosterol, campesterol, and stigmasterol) for both sediment trap deployments yielded a $\delta^{13}C$ range from -31.9 to -19.3‰ with no statistical difference (Student's t-Test; $P \geq 0.05$) between deployment years and an average sterol $\delta^{13}C$ signature of -24.8 ± 2.4‰ for both years (Table 5.6a,b). Cholesterol, the dominant algal and zooplankton sterol (C_{27}), had a $\delta^{13}C$ value of -25.1 ± 1.7‰. The sediment trap sterols were depleted in ^{13}C by approximately 3–4‰ relative to the sediment trap bulk $\delta^{13}C$ values, and the *n*-alkanes were depleted by ~10‰, reflecting the isotopic discrimination during lipid biosynthesis (Collister et al. 1994; Lockheart et al. 1997).

Table 5.6a Carbon Isotopic ($\delta^{13}C$; ‰) Composition of Select *n*-alkanes and Sterols for the 2008–2009 Sediment Trap Samples

The sterol $\delta^{13}C$ values were corrected for added derivative carbons using a functional relationship estimation by maximum likelihood equation from Ripley and Thompson (1987). Missing values indicate individual biomarker concentration insufficient for isotopic analysis.

														cholesterol	brassicasterol	campesterol	stigmasterol	β-sitosterol
Date	*n*-C_{15}	*n*-C_{17}	*n*-C_{18}	*n*-C_{19}	*n*-C_{20}	*n*-C_{21}	*n*-C_{22}	*n*-C_{27}	*n*-C_{29}	*n*-C_{31}	*n*-C_{33}	*n*-C_{34}	*n*-C_{35}	C_{27}	C_{28}	C_{28}	C_{29}	C_{29}
10/26/08	-26.9	-27.4	-28.4	-28.2	-28.3		-27.3	-32.5	-36.7		-30.7	-28.2	-25.7	-29.5	-27.9	-23.0	-23.6	-25.2
11/22/08		-29.9	-30.9	-35.4	-29.5									-25.0	-24.8	-24.4	-25.1	-26.7
12/19/08			-30.5	-35.6	-31.6	-33.7								-26.8	-25.3	-31.9	-24.5	-27.5
1/15/09			-31.2	-34.9	-31.9	-35.6								-26.8	-25.2	-22.1	-23.7	-25.7
2/11/09			-31.5	-34.7	-31.2	-34.3												
3/10/09	-43.4		-33.1	-34.4	-31.1	-34.2								-26.7	-25.5	-23.8	-24.7	-24.7
4/6/09		-27.6	-30.7	-32.8	-31.4	-33.4			-33.3	-30.5				-24.4	-23.2	-21.7	-21.4	-23.0
5/3/09			-31.0	-35.4	-32.2	-34.4												
5/30/09	-40.1	-30.3	-31.0	-34.8	-32.3	-34.4			-33.0					-25.7	-24.6	-22.4	-23.3	-24.1
6/26/09														-24.9				
7/23/09					-32.2									-22.0	-24.2	-21.4	-19.7	-29.3
8/19/09			-30.0	-33.5	-30.6	-32.3								-24.4	-24.8	-22.8	-22.4	-28.3

Table 5.6b Carbon Isotopic ($\delta^{13}C$; ‰) Composition of Select *n*-alkanes and Sterols for the 2010–2011 Sediment Trap Samples

The sterol $\delta^{13}C$ values were corrected for added derivative carbons using a functional relationship estimation by maximum likelihood equation from Ripley and Thompson (1987). Missing values indicate individual biomarker concentration insufficient for isotopic analysis.

Date	*n*-C_{15}	*n*-C_{17}	*n*-C_{18}	*n*-C_{19}	*n*-C_{20}	*n*-C_{21}	*n*-C_{22}	*n*-C_{27}	*n*-C_{29}	*n*-C_{31}	*n*-C_{33}	*n*-C_{34}	*n*-C_{35}	cholesterol C_{27}	brassicasterol C_{28}	campesterol C_{28}	stigmasterol C_{29}	β-sitosterol C_{29}
11/4/10					-36.6									-24.5	-23.3	-24.2	-24.2	-24.6
12/4/10														-25.2	-25.8	-24.4	-23.5	
1/3/11					-32.8									-22.8	-25.1	-24.6	-25.5	-27.3
2/2/11														-22.7	-22.7	-24.0	-28.3	-31.0
3/4/11					-31.4	-30.9	-30.9		-35.3					-24.6	-26.2	-26.3	-28.2	-27.6
4/3/11					-37.5									-23.1	-21.4	-20.8	-19.3	-21.9
5/3/11					-28.8	-31.8	-30.9		-32.1					-24.0	-23.3	-22.6	-24.1	-22.0
6/2/11	-44.0				-31.7	-31.5	-28.6							-25.3	-24.2	-23.9	-25.4	-31.8
7/2/11														-26.7		-24.7	-24.8	-30.6
8/1/11									-32.3	-32.3				-26.2	-25.0	-23.7	-24.7	-29.0
8/31/11																		
9/30/11														-25.1	-24.5	-25.2	-25.9	-27.3

5.4 Discussion

5.4.1 Provenance of Organic Matter

5.4.1.1 Radiocarbon

The ^{14}C ages capture the predominance of marine OM to the VK region, reflecting an autochthonous origin primarily composed of fresh planktonic detritus. Terrestrial OM typically yields older ^{14}C ages, ranging from 2,580 to 6,770 years BP (Goñi et al. 1997). For example, Goñi et al. (1998) suggest that the older ^{14}C ages measured in surface sediment samples collected in northwestern Gulf are indicative of allochthonous OM, reflecting significant terrigenous input to that area as well as preferential removal of young, labile OM. Changes in the contribution of terrestrial OM have been linked to the POC age structure in the MAR basin, with higher discharge contributing to a greater proportion of older POC (Rosenheim et al. 2013). However, in this present study discharge was consistently low from Oct 2010 through Feb 2011, and the depleted $\Delta^{14}C$ signal in the fall-winter of 2010 preceded the May discharge peak in the MAR System (Aulenbach et al. 2007). Changes in discharge cannot sufficiently explain the relatively low $\Delta^{14}C$ during this period. Instead, previous work documenting depleted $\Delta^{14}C$ in suspended POC collected in 2011 in the Gulf following the *Deepwater Horizon* event suggests that fossil carbon may have been incorporated in the sedimentary OC pool and planktonic food web (Graham et al. 2010; Chanton et al. 2012; Cherrier et al. 2013; Prouty et al. 2014b). For example, Cherrier et al. (2013) concluded that depleted POC $\Delta^{14}C$ values could be attributed to a fossil methane contribution of approximately 28-43%. The dilution from a low-^{14}C carbon source (e.g., -1,000 ‰) was estimated using a mass-balance-isotope mixing model (Fry and Anderson 2014) according to:

$$\% \text{ oil} = 100 * (\Delta^{14}C_{control} - \Delta^{14}C_{sample}) / (\Delta^{14}C_{control} - (-1000)),$$

where the average pre-spill $\Delta^{14}C$ sediment trap value was assigned the $\Delta^{14}C_{control}$ and the average post-spill $\Delta^{14}C$ sediment trap value was assigned the $\Delta^{14}C_{sample}$. The % oil contribution was calculated at 3.8%. For comparison, Chanton et al. (2015) found fossil petroleum derived carbon on the seafloor represented 3.0-4.9% of the $\Delta^{14}C$ signature on surface (0-1 cm) sediment organic matter. In summary, the overall $\Delta^{14}C$ signature in the sediment traps from both years of this study support a marine source of OM, with a small dilution (<4%) from a low-^{14}C carbon source (e.g., petro-carbon) potentially linked to the *Deepwater Horizon* oil spill.

5.4.1.2 Molecular Level Characterization and Organic Matter Sources

The distribution of biomarkers in the sediment traps suggests that OM delivery to the deep-sea of the Viosca Knoll region is a composite of sources (e.g., algal-phytoplankton-zooplankton productivity and land-plant productivity) and transport processes. This mixture of sources is reflected in the CPI range, spanning from those values associated with marine microorganisms to those representing a terrestrial-plant source. Despite this range, the biomarker composition in the sterol and *n*-alkane fractions during both years was dominated by marine sources (Figure 5.6), consistent with high primary production in this region (e.g., Lohrenz et al. 1990; 1994). The marine signal was particularly strong in the 2008–2009 sediment trap samples when the LMW *n*-alkanes contributed up to 76% of the total *n*-alkane composition. The dominance of a marine signature was also captured in the C_{max} values, which were characterized by *n*-C_{19} and *n*-C_{21} in the 2008–2009 and 2010–2011 samples, respectively. These values are indicative of marine phytoplankton (Blumer et al. 1971), whereas terrestrial sources typically yield a $C_{max} \geq 25$ due to incorporation of higher plant waxes (Eglinton and Hamilton 1967), as observed in estuary and salt marsh

sediments (e.g., Tanner et al. 2010; Maioli et al. 2012). The enriched ACL values, centered at mean of 28, and P_{aq} range further supports the interpretation that there is a minor contribution from terrestrial sources and that the long-chain *n*-alkanes are most likely linked to aquatic plants (i.e., emergent and submerged macrophytes) rather than terrestrial plants (Jeng 2006).

The predominance of marine-derived OM sources was also observed in the sterol composition. The dominant sterol during both years was cholesterol, a sterol typically sourced from zooplankton lipids (e.g., Gagosian et al. 1983; Volkman 1986) and also enriched in offshore suface sediment samples from the canyon regions of the Gulf (Waterson and Canuel 2008). Huang and Meinschein (1979) interpreted elevated cholesterol concentrations to represent a high production of zooplankton biomass per unit of phytoplankton biomass. These results are consistent with an enriched (4:1) C_{27}:C_{29} ratio. The elevated ratio of cholesterol relative to those sterols associated with land plants (e.g., β-sitosterol) represents the contribution of sterols associated with aquatic plants. Phytoplankton is also a probable source of C_{28} sterols, which are related to the presence of diatoms (Orcutt and Patterson 1975). The strong marine signature is further illustrated by a consistent trend of sterol enrichment, C_{27}>C_{28}>C_{29}. Taken together, the sterol and *n*-alkane compositions provide compelling evidence that during both years the source of OM is autochthonous, highlighting the dependence of these deep-sea communities on surface primary production, but in the months of November 2010–October 2011 after the spill was started (July 15, 2010) downward transport of marine-derived OM decreased.

5.4.1.3 Bulk Sediment and Compound Specific Source Indicators

Elemental, isotopic, and petrologic composition of sediment can provide OM provenance information, but given the range of overlap between marine and terrestrial source signals, these parameters taken alone can be difficult to interpret (e.g., Goñi et al. 1997; 1998). For example, the $\delta^{13}C$ signatures of marine and terrestrial OM, often used to identify source, can overlap when there is a combination of C_3 and C_4 plants of terrestrial origin, resembling a marine $\delta^{13}C$ signature (-20 to -22‰; Meyers 1994). In this study it was difficult to distinguish between a mixture of marine algae plus terrestrial C_3 plants versus a mixture of terrestrial C_3 plus C_4 plants given sediment trap bulk $\delta^{13}C$ values between -20.4 to -22.7‰. However, combined with relatively young $\Delta^{14}C$ ages from the sediment trap samples, the bulk sediment trap $\delta^{13}C$ values are inferred to represent marine phytodetritus. The range of C/N ratios (8–12) support this interpretation, whereas fluvial sources would drive C/N ratios towards those reflective of land-derived organic debris (12–20) (Meyers 1994). The high C/N ratios in the sediment trap samples relative to the Redfield ratio (6.7) may be a function of C overconsumption (i.e., more carbon fixed per unit of nitrate used) during phytoplankton blooms (Kähler and Koeve 2001). For example, in 2008–2009 the C/N values peak in the spring when discharge and nutrient loading (Figure 5.2b) are typically the greatest and when phytoplankton blooms develop (e.g., Lohrenz et al. 1999; Walker et al. 2005).

The relative contribution of terrestrial OM sources to the sediment traps deployed in the VK region are lower than those previously reported from surface sediments collected at study sites in northwestern Gulf (Goñi et al. 1997; 1998; Onstad et al. 2000; Bianchi et al. 2002; Waterson and Canuel, 2008; Bianchi et al. 2011). This comparison may reflect preferential removal of labile components and enrichment of residual recalcitrant matter in surface sediment relative to trap material (e.g., Wakeham and Canuel 2006; Wakeham and McNichol 2014). However, Goñi et al. (1998) found significant terrigenous input and interpreted the low C/N ratios and marine-like sediment $\delta^{13}C$ values as C_4 organic matter originating from eroded soils in the northwestern grasslands of the Mississippi River drainage basin. Their interpretation is supported by depleted sediment $\Delta^{14}C$ values, as well as depleted $\delta^{13}C$ lignin phenol values (e.g., -26.3‰), both of which indicate a significant fraction of allochthonous OM. Outside the primary dispersal system of the Mississippi River, Goñi et al. (1998) and Bianchi et al. (2002) concluded that terrestrial OM is

dominated by C_4 (non-woody angiosperms) carbon because of its association with finer size fraction of sediments (e.g., clays), whereas C_3 woody plant tissue can be preferentially retained in inner bays and estuaries due to the coarse-grained nature of the sediment.

In contrast to sampling sites in the northwestern Gulf, results from CSIA on sterols and *n*-alkanes from this study suggest that OM in the offshore region of VK is primarily from marine algae with a contribution from C_3 vascular plants rather than a mixture of terrestrial C_3 plus C_4 plants. Neither the sterol nor *n*-alkane $\delta^{13}C$ values (<-21‰) captured a terrestrial C_4 plant contribution. The input of C_3 plants to the VK region is most likely from input of fine-grained POC sourced from select tributaries in the upper Mississippi River drainage basin that are characterized by woody angiosperms (Onstad et al. 2000), as well as from sedimentary carbon sourced in the lower Mississippi River that has a relatively high concentration of woody angiosperms (Bianchi et al. 2002). Comparing results from the northwestern Gulf to sites of the Viosca Knoll region illustrates the spatial variability of both terrestrial and marine OM delivery in the Northern Gulf.

5.4.2 Temporal Shift in Organic Matter Sources

Results from this present study also suggest there is temporal variability. The relative shift away from marine OM sources in the 2010–2011 sediment trap samples could be interpreted as an increase in the terrestrial-derived OM component. However, neither the $\delta^{13}C$ values nor C/N ratios in 2010–2011 are indicative of a terrestrial OM source. Whereas the sediment trap $\Delta^{14}C$ values are on average 30‰ more depleted in 2010–2011, the ^{14}C ages are not reflective of an aged terrestrial origin. Instead, the depleted-^{14}C signal in the 2010–2011 sediment trap samples can be explained by incorporation of a depleted-^{14}C carbon source into the planktonic food web as previously described (Graham et al. 2010; Chanton et al. 2012; Cherrier et al. 2013; Prouty et al. 2014b). Potential sources of depleted-^{14}C carbon (e.g., petrogenic) to the Gulf can include natural sources, such as seeps, as well as anthropogenic sources including accidental oil spills from commercial vessel traffic and offshore drilling activities. Whereas there is a discernable change in petrogenic composition in the 2010–2011 sediment trap samples relative to the 2008–2009 sediment trap samples (Figure 5.8), comparison of the hopanoid portion of the GC-MS chromatograms of the sediment trap samples to Macondo 252-1 well oil indicates that the petrogenic signature in the samples is most likely a combination of sources. Therefore, the complexity of various input sources to the Gulf prevents assigning specific sources of oil inputs to the samples given the methods we used.

The potential influence of the *Deepwater Horizon* spill was also evident in the $\delta^{34}S$ sediment trap data where $\delta^{34}S$ values decrease in the 2010–2011 samples. The fate of oil and gas in both the subsurface and surface water involved bacteria degradation. As reviewed by King et al. (2015), the microbial response after the spill simulated hydrocarbon-degrading bacteria. This may have included anaerobic degradation of petroleum hydrocarbons by sulfate reducing bacteria (Suárez-Suárez et al. 2011), as was observed in surface waters and oil mousse samples in the nearshore Gulf (Liu and Liu 2013). The altered bacterioplankton community composition and succession following the spill may have altered the sulfur cycle (e.g., sulfate reduction and assimilation), resulting in a shift in $\delta^{34}S$ values that is captured in the sediment trap samples.

5.4.3 Impact on Biomass Production

Whereas the spatial extent of the *Deepwater Horizon* acute impact on the deep-sea benthos may be constrained (e.g., Montagna et al. 2013; Fisher et al. 2014a), quantifying secondary impacts like changes in biomass production and carbon export to the deep-sea remain unresolved. Though the sediment traps

were placed beneath known surface slicks that covered as much as 75,000 km^2 (Figure 5.1) (Cleveland et al. 2011), no visible signs of impact to the deep-sea corals were identified in the area to the north of the Macondo wellhead (lease blocks VK906 and VK826) (Fisher et al. 2014a). Instead, findings from our study suggest that sub-acute impacts may be detectible in the VK region. The reduction in the total concentration of marine-sourced sterols and *n*-alkane describes a provenance shift driven by a reduction in marine sources potentially linked to a decrease in surface ocean primary production. This interpretation is further emphasized by a concomitant decrease in marine biomarkers and $\%C_{org}$ (Figure 5.7). Satellite-derived estimates of surface POC also decreased in 2010–2011 relative to 2008–2009 (Hu et al. 2011), potentially in response to a reduction in primary productivity in 2010–2011. This scenario is further supported by a reduction in pigment flux in the 2010–2011 sediment trap samples (Figure 5.4f). The reduction in carbon export after the spill may have impacted benthic ecosystems, including a shift in community distribution and density. Fisher et al. (2014b) reported a decrease in macrofaunal and meiofaunal densities at the OCS lease block study site of MC294, approximately 11 km SW of the Macondo well, after the *Deepwater Horizon* spill. The subsequent reduction in sediment trap $\%C_{org}$ coupled to a decrease in marine-derived OM and pigment flux is consistent with indirect impacts and as such warrants more in depth study at future oil spills to ascertain the significance of such impacts (short and long term) within the context of normal geospatial and interannual and decadal variability.

5.5 Conclusion

The economics of the Gulf region depend greatly on the health of the Gulf and its ability to provide ecosystem services, including those provided by the deep-sea (e.g., Thurber et al. 2014). Detecting changes in plankton abundance and diversity and their link to the biological pump is complex but critical to evaluate the full extent of the *Deepwater Horizon* spill on Gulf ecosystem health. By integrating a set of powerful geochemical tracers (e.g., stable and radio-isotopes, lipid biomarkers, and compound specific isotopes) from sediment traps deployed before and after the spill, this study quantifies the reduction in biomass export in 2010–2011, at least 6–18 months after the spill started. Though satellite observations indicate an initial increase in phytoplankton biomass, results from this sediment trap study define a prolonged reduction in primary production and carbon export to the deep-sea community. These data address a gap in our knowledge of the biogeochemical processes that ensued after the 2010 *Deepwater Horizon* spill. Furthermore, these data identify potentially important sub-acute impacts to the deep-sea that must be better understood as we pursue long-term restoration and mitigation efforts in the Gulf and other areas.

5.6 Acknowledgments

The USGS Terrestrial, Marine, and Freshwater Environments-OCS Ecosystem Program and USGS Coastal and Marine Geology Program supported this work. We thank A. Lam (USGS) for lipid extraction, C. Yarnes (UC Davis) for CSIA, A. Davies (Bangor University) for hydrographic data, C. Hu (USF) for satellite data, B. Harlow (WSU) for sulfur isotope analyses, T. Guilderson (LLNL) for radiocarbon analyses, and T. Lorenson (USGS) for HCA and C. German (WHOI) for helpful discussion. USGS funded ship time for the first lander deployment and retrieval, and Greenpeace International funded the second lander deployment; USGS supported retrieval of the second lander. We thank M. Rhode (UNC-Wilmington) and G. Brewer (USGS) for assistance with many aspects of this project and comments from J. Richey and B. Thomas (USGS) and two anonymous reviewers. Any use of trade, product, or firm names is for descriptive purposes only and does not imply endorsement by the U.S. Government.

Appendix 5.1 Geochemical Parameters for Sediment Trap Samples

Parameter definitions are in Appendix 5.2.

Date	Ts/Tm	24Tri/23Tri	28Tri/29Tri	C29/C30	29D/29H	C31S/C30	35S/34S	C27DS/C27DR	C27DS/C29S
11/4/10	1.06	0.52	0.83	0.51	0.36	0.41	0.75	1.88	0.45
12/4/10	1.10	0.54	1.02	0.53	0.36	0.41	0.75	1.92	0.45
1/3/11	1.08	0.39	0.85	0.58	0.34	0.41	0.69	1.81	0.61
3/4/11	1.10	0.36	1.00	0.62	0.33	0.39	0.80	1.86	0.78
4/3/11	1.08	0.33	0.99	0.58	0.30	0.38	0.77	1.81	0.78
5/3/11	1.13	0.32	1.18	0.59	0.31	0.37	0.92	1.92	0.87
6/2/11	1.03	0.32	0.93	0.60	0.30	0.40	0.76	1.86	0.73
7/2/11	0.98	0.33	1.34	0.69	0.39	0.34	n/d	1.84	0.84
8/31/11	0.98	0.13	1.13	0.62	0.35	0.40	0.71	1.80	0.77
9/30/11	1.10	0.32	1.47	0.62	0.25	0.38	0.74	1.87	0.75
10/26/08	0.95	0.00	1.29	0.63	0.27	0.39	0.87	1.82	0.94
11/22/08	0.95	0.00	1.24	0.60	0.28	0.37	0.80	1.71	1.00
12/19/08	0.96	0.27	1.36	0.68	0.28	0.36	0.87	1.89	1.01
1/15/09	0.74	0.26	0.90	0.70	0.21	0.41	0.94	1.82	1.04
2/11/09	0.73	0.26	0.98	0.70	0.23	0.40	0.89	1.87	1.03
3/10/09	0.83	0.25	1.97	0.66	0.24	0.38	0.96	1.87	0.93
4/6/09	0.82	0.26	1.19	0.68	0.23	0.40	0.96	1.82	0.96
5/3/09	0.75	0.26	0.91	0.73	0.25	0.37	0.90	1.81	1.01
5/30/09	0.88	0.28	1.08	0.68	0.26	0.37	0.78	1.84	0.94
6/26/09	0.96	0.28	1.00	0.66	0.24	0.37	0.77	1.79	0.80
7/23/09	0.69	0.27	0.98	0.70	0.30	0.35	0.77	1.78	0.92
8/19/09	0.69	0.26	1.28	0.70	0.31	0.35	0.85	1.79	0.92

Appendix 5.2. Abbreviations Defined for Geochemical Parameters Calculated from Peak Heights and/or Areas

Triterpanes (hopanes), m/z 191 SIM chromatograms:

1. **Ts/Tm**, 18α-22,29,30-trisnorneohopane/17α-22,29,30-trisnorhopane.

2. **24Tri/23Tri**, C_{24} tricyclic terpane/C_{23} tricyclic terpane.

3. **28Tri/29Tri**, C_{28} tricyclic terpane/C_{29} tricyclic terpane.

4. **C_{29}/C_{30},** 17α,21β(H)-30-norhopane/17α,21β(H)-hopane.

5. **29D/29H**, 18α(H)-30-norneohopane/17α,21β(H)-30-norhopane.

6. **C_{31}S/C_{30},** 17α,21β(H)-homohopane (22S)/ 17α,21β(H)-hopane.

7. **35S/34S**, 17α,21β(H)-29-pentakishomohopane (22S)/17α,21β(H)-29-tetrakishomohopane (22S).

Steranes, m/z 217 SIM chromatograms:

1. **C_{27}S/ C_{29}S**: 20S-5α,14α,17α(H)–cholestane/20S-13β, 17α(H)–diasterane.

2. **C_{27}S /C_{27}R**: 20S-5α,14α,17α(H)-cholestane /20R-5α,14α,17α(H)-cholestane.

6 Works Cited

Abbriano RM, Carranza MM, Hogle SL, Levin RA, Netburn AN. 2011. Deepwater Horizon oil spill: A review of the planktonic response. Oceanography. 24(3):294–301.

Adeyemo, OK, Kroll, KJ, Denslow, ND. 2015. Developmental abnormalities and differential expression of genes induced in oil and dispersant exposed *Menidia beryllina*embryos. Aquat toxicol. 168: 60-71. doi: 10.1016/j.aquatox.2015.09.012

Adkins JF, Henderson GM, Wang SL, O'Shea S, Mokadem F. 2004. Growth rates of the deep-sea scleractinia *Desmophyllum cristagalli* and *Enallopsammia rostrata*. Earth Planet Sci Lett. 227: 481–490.

Afgan E, Baker D, van den Beek M, Blankenberg D, Bouvler D. 2016. The Galaxy platform for accessible, reproducible and collaborative biomedical analyses: 2016 update. Nucleic Acid Res. 44: W3-W10.

Ainsworth TD, Gates RD. 2016. Corals' microbial sentinels. Science. 352(6293):1518-1519.

Ainsworth TD, Krause L, Bridge T, Torda G, Raina J-B, et al. 2015. The coral core microbiome identifies rare bacterial taxa as ubiquitous endosymbionts. ISME J. 9:2261-2274.

Al-Dahash LM, Mahmoud HM. 2013. Harboring oil-degrading bacteria: A potential mechanism of adaptation and survival in corals inhabiting oil-contaminated reefs. Marine Poll Bull. 72:364-374.

Aliyari R, Ding SW. 2009. RNA-based viral immunity initiated by the Dicer family of host immune receptors. Immunol Rev. 227, 176-188.

Almeda R, Wambaugh Z, Chai C, Wang Z, Liu Z, et al. 2013. Effects of crude oil exposure on bioaccumulation of polycyclic aromatic hydrocarbons and survival of adult and larval stages of gelatinous zooplankton. PLoS One. 8:e74476.

Andrews AH, DeMartini EE, Brodziak J, Nichols RS, Humphreys RL. 2012. A long-lived life history for a tropical, deepwater snapper (*Pristipomoides filamentosus*): Bomb radiocarbon and lead–radium dating as extensions of daily increment analyses in otoliths. C. Can J Fish Aquat Sci. 69:1850-1869.

Andrews S. 2010. FastQC: A quality control tool for high throughput sequence data. http://www.bioinformatics.babraham.ac.uk/projects/ fastqc

Apprill A. 2017. Marine animal microbiomes: Toward understanding host-microbiome interactions in a changing ocean. Front Mar Sci. 4:222.

Arthur JS, Ley SC. 2013. Mitogen-activated protein kinases in innate immunity. Nature reviews. Immunol 13: 679-92.

Ashburner M, Ball CA, Blake JA, Botstein D, Butler H, et al. 2000. Gene ontology: Tool for the unification of biology. Nat Genet. 25(1):25-29.

Aulenbach BT, Buxton HT, Battaglin WT, Coupe RH. 2007. Streamflow and nutrient fluxes of the Mississippi-Atchafalaya River Basin and subbasins for the period of record through 2005.

Baker EJ, Kellogg CA. 2014. Comparison of three DNA extraction kits to establish maximum yield and quality of coral-associated microbial DNA. USGS Open-File Report 2014-1066. Reston (VA): US Geological Survey. doi.org/10.3133/ofr20141066

Baker MS, Wilson CA. 2001. Use of bomb radiocarbon to validate otolith section ages of red snapper lutjanus campechanus from the northern gulf of mexico. Limnol Oceanog. 46(7):1819-1824.

Barshis DJ, Ladner JT, Oliver TA, Senesa FO, Tralor-Knowles N. 2013. Genomic basis for coral resilience to climate change. PNAS 110(4):1387-1392.

Bhattacharya D, Agrawal S, Aranda M, Baumgarten S, Belcaid M, et al. 2016. Comparative genomics explains the evolutionary success of reef-forming corals. Elife 5.

Bautista AT, Matsuzaki H, Siringan FP. 2016. Historical record of nuclear activities from 129i in corals from the northern hemisphere (Philippines). J Environ Radioact. 164:174-181.

Bayha KM, Ortell N, Ryan CN, Griffitt KJ, Krasnec M, et al. 2017. Crude oil impairs immune function and increases susceptibility to pathogenic bacteria in southern flounder. PLoS One. 12:e0176559.

Beaulieu C, Chen J, Sarmiento J. 2012. Change-point analysis as a tool to detect abrupt climate variations. Phil Trans R Soc. A 370: 1228-1249.

Becker EL, Cordes EE, Macko SA, Fisher CR. 2009. Importance of seep primary production to *Lophelia pertusa* and associated fauna in the Gulf of Mexico. Deep Sea Res Part I. 56:786-800.

Beyer J, Trannum HC, Bakke T, Hodson PV, Collier TK. 2016. Environmental effects of the Deepwater Horizon oil spill: A review. Mar Pollut Bull. 110:28-51.

Bianchi T, Wysocki L, Schreiner K, Filley T, Corbett DR, et al. 2011. Sources of terrestrial organic carbon in the Mississippi plume region: Evidence for the importance of coastal marsh inputs. Aquat Geochem. 17(4-5):431-456.

Bianchi TS, Lambert CD, Santschi PH, Guo L. 1997. Sources and transport of land-derived particulate and dissolved organic matter in the Gulf ofMmexico (Texas shelf/slope): The use of ligninphenols and loliolides as biomarkers. Org Geochem. 27(1–2):65-78.

Bianchi TS, Mitra S, McKee BA. 2002. Sources of terrestrially-derived organic carbon in lower Mississippi River and Louisiana Shelf sediments: Implications for differential sedimentation and transport at the coastal margin. Mar Chem. 77(2–3):211-223.

Bianchi TS, Filley T, Dria K, Hatcher PG. 2004. Temporal variability in sources of dissolved organic carbon in the lower Mississippi River. Geochim Cosmochim Acta. 68:959–967.

Bianchi TS, Wysocki LA, Stewart M, Filley TR, McKee BA. 2007. Temporal variability in terrestrially-derived sources of particulate organic carbon in the lower Mississippi River and its upper tributaries. Geochim Cosmochim Acta. 71:4425–4437.

Biddulph DL. 2004. Development and applications of the NSF-Arizona AMS iodine-129 program [dissertation]. Tucson: University of Arizona.

Biddulph DL, Beck JW, Burr GS, Donahue DJ. 2006. Two 60-year records of 129i from coral skeletons in the south Pacific Ocean. In: Povinec PP, Sanchez-Cabeza JA, editors. Radioactivity in the environment. Berlin, Heidelberg (DE): Elsevier. p. 592-598.

Biddulph DL, Beck JW, Burr GS, Donahue DJ, Hatheway AL, et al. 2000. Measurement of the radioisotope 129I at the NSF-Arizona AMS laboratory. Nuclear instruments and methods in physics research section b: Beam interactions with materials and atoms. 172(1–4):693-698.

Bik HM, Halanych KM, Sharma J, Thomas WK. 2012. Dramatic shifts in benthic microbial eukaryote communities following the Deepwater Horizon oil spill. PLoS One. 7:e38550.

Blumer M, Guillard RRL, Chase T. 1971. Hydrocarbons of marine phytoplankton. Mar Biol. 8 183–189.

Blumer M, Mullin MM, Thomas DW. 1963. Pristane in zooplankton. Science. 140 974-974.

Boland GS, Etnoyer PJ, Fisher CR, Hickerson EL. 2017. State of deep-sea coral and sponge ecosystems of the U.S. Gulf of Mexico: Texas to the Florida Straits. In: Hourigan TF, Etnoyer PJ, Cairns SD, Tsao C-F, editors. State of deep-sea coral and sponge ecosystems of the United States. NOAA Technical Memorandum No.: NMFS HC-4. Silver Spring (MD): NOAA, National Marines Fisheries Service. p. 321–378.

Bonnin J, van Raaphorst W, Brummer G-J, van Haren H, Malschaert H. 2002. Intense mid-slope resuspension of particulate matter in the faeroe–shetland channel: Short-term deployment of near-bottom sediment traps. Deep Sea Res I. 49(8):1485-1505.

Boone DR, Mah RA. 2001. Genus I: *Methanosarcina*. Bergey's Man Syst Bacteriol. 1:269-276.

Bourguignon LY, Zhu H, Shao L, Chen YW. 2000. Ankyrin–Tiam1 interaction promotes Rac1 signaling and metastatic breast tumor cell invasion and migration. J Cell Biol. 150, 177-192.

Bourne D, Iida Y, Uthicke S, Smith-Keune C. 2008. Changes in coral-associated microbial communities during a bleaching event. ISME J. 2:350-363.

Bray EE, Evans ED. 1961. Distribution of n-paraffins as a clue to recognition of source beds. Geochim Cosmochim Acta. 22(1):2-15.

Brooke S, SW Ross. 2014. First observations of the cold-water coral *Lophelia pertusa* in mid-Atlantic canyons of the USA. Deep Sea Res II. 104:245-251.

Brooke S, Schroeder WW. 2007. State of deep coral ecosystems in the Gulf of Mexico region: Texas to the Florida Straits In: Lumsden SE, Hourigan TF, Bruckner AW, Dorr G, editors. The state of deep coral ecosystems of the United States. Silver Spring (MD): Department of Commerce, National Oceanic and Atmospheric Administrction. NOAA Technical Memorandum CRCP-3. p. 271–306.

Bryant WR, Lugo J, Cordova C, Salvador A. 1991. Physiography and bathymetry. In: Salvador A, ed. The Gulf of Mexico Basin. The Geology of North America, Volume J. Boulder (CO): Geological Society of America. p. 13–30.

Bugyi B, Carlier M-F. 2010. Control of actin filament treadmilling in cell motility. Annu Rev Biophys 39: 449-470.

Buhl-Mortensen L, Vanreusel A, Gooday AJ, Levin LA, Priede IG, et al. 2010. Biological structures as a source of habitat heterogeneity and biodiversity on the deep ocean margins. Mar Ecol. 31(1):21-50.

Bushnell B. (2017). BBTools software package. Available at: http://sourceforge.net/projects/bbmap

Cai WJ, Lohrenz SE. 2010. The Mississippi River plume and adjacent margin in the Gulf of Mexico. In: Liu, K.K., Atkinson, L.P., Quinones, R., Talaue-McManus, L., editors. Carbon and nutrient fluxes in continental margins: A global synthesis. New York: Springer-Verlag. p. 406–422.

Cairns SD. 2000. A revision of the shallow-water azooxanthellate Scleractinia of the Western Atlantic. Stud Nat Hist Caribb Reg. 75:1–231.

Cairo G, Tacchini L, Pogliaghi G, Anzon E, Tomasi A, et al. 1995. Induction of ferritin synthesis by oxidative stress. J Biol Chem. 270, 700–703.

Calvin S. 2013. XAFS for Everyone. CRC Press. 457 p.

Camilli R, Reddy CM, Yoerger DR, Van Mooy BAS, Jakuba MV, et al. 2010. Tracking hydrocarbon plume transport and biodegradation at Deepwater Horizon. Science. 330:201-204.

Caporaso JG, Kuczynski J, Stombaugh J, Bittinger K, Bushman FD. 2010. QIIME allows analysis of high-throughput community sequencing data. Nat Methods. 7:335-336.

Carassou L, Hernandez FJ, Graham WM. 2014. Change and recovery of coastal mesozooplankton community structure during the Deepwater Horizon oil spill. Environ Res Lett. 9.

Chance R, Malin G, Jickells T, Baker AR. 2007. Reduction of iodate to iodide by cold water diatom cultures. Mar Chem. 105(1–2):169-180.

Chang C-C, Burr GS, Jull AJT, Russell JL, Biddulph D, et al. 2016. Reconstructing surface ocean circulation with 129i time series records from corals. J Environ Radioact. 165:144-150.

Chanton J, Zhao T, Rosenheim BE, Joye S, Bosman S, et al. 2015. Using natural abundance radiocarbon to trace the flux of petrocarbon to the seafloor following the Deepwater Horizon oil spill. Environ Sci Technol. 49(2):847-854.

Chanton JP, Cherrier J, Wilson RM, Sarkodee-Adoo J, Boseman S,et al. 2012. Radiocarbon indicates that carbon from the Deepwater Horizon spill entered the planktonic food web of the Gulf of Mexico. Environ Res Lett. 7.

Cherrier J, Sarkodee-Adoo J, Guilderson TP, Chanton JP. 2013. Fossil carbon in particulate organic matter in the Gulf of Mexico following the Deepwater Horizon event. Environ Sci Technol Lett.

Claesson MJ, Wang Q, O'Sullivan O, Greene-Diniz R, Cole JR. 2010. Comparison of two next-generation sequencing technologies for resolving highly complex microbiota composition using tandem variable 16S rRNA gene regions. Nucleic Acids Res. 38(22):e200.

Cleveland CJ, Hogan M, Saundry P. 2011. Deepwater Horizon oil spill. In: Cleveland C, editor. Encyclopedia earth. Washington (DC): Environmental Information Coalition, National Council for Science and the Environment.

Coleman FC, Baker PB, Koenig CC. 2004. A review of Gulf of Mexico marine protected areas: Successes, failures, and lessons learned. Fisheries. 29(2):10-21.

Collister JW, Rieley G, Stern B, Eglinton G, Fry B. 1994. Compound-specific δ 13c analyses of leaf lipids from plants with differing carbon dioxide metabolisms. Org Geochem. 21(6-7):619-627.

Cordes EE, Carney SL, Hourdez S, Carney RS, Brooks JM, et al. 2007. Cold seeps of the deep Gulf of Mexico: Community structure and biogeographic comparisons to Atlantic equatorial belt seep communities. Deep Sea Res Part I. 54(4):637-653.

Cordes EE, McGinley MP, Podowski EL, Becker EL, Lessard-Pilon S, et al. 2008. Coral communities of the deep Gulf of Mexico. Deep Sea Res Part I. 55(6):777-787.

Conesa A, Madrigal P, Tarazona S, Gomez-Cabrero D, Cervera A, et al. 2016. A survey of best practices for RNA-seq data analysis. Genome Biol. 17:13.

Daly KL, Passow U, Chanton J, Hollander D. 2016. Assessing the impacts of oil-associated marine snow formation and sedimentation during and after the Deepwater Horizon oil spill. Anthropocene. 13:18-33.

Davies AJ, Duineveld GCA, van Weering TCE, Mienis F, Quattrini AM, et al. 2010. Short-term environmental variability in cold-water coral habitat at Viosca Knoll, Gulf of Mexico. Deep Sea Res Part I. 57(2):199-212.

Deines P. 1980. The isotopic composition of reduced organic carbon. In: Fritz P, Fontes JC, editors. Handbook of environmental isotope geochemistry. Amsterdam (NL): Elsevier Scientific Pub Co. p. 329-406.

de la Cuesta JL, Manley SL. 2009. Iodine assimilation by marine diatoms and other phytoplankton in nitrate-replete conditions. Limnol Oceanogr. 54(5):1653-1664.

De Leo DM, Ruiz-Ramos DV, Baums IB, and EE Cordes. 2015. Response of deep-water corals to oil and chemical dispersant. Deep Sea Res II. 129:137-147.

Delmont TO, Malandain C, Prestat E, Larose C, Monier J-M, et al. 2011. Metagenomic mining for microbiologists. ISME J. 5:1837-1843.

Demopoulos AWJ, Bourque JR, Frometa J. 2014. Biodiversity and community composition of sediment macrofauna associated with deep-sea *Lophelia pertusa* habitats in the Gulf of Mexico. Deep Sea Res Part I. 93(0):91-103.

Demopoulos AWJ, Ross SW, Kellogg CA, Morrison CL, Nizinski M, et al. 2017. Deepwater program: *Lophelia* II, continuing ecological research on deep-sea corals and deep-reef habitats in the Gulf of Mexico. U.S. Geological Survey Open-File Report 2017–1139. BOEM OCS Study 2016-023. Washington (DC): Department of the Interior US Geological Survey; Reston (VA): Department of the Interior Bureau of Ocean Energy Management.

DeSantis TZ, Hugenholtz P, Larsen N, Rojas M, Brodie EL, et al. 2006. Greengenes, a chimera-checked 16S rRNA gene database and workbench compatible with ARB. Appl Environ Microbiol. 72:5069-5072.

Dobin A, Davis CA, Schlesinger F, Drenkow J, Zaleski C, et al. 2013. STAR: ultrafast universal RNA-seq aligner. Bioinform. 29:15-21

Dorschel B, Hebbeln D, Foubert A, White M, Wheeler AJ. 2007. Hydrodynamics and cold-water coral facies distribution related to recent sedimentary processes at Galway Mound west of Ireland. Mar Geol. 244(1-4):184-195.

Doughty CL, Quattrini AM, Cordes EE. 2014. Insights into the population dynamics of the deep-sea coral genus *Paramuricea* in the Gulf of Mexico. Deep Sea Res Part II. 99:71-82.

Druffel E. 2002. Radiocarbon in corals: Records of the carbon cycle, surface circulation and climate. Oceanography. 15(1).

Druffel ERM, Griffin S, Witter A, Nelson E, Southon J, et al. 1995. Gerardia: Bristlecone pine of the deep-sea? Geochim Cosmochim Acta. 59(23):5031-5036.

Dubansky B, Whitehead A, Miller JT, Rice CD, Galvez F. 2013. Multitissue molecular, genomic, and developmental effects of the Deepwater Horizon oil spill on resident Gulf killifish (Fundulus grandis). Environ Sci Technol. 47:5074-5082.

Dubois KD, Lee D, Veizer J, 2010. Isotopic constraints on alkalinity, dissolved organic carbon, and atmospheric carbon dioxide fluxes in the Mississippi River. J Geophys Res Biogeosci. 115(G-2). doi: 10.1029/2009JG001102

Dunstan WM, Atkinson LP, Natoli J. 1975. Stimulation and inhibition of phytoplankton growth by low molecular weight hydrocarbons. Mar Biol. 31(4):305-310.

Edge S, Morgan M, Gleason D, Snell T. 2005. Development of a coral cDNA array to examine gene expression profiles in *Montastraea faveolata* exposed to environmental stress. Mar Pollut Bull. 51:5–7.

Eglinton G, Hamilton RJ. 1967. Leaf epicuticular waxes. Science. 156:1322-1335.

Elderfield H, Truesdale VW. 1980. On the biophilic nature of iodine in seawater. Earth Planet Sci Lett. 50(1):105-114.

Emblem Å, Karlsen BO, Evertsen J, Miller DJ, Moum T, et al. 2012. Mitogenome polymorphism in a single branch sample revealed sequencing of the *Lophelia pertusa* coral genome. Gene. 506:344-349.

Fadok V, Xue D, Henson P. 2001. If phosphatidylserine is the death knell, a new phosphatidylserine-specific receptor is the bellringer. Cell Death Differ. 8:582-587.

Fan Y, Ho, X, Zhou W, Liu G. 2016. 129I record of nuclear activities in marine sediment core from Jiaozhou Bay in China. J Environ Radioact 154, 15-24.

Farrenkopf AM, Dollhopf ME, Chadhain SN, Luther Iii GW, Nealson KH. 1997. Reduction of iodate in seawater during Arabian Sea shipboard incubations and in laboratory cultures of the marine bacterium Shewanella putrefaciens strain MR-4. Mar Chem. 57:347–354.

Feiters MC, Kupper FC, Meyer-Klaucke W. 2005. X-ray absorption spectroscopic studies on model compounds for biological iodine and bromine. J Synchrotron Radiat. 12: 85–93.

Feske S, Okamura H, Hogan PG, Rao A. 2003. Ca 2+calcineurin signalling in cells of the immune system. Biochem Biophys Res Commun. 311:1117-1132.

Ficken KJ, Li B, Swain DL, Eglinton G. 2000 An *n*-alkane proxy for the sedimentary input of submerged/floating freshwater aquatic macrophytes. Org Geochem. 31(7–8): 745-749.

Fisher CR, Demopoulos AWJ, Cordes EE, Baums IB, White HK, et al. 2014a. Coral communities as indicators of ecosystem-level impacts of the Deepwater Horizon Spill. BioScience. 64:796-807.

Fisher CR, Hsing PY, Kaiser CL, Yoerger DR, Roberts HH. 2014b. Footprint of Deepwater Horizon blowout impact to deep-water coral communities. Proc Natl Acad Sci USA. 111:11744-11749.

Flannagan RS, Jaumouille V, Grinstein S. 2012. The cell biology of phagocytosis. Annual Review of Pathology. 7:61-98.

Formolo MJ, Lyons TW, Zhang C, Kelley C, Sassen R, et al. 2004. Quantifying carbon sources in the formation of authigenic carbonates at gas hydrate sites in the Gulf of Mexico. Chem Geol. 205(3–4):253-264.

Fry B, Anderson LC. 2014. Minimal incorporation of Deepwater Horizon oil by estuarine filter feeders. Mar Pollut Bull. 80(1–2):282-287.

Fuge R, Johnson CC. 1986. The geochemistry of iodine–A review. Environ Geochem Health. 8(2):31-54.

Fuge R, Johnson CC. 2015. Iodine and human health, the role of environmental geochemistry and diet, a review. Appl Geochem. 63:282-302.

Galkiewicz JP, Stellick SH, Gray MA, Kellogg CA. 2012. Cultured fungal associates from the deep-sea coral *Lophelia pertusa*. Deep Sea Res Part I. 67:12-20.

Gagosian R, Nigrelli G, Volkman J. 1983. Vertical transport and transformation of biogenic organic compounds from a sediment trap experiment off the coast of Peru. In: Suess E, Thiede J, editors. Coastal upwelling its sediment record. NATO Conference Series, Series IV. New York (NY): Plenum Press. p. 241-272.

Gaur A, Shrivastava BD, Joshi SK. 2009. Copper K-edge XANES of Cu(I) and Cu(II) oxide mixtures. Journal of Physics: Conference Series 190, 012084.

Gasch A, Spellman P, Kao C, Carmel-Harel O, Eisen M, et al. 2000. Genomic expression programs in the response of yeast cells to environmental changes. Mol Biol Cell. 11, 4241–4257.

Gavins FNE, Hickey MJ. 2012. Annexin A1 and the regulation of innate and adaptive immunity. Front Immunol. 3:354.

Gene Ontology Consortium. 2017. Expansion of the Gene Ontology knowledgebase and resources. Nucleic Acids Res. 45(D1):D331-D338.

Gilbert DG. 2002. euGenes, a eukaryote organism genome information service. Nucleic Acids Res. 30, 145-148.

Gene Ontology Consortium. 2017. Expansion of the Gene Ontology knowledgebase and resources. Nucleic Acids Res. 45(D1):D331-D338.

Glasl B, Bourne DG, Frade PR, Webster NS. 2018. Establishing microbial baselines to identify indicators of coral reef health. Microbiol Aust. (March 2018):42-46.

Goldberg WM. 1978. Chemical changes accompanying maturation of the connective tissue skeletons of gorgonian and antipatharian corals. Mar Biol. 49(3):203-210.

Goldberg WM. 1991. Chemistry and structure of skeletal growth rings in the black coral antipathes fiordensis (cnidaria, antipathatia). Hydrobiologia. 216:403-409.

Goldberg WM, Hopkins TL, Holl SM, Schaefer J, Kramer KJ, Morgan TD, Kim K. 1994. Chemical composition of the sclerotized black coral skeleton (Coelenterata: Antipatharia): a comparison of two species. Comp Biochem Physiol B. 107:633–643.

Goldstone JV, Hamdoun A, Cole BJ, Howard-Ashby M, Nebert DW, et al. 2006. The chemical defensome: environmental sensing and response genes in the *Strongylocentrotus purpuratus* genome. Dev Biol. 300:366–384

Goñi MA, Ruttenberg KC, Eglinton TI. 1997. Sources and contribution of terrigenous organic carbon to surface sediments in the Gulf of Mexico. Nature. 389(6648):275-278.

Goñi MA, Ruttenberg KC, Eglinton TI. 1998. A reassessment of the sources and importance of land-derived organic matter in surface sediments from the Gulf of Mexico. Geochim Cosmochim Acta. 62(18):3055-3075.

Götz S, García-Gómez JM, Terol J, Williams TD, Nagaraj SH, et al. 2008. High-throughput functional annotation and data mining with the Blast2GO suite. Nucleic Acids Res. 36(10):3420-3435.

Grabherr MG, Haas BJ, Yassour M, Levin JZ, Thompson DA, et al. 2011. Full-length transcriptome assembly from RNA-seq data without a reference genome. Nat Biotechnol. 29:644–52.

Graham WM, Condon RH, Carmichael RH, A'Ambra I, Pattersn HK, et al. 2010. Oil carbon entered the coastal planktonic food web during the Deepwater Horizon oil spill. Environ Res Lett. 5(4):045301.

Griffiths SK. 2012. Oil release from Macondo well MC252 following the Deepwater Horizon accident. Environ Sci Technol. 46(10):5616-5622.

Grigg RW. 1974. Growth rings: Annual periodicity in two gorgonian corals. Ecology. 55(4):876-881.

Gross O, Thomas CJ, Guarda G, Tschopp J. 2011. The inflammasome: An integrated view. Immunol Rev. 243:136-151.

Gruffat H, Lupo J, Morand P, Boyer V, Manet E. 2011. The nuclear and adherent junction complex component protein ubinuclein negatively regulates the productive cycle of Epstein-Barr virus in epithelial cells. J Virol. 85:784-94.

Guilderson TP, Caldeira K, Duffy PB. 2000. Radiocarbon as a diagnostic tracer in ocean and carbon cycle modeling. Global Biogeochem Cycles. 14(3):887-902.

Guilderson TP, Tumey SJ, Brown TA, Buesseler KO. 2014. The 129-iodine content of subtropical pacific waters: Impact of Fukushima and other anthropogenic 129-iodine sources. Biogeosciences. 11: 4839-4852.

Gurevich A, Saveliev V, Vyahhi N, Tesler G. 2013. QUAST: Quality assessment too for genome assemblies. Bioinformatics. 29(8):1072-1075.

Handl J. 1996. Concentrations of 129i in the biosphere. Radiochimica Acta. 72(1):33-38.

Harada H, Fujita T, Miyamoto M, Kimura Y, Maruyama M, et al. 1989. Structurally similar but functionally distinct factors, IRF-1 and IRF-2, bind to the same regulatory elements of IFN and IFN-inducible genes. Cell. 58:729-739.

He P, Hou X, Aldahan A, Possnert G, Yi P. 2013. Iodine isotopes species fingerprinting environmental conditions in surface water along the northeastern Atlantic Ocean. Sci Rep. 3.

Hedges JI, Parker PL. 1976. Land-derived organic matter in surface sediments from the Gulf of Mexico. Geochim Cosmochim Acta. 40(9):1019-1029.

Henry LA, Roberts JM. 2007. Biodiversity and ecological composition of macrobenthos on cold-water coral mounds and adjacent off-mound habitat in the bathyal porcupine seabight, NE Atlantic. Deep Sea Res Part I. 54(4):654-672.

Herzog C, Haun RS, Kaushal V, Mayeux PR, Shah SV, et al. 2009. Meprin A and meprin α generate biologically functional IL-1β from pro-IL-1β. Biochem Biophys Res Commun. 379:904-908.

Hester ER, Barott KL, Nulton J, Vermeij MJA, Rohwer FL. 2016. Stable and sporadic symbiont communities of coral and algal holobionts. ISME J. 10:1157-1169.

Hewson I, Brown JM, Burge CA, Couch CS, LaBarre BA, et al. 2012. Description of viral assemblages associated with the *Gorgonia ventalina* holobiont. Coral Reefs. 31:487-491.

Hoff KJ, Stanke M. 2013. WedAUGUSTUS-A web service for training AUGUSTUS and predicting genes in eukaryotes. Nucleic Acids Res. 41(W1):W123-W128.

Hormann V, Fischer HW. 2017. The physicochemical distribution of 131i in a municipal wastewater treatment plant. J Environ Radioact. 178:55-62.

Hostettler FD, Rosenbauer RJ, Lorenson TD, Dougherty JG. 2004. Geochemical characterization of tarballs on beaches along the California coast. Part I—Shallow seepage impacting the Santa Barbara Channel Islands, Santa Cruz, Santa Rosa, and San Miguel. Org Geochem. 35:725–746.

Hou X, Hansen V, Aldahan A, Possnert G, Lind OC, et al. 2009. A review on speciation of iodine-129 in the environmental and biological samples. Anal Chim Acta. 632(2):181-196.

Hou X, Yan X, Chai C. 2000. Chemical species of iodine in some seaweeds II. Iodine-bound biological macromolecules. J Radioanal Nuc Chem. 245:461–467.

Hsing P-Y, Fu B, Larcom EA, Berlet SP, Shank TM, et al. 2013. Evidence of lasting impact of the Deepwater Horizon oil spill on a deep Gulf of Mexico coral community. Elem Sci Anth. 1(1):000012.

Hu C, Weisberg RH, Liu Y, Zheng L, Daly KL, et al. 2011. Did the northeastern Gulf of Mexico become greener after the Deepwater Horizon oil spill? Geophys Res Lett. 38(9):L09601.

Hu X, Chung AY, Wu I, Foldi J, Chen J, et al. 2008. Integrated regulation of toll-like receptor responses by notch and Interferon-γ pathways. Immunity. 29:691-703.

Hu Q, Zhao P, Moran JE, Seaman JC. 2005. Sorption and transport of iodine species in sediments from the Savannah River and Hanford Sites. J Contam Hydrol. 78:185–205.

Huang W-Y, Meinschein WG. 1979. Sterols as ecological indicators. Geochim Cosmochim Acta. 43(5):739-745.

Hughen KA, Baillie MGL, Bard E, Beck JW, Bertrand CJH, et al. 2004. Marine04 marine radiocarbon age calibration, 0–26 cal kyr bp. Radiocarbon. 46(3):1059-1086.

Incardona JP, Gardner LD, Linbo TL, Brown TL, Esbaugh AJ, et al. 2014. Deepwater Horizon crude oil impacts the developing hearts of large predatory pelagic fish. Proc Natl Acad Sci USA. 111:E1510-1518.

Jeng W. 2006. Higher plant n-alkane average chain length as an indicator of petrogenic hydrocarbon contaimination of the marine environment. Mar Chem. 102:242-251.

Jensen A, Frederiksen R. 1992. The fauna associated with the bank-forming deepwater coral *Lophelia pertusa (scleractinaria)* on the Faroe shelf. Sarsia. 77(1):53-69.

Jernelov A, Linden O. 1981. Ixtoc 1: A case study of the world's largest oil spill. Ambio. 10(6):299-306.

Jones ER, Martyniuk CJ, Morris JM, Krasnec MO, Griffitt RJ. 2017. Exposure to Deepwater Horizon oil and Corexit 9500 at low concentrations induces transcriptional changes and alters immune transcriptional pathways in sheepshead minnows. Comp Biochem Physiol D: Genomics Proteomics. 23:8-16.

Joye SB, Bracco A, Özgökmen TM, Chanton JP, Grosell M, et al. 2016. The Gulf of Mexico ecosystem, six years after the Macondo oil well blowout. Deep Sea Res Part II. 129:4-19.

Joye SB, MacDonald IR, Leifer I, Asper V. 2011. Magnitude and oxidation potential of hydrocarbon gases released from the BP oil well blowout. Nature Geosci. 4:160-165.

Kaczorowska B, Hacura A, Kupka T, Wrzalik R, Talik E, Pasterny,G. Matuszewska A. 2003. Spectroscopic characterization of natural corals. Anal Bioanal Chem 377, 1032-1037.

Kähler P, Koeve W. 2001. Marine dissolved organic matter: can its C:N ratio explain carbon overconsumption? Deep Sea Res Part II. 48(1): 49–62.

Kanehisa M, Goto S, Kawashima S, Okuno Y, Hattori M. 2004. The KEGG resource for deciphering the genome. Nucleic Acids Res. 32:D277-D280.

Kaplan DI, Denham ME, Zhang S, Yeager C, Xu C, et al. 2014. Radioiodine biogeochemistry and prevalence in groundwater. Crit Rev Environ Sci Technol. 44(20):2287-2335.

Kellogg CA. 2008. Microbial ecology of *Lophelia pertusa* in the northern Gulf of Mexico. In: Characterization of Northern Gulf of Mexico deepwater hard bottom communities with emphasis on *Lophelia* coral–*Lophelia* reef megafaunal community structure, biotopes, microbial ecology, and geology. Reston (VA): Department of the Interior US Geologic Survey. No. Open-File Report 2008-1148. New Orleans (LA): US Department of the Interior Minerals Management Service. OCS Study MMS 2008-015. Chapter 6.

Kellogg CA, Goldsmith DB. 2017. Cold-water coral microbiomes (*Lophelia pertusa*) from Gulf of Mexico and Atlantic Ocean: Raw data. U.S. Geological Survey data release. DOI: 10.5066/F7M32SXM.

Kellogg CA, Goldsmith DB, Gray MA. 2017. Biogeographic comparison of *Lophelia*-associated bacterial communities in the western Atlantic reveals conserved core microbiome. Front Microbiol. 8:796.

Kellogg CA, Lisle JT, Galkiewicz JP. 2009. Culture-independent characterization of bacterial communities associated with the cold-water coral *Lophelia pertusa* in the northeastern Gulf of Mexico. Appl Environ Microbiol. 75(8):2294-2303.

Kellogg CA, Neulinger SC. 2018. Metagenomic analysis of the microbial community associated with the deep-sea coral *Lophelia pertusa*. ASM Microbe 2018. American Society for Microbiology; Atlanta, Georgia; 2018 June 7–11.

Keppler F, Biester H, Putschew A, Silk PJ, Schöler HF, Müller G. 2003. Organoiodine formation during humification in peatlands. Environ Chem Lett. 1:219–223.

Kessler JD, Valentine DL, Redmond MC, Du M, Chan EW, et al. 2011. A persistent oxygen anomaly reveals the rate of spilled methane in the deep Gulf of Mexico. Science. 331(6015):312-315.

King GM, Kostka JE, Hazen TC, Sobecky PA. 2015. Microbial responses to the deepwater horizon oil spill: From coastal wetlands to the deep sea. Annu Rev Mar Sci. 7:377-401.

Koenig AE, Rogers RR, Trueman CN. 2009. Visualizing fossilization using laser ablation–inductively coupled plasma–mass spectrometry maps of trace elements in late cretaceous bones. Geology. 37(6):511-514.

Komugabe AF, Fallon SJ, Thresher RE, Eggins SM. 2014. Modern Tasman Sea surface reservoir ages from deep-sea black corals. Deep Sea Res Part II. 99(0):207-212.

Kraal G, van der Laan LJW, Elomaa O, Tryggvason K. 2000. The macrophage receptor MARCO. Microbes Infect. 2:313-316.

Kujawinski EB, Kido Soule MC, Valentine DL, Boysen AK, Longnecker K, et al. 2011. Fate of dispersants associated with the Deepwater Horizon oil spill. Environ Sci Technol 45:1298-1306.

Kumar H, Kawai T, Akira S. 2009. Toll-like receptors and innate immunity. Biochem Biophys Res Commun. 388:621-625.

Küpper FC, Carpenter LJ, McFiggans GB, Palmer CJ, Waite TJ, et al. 2008. Iodide accumulation provides kelp with an inorganic antioxidant impacting atmospheric chemistry. Proc Natl Acad Sci USA. 105(19):6954-6958.

Küpper FC, Schweigert N, Ar Gall E, Legendre JM, Vilter H. Kloareg B. 1998. Iodine uptake in Laminariales involves extracellular, haloperoxidase-mediated oxidation of iodide. Planta. 207: 163–171.

Kurogane Y, Miyata M, Kubo Y, Nagamatsu Y, Kundu RK, et al. 2012. FGD5 mediates proangiogenic action of vascular endothelial growth factor in human vascular endothelial cells. Arteriosclerosis Thromb Vasc Biol. 32:988-996.

Le Hénaff M, Kourafalou VH, Paris CB, Helgers J, Aman ZM, et al. 2012. Surface evolution of the Deepwater Horizon oil spill rpatch: Combined effects of circulation and eind-induced drift. Environ Sci Technol. 46(13):7267-7273.

Lebel LS, Dickson RS, Glowa GA. 2016. Radioiodine in the atmosphere after the Fukushima Dai-Ichi nuclear accident. J Environ Radioact. 151:82-93.

Leblanc C, Colin C, Cosse A, Delage L, La Barre S, et al. 2006. Iodine transfers in the coastal marine environment: The key role of brown algae and of their vanadium-dependent haloperoxidases. Biochimie. 88(11):1773-1785.

Leito JT, Lightenberg AJ, Van Houdt M, Van den Berg TK, Wouters D. 2011. The bacteria binding glycoprotein salivary agglutinin (SAG/gp340) activates complement via the lectin pathway. Mol Immunol. 49:185-190.

Li FJ, Duggal RN, Oliva OM, Karki S, Surolia R. 2015. Heme Oxygenase-1 protects Corexit 9500A-induced respiratory epithelial injury across species. PloS ONE. 10(4):e0122275. https://doi.org/10.1371/journal.pone.0122275

Littman RA, Willis BL, Bourne DG. 2011. Metagenomic analysis of the coral holobiont during a natural bleaching event on the Great Barrier Reef. Environ Microbiol Rep. 3(6):651-660.

Liu Z, Liu J. 2013. Evaluating bacterial community structures in oil collected from the sea surface and sediment in the northern Gulf of Mexico after the Deepwater Horizon oil spill. MicrobiologyOpen. 2(3):492-504.

Lockheart MJ, Van Bergen PF, Evershed RP. 1997. Variations in the stable carbon isotope compositions of individual lipids from the leaves of modern angiosperms: Implications for the study of higher land plant-derived sedimentary organic matter. Org Geochem. 26(1-2):137-153.

Lohrenz SE, Dagg MJ, Whitledge TE. 1990. Enhanced primary production at the plume/oceanic interface of the Mississippi River. Cont Shelf Res. 10(7):639-664.

Lohrenz SE, Fahnenstiel GL, Redalje DG. 1994. Spatial and temporal variations of photosynthetic parameters in relation to environmental conditions in coastal waters of the northern Gulf of Mexico. Estuaries. 17(4):779-795.

Lohrenz SE, Fahnenstiel GL, Redalje DG, Lang GA, Dagg MJ, et al. 1999. Nutrients, irradiance, and mixing as factors regulating primary production in coastal waters impacted by the Mississippi River plume. Cont Shelf Res. 19(9):1113-1141.

Longerich HP, Jackson SE, Günther D. 1996. Inter-laboratory note. Laser ablation inductively coupled plasma mass spectrometric transient signal data acquisition and analyte concentration calculation. J Anal At Spectrom. 11(9):899-904.

Lozupone C, Knight R. 2005. UniFrac: A new phylogenetic method for comparing microbial communities. Appl Environ Microbiol. 71:8228-8235.

Lukashchuk V, Everett RD. 2010. Regulation of ICP0-null mutant herpes simplex virus type 1 infection by ND10 components ATRX and hDaxx. J Virol. 84. 4026-4040.

Lunden JJ, Georgian SE, Cordes EE. 2013. Aragonite saturation states at cold-water coral reefs structured by *Lophelia pertusa* in the Northern Gulf of Mexico. Limnol Oceanogr. 58(1):354-362.

MacDonald IR, Guinasso NL, Jr, Reilly JF, Brooks JM, Callender WR, et al. 1990. Gulf of Mexico hydrocarbon seep communities: VI. Patterns in community structure and habitat. Geo-Mar Lett. 10:244-252.

Maddaluno L, Verbrugge SE, Martinoli C, Matteoli G, Chiavelli A, et al. 2009. The adhesion molecule L1 regulates transendothelial migration and trafficking of dendritic cells. J Exper Med. 206:623-35.

Madsen J, Mollenhauer J, Holmskov U. 2010. Review: Gp-340/DMBT1 in mucosal innate immunity. Innate immun. 16:160-167.

Mager EM, Esbaugh AJ, Stieglitz JD, Hoenig R, Bodinier C, et al. 2014. Acute embryonic or juvenile exposure to Deepwater Horizon crude oil impairs the swimming performance of mahi-mahi (*Coryphaena hippurus*). Environ Sci Technol 48:7053-7061.

Mahmoud H, Jose L. 2017. Phage and nucleocytoplasmic large viral sequences dominate coral viromes from the Arabian Gulf. Front Microbiol. 8:2063.

Maioli OLG, de Oliveira CR, Dal Sasso MA, Madureira LAdS, Azevedo DdA, et al. 2012. Evaluation of the organic matter sources using the δ13c composition of individual n-alkanes in sediments from Brazilian estuarine systems by gc/c/irms. Estuar Coast Shelf Sci. 114(0):140-147.

Marhaver KL, Edwards RA, Rohwer F. 2008. Viral communities associated with healthy and bleaching corals. Environ Microbiol. 10(9):2277-2286.

Mason OU, Hazen TC, Borglin S, Chain PS, Dubinsky EA, et al. 2012. Metagenome, metatranscriptome and single-cell sequencing reveal microbial response to Deepwater Horizon oil spill. ISME J. 6:1715-1727.

McClellan SA, Huang X, Barrett RP, Lighvani S, Zhang Y, et al. 2006. Matrix metalloproteinase-9 amplifies the immune response to Pseudomonas aeruginosa corneal infection. Invest Ophthalmol Vis Sci. 47:256-64.

McDonald D, Price MN, Goodrich J, Nawrock EP, DeSantis TZ, et al. 2012. An improved Greengenes taxonomy with explicit ranks for ecological and evolutionary analyses of bacteria and archaea. ISME J. 6:610-618.

McIsaac GF, David MB, Gertner GZ, Goolsby DA. 2001. Eutrophication: nitrate flux in the Mississippi River. Nature. 414:166–167.

McNutt MK, Camilli R, Crone TJ, Guthrie GD, Hsieh PA, et al. 2012a. Review of flow rate estimates of the Deepwater Horizon oil spill. Proc Natl Acad Sci USA. 109:20260-20267.

McNutt MK, Chu S, Lubchenco J, Hunter T, Dreyfus G, et al. 2012b. Applications of science and engineering to quantify and control the Deepwater Horizon oil spill. Proc Natl Acad Sci USA. 109(50):20222-20228.

Mead R, Goñi MA. 2006. A lipid molecular marker assessment of sediments from the northern Gulf of Mexico before and after the passage of Hurricane Lili. Org Geochem. 37(9):1115-1129.

Meistertzheim A-L, Lartaud F, Arnaud-Haond S, Kalenitchenko D, Bessalam M, et al. 2016. Patterns of bacteria-host associations suggest different ecological strategies between two reef building cold-water coral species. Deep Sea Res Part I. 114:12-22.

Messing CG, Reed JK, Brooke SD, Ross SW. 2008. Ch. 27: Deep-water coral reefs of the United States. In Pseudonocardiaceae: Riegl B, Dodge, RE, editors. Coral reefs of the USA. Berlin, Heidelberg (DE): Springer. p. 763–788.

Meyers PA. 1994. Preservation of elemental and isotopic source identification of sedimentary organic matter. Chem Geol. 114(3–4):289-302.

Middelburg JJ, Mueller CE, Veuger B, Larsson AI, Form A, et al. 2015. Discovery of symbiotic nitrogen fixation and chemoautotrophy in cold-water corals. Sci Rep. 5:17962.

Mienis F, Duineveld GCA, Davies AJ, Ross SW, Seim H, et al. 2012. The influence of near-bed hydrodynamic conditions on cold-water corals in the Viosca Knoll area, Gulf of Mexico. Deep-Sea Res I. 60:32–45.

Miller MC, Alexander V, Barsdate RJ. 1978. The effects of oil spills on phytoplankton in an Arctic lake and ponds. Arctic. 31:192–218.

Milliman JD, Meade RH. 1983. World-Wide delivery of river sediment to the oceans. J Geol. 91:1-21.

Montagna PA, Baguley JG, Cooksey C, Hartwell I, Hyde LJ, et al. 2013. Deep-sea benthic footprint of the Deepwater Horizon blowout. PLoS One. 8:e70540.

Moran JE, Oktay S, Santschi PH, Schink DR, Fehn U, et al. 1999. World-wide redistribution of 129iodine from nuclear fuel reprocessing facilities: Results from meteoric, river and seawater tracer studies. IAEA-SM-354/101.

Motohashi H, O'Connor T, Katsuoka F, Engel JD, Yamamoto M. 2002. Integration and diversity of the regulatory network composed of Maf and CNC families of transcription factors. Gene. 294:1-12.

Moya A, Huisman L, Ball EE, Hayward DC, Grasso LC, et al. 2012. Whole transcriptome analysis of the coral *Acropora millepora* reveals complex responses to CO_2-driven acidification during the initiation of calcification. Mol Ecol. 21:2440–2454.

Moya A, Huisman L, Forêt S, Gattuso J-P, Hayward DC, et al. 2015. Rapid acclimation of juvenile corals to CO_2-mediated acidification by upregulation of heat shock protein and Bcl-2 genes. 2015. Mol Ecol. 24:438-452.

Müller PJ, Suess E. 1979. Productivity, sedimentation rate, and sedimentary organic matter in the oceans—I. Organic carbon preservation. Deep Sea Res Part A. 26(12):1347-1362.

Muramatsu Y, Hans Wedepohl K. 1998. The distribution of iodine in the earth's crust. Chem Geol. 147(3):201-216.

Muramatsu Y, Yoshida S, Fehn U, Amachi S, Ohmomo Y. 2004. Studies with natural and anthropogenic iodine isotopes: Iodine distribution and cycling in the global environment. J Environ Radioact. 74(1–3):221-232.

Murawski SA, Hogarth WT, Peebles EB, Barbeiri L. 2014. Prevalence of external skin lesions and polycyclic aromatic hydrocarbon concentrations in Gulf of Mexico fishes, post-Deepwater Horizon. Trans Am Fish Soc. 143:1084-1097.

Nagy L, Szanto A, Szatmari I, Széles L. 2012. Nuclear hormone receptors enable macrophages and dendritic cells to sense their lipid environment and shape their immune response. Phys Rev. 92(4):1965.

Neulinger SC, Järnegren J, Ludvigsen M, Lochte K, Dullo W-C. 2008. Phenotype-specific bacterial communities in the cold-water coral *Lophelia pertusa* (Scleractinia) and their implications for the coral's nutrition, health, and distribution. Appl Environ Microbiol. 74(23):7272-7285.

Newton K, Dixit VM. 2012. Signaling in innate immunity and inflammation. Cold Spring Harb Persp Biol. 4(3):a006049.

Ng TH, Chiang YA, Yeh YC, Wang HC. 2014. Review of Dscam-mediated immunity in shrimp and other arthropods. Dev Comp Immunol. 46:129-38.

Nishiizumi K, Elmore D, Honda M, Arnold JR, Gove HE, 1983. Measurements of 129I in meteorites and lunar rock by tandem accelerator mass spectrometry. Nature. 305:611.

Nowak D, Florek M, Nowak J, Kwiatek W, Lekki J, et al. 2009. Morphology and the chemical make-up of the inorganic components of black corals. Mater Sci Engin, C. 29(3):1029-1038

Nuzzi R. 1973. Effects of water soluble extracts of oil on phytoplankton, in proceedings of joint conference on prevention and control of oil spills. Washington (DC): American Petroleum Institute.

Odunuga O, Longshaw V, Blatch GL. 2004. Hop: More than an Hsp70/Hsp90 adaptor protein. BioEssays. 26: 1058-1068.

Oktay SD, Santschi PH, Moran JE, Sharma P. 2000. The 129iodine bomb pulse recorded in mississippi river delta sediments: Results from isotopes of i, pu, cs, pb, and c. Geochim Cosmochim Acta. 64(6):989-996.

Oktay SD, Santschi PH, Moran JE, Sharma, P. 2001. 129I and 127I transport in the Mississippi River. Environ Sci Technol. 35:4470-4476.

O'Mahony L, Akdis M, Akdis CA. 2011. Regulation of the immune response and inflammation by histamine and histamine receptors. J Allergy Clin Immunol. 128:1153-1162.

Onstad GD, Canfield DE, Quay PD, Hedges JI. 2000. Sources of particulate organic matter in rivers from the continental USA: Lignin phenol and stable carbon isotope compositions. Geochim Cosmochim Acta. 64(20):3539-3546.

Orcutt DM, Patterson GW. 1975. Sterol, fatty acid and elemental composition of diatoms grown in chemically defined media. Comp Biochem Physiol B. 50(4):579-583.

Orsini L, Gilbert D, Podicheti R, Jansen M, Brown JB, et al. 2016. *Daphnia magna* transcriptome by RNA-Seq across 12 environmental stressors. Sci Data. 3:160030.

Pantos O, Cooney RP, Le Tissier MDA, Barer MR, O'Donnell AG, et al. 2003. The bacterial ecology of a plague-like disease affecting the Caribbean coral *Montastrea annularis*. Environ Microbiol. 5(5):370-382.

Pascall JC, Rotondo S, Mukadam AS, Oxley D, Webster J, et al. 2013. The immune system GTPase GIMAP6 interacts with the Atg8 homologue GABARAPl2 and is recruited to autophagosomes. Plos One. 8: e77782.

Passow U. 2016. Formation of rapidly-sinking, oil-associated marine snow. Deep Sea Res Part II. 129:232-240.

Passow U, Ziervogel K, Asper V, Diercks A. 2012. Marine snow formation in the aftermath of the Deepwater Horizon oil spill in the Gulf of Mexico. Environ Res Lett. 7(3):035301.

Patro R, Duggal G, Love MI, Irizarry RA, Kingsford C. 2017 Salmon provides fast and bias-aware quantification of transcript expression. Nat Methods. 14:417-419.

Pertoft H. 2000. Fractionation of cells and subcellular particles with Percoll. J Biochem Bioph Methods. 44:1-30.

Peters KE, Hostettler FD, Lorenson TD, Rosenbauer RJ. 2008. Families of Miocene Monterey crude oil, seep, and tarball samples, coastal California. Am Assoc Pet Geol Bull. 92(9):1131e1152.

Pilcher W, Miles S, Tang S, Mayer G, Whitehead A. 2014. Genomic and genotoxic responses to controlled weathered-oil exposures confirm and extend field studies on impacts of the Deepwater Horizon oil spill on native killifish. PLoS One. 9:e106351.

Pisani O, Oros DR, Oyo-Ita OE, Ekpo BO, Jaffé R, et al. 2013. Biomarkers in surface sediments from the cross river and estuary system, SE Nigeria: Assessment of organic matter sources of natural and anthropogenic origins. Appl Geochem. 31(0):239-250.

Poynter J, Eglington G. 1990. Molecular composition of the three sediments from Hole 717C: The Bengal Fan. In: Cochran JR, Stow DAV, et al., editors. Proc Ocean Drill Program. (116):155-161.

Prouty NG, Roark EB, Holmes C, Buster NA, Ross SW. 2010. Sub-decadal records of surface water properties recorded in deep-sea corals spanning the last millennium from the Gulf of Mexico. Paper presented at USGS Climate Change Science Workshop March 1–5. Denver, CO.

Prouty NG, Roark EB, Buster NA, Ross SW. 2011. Growth rate and age distribution of deep-sea black corals in the Gulf of Mexico. Marine Ecol Prog Ser. 423:101-115.

Prouty NG, Roark EB, Koenig AE, Demopoulos AWJ, Batista FC. 2014a. Deep-sea coral record of human impact on watershed quality in the Mississippi River basin. Global Biogeochem Cycles. 28(1):2013GB004754.

Prouty NG, Fisher CR, Demopoulos AWJ, Druffel E. 2014b. Growth rates and ages of deep-sea corals impacted by the Deepwater Horizon oil spill. Deep Sea Res Part II.

Prouty NG, Campbell PL, Mienis F, Duineveld G, Demopoulos AWJ, Ross SW, Brooke S. 2016. Impact of Deepwater Horizon spill on food supply to deep-sea benthos communities. Estuar Coast Shelf Sci. 169:248–264.

Qiao Y, Wang P, Qi J, Zhang L, Gao C. 2012. TLR-induced NF-κB activation regulates NLRP3 expression in murine macrophages. FEBS lett. 586(7): 1022-1026.

Quintana-Rizzo E, Torres JJ, Ross SW, Romero I, Watson K, et al. 2015. Δ13c and δ15n in deep-living fishes and shrimps after the Deepwater Horizon oil spill, Gulf of Mexico. Mar Pollut Bull.

Raftopoulou M and Hall A. 2004. Cell migration: Rho GTPases lead the way. Dev Biol. 265:23-32.

Raisbeck GM, Yiou F. 1999. ^{129}I in the oceans: Origins and applications. Sci Total Environ. 237:31-41.

Raisbeck GM, Yiou F, Zhou ZQ, Kilius LR. 1995. ^{129}I from nuclear fuel reprocessing facilities at Sellafield (U.K.) and La Hague (France); potential as an oceanographie tracer. J Mar Syst. 6(5–6):561-570.

Ravel B, Newville M. 2005. Athena, Artemis, Hephaestus: Data analysis for x-ray absorption spectroscopy using ifeffit. J Synchrotron Rad. 12:537-541.

Raymond PA, Oh N.-H, Turner RE, Broussard W. 2008. Anthropogenically enhanced fluxes of water and carbon from the Mississippi River. Nature. 451: 449-452.

Reddy CM, Arey JS, Seewald JS, Sylva SP, Lemkau KL, et al. 2012. Composition and fate of gas and oil released to the water column during the Deepwater Horizon oil spill. Proc Natl Acad Sci USA. 109:20229-20234.

Redfield AC, Ketchum BH, Richards FA. 1963. The influence of organisms on the composition of seawater. In: Hill MN, editor. The sea. New York: Interscience. p. 26–77.

Reed WA, May I, Livens FR, Charnock JM, Jeapes AP, Gresley M, Mitchell RM, Knight P. 2002. XANES fingerprinting of iodine species in solution and speciation of iodine in spent solvent from nuclear fuel reprocessing. J Anal At Spectrom. 17:541-543.

Reed JK, Weaver DC, Pomponi SA. 2006. Habitat and fauna of deep-water *Lophelia pertusa* coral reefs off the southeastern U.S.: Blake Plateau, Straits of Florida, and Gulf of Mexico. Bull Mar Sci. 78(2):343-375.

Rhee SG, Kang SW, Chang TS, Jeong W, Kim K. 2001. Peroxiredoxin, a novel family of peroxidases. IUBMB Life. 52:35-41.

Riddell JR, Wang X-Y, Minderman H, Gollnick SO. 2010. Peroxiredoxin 1 stimulates secretion of proinflammatory cytokines by binding to TLR4. J Immunol. 184:1022-1030.

Rideout JR, He Y, Navas-Molina JA, Walters WA, Ursell LK, et al. 2014. Subsampled open-reference clustering creates consistent, comprehensive OTU definitions and scales to billions of sequences. PeerJ. 2:e545.

Ripley BD, Thompson M. 1987. Regression techniques for the detection of analytical bias. Analyst. 112(4):377-383.

Risk MJ, Sherwood OA, Nairn R, Gibbons C. 2009. Tracking the record of sewage discharge off Jeddah, Saudi Arabia, since 1950, using stable isotope records from antipatharians. Mar Ecol Prog Ser. 397:219-226.

Roark EB, Guilderson TP, Dunbar RB, Fallon SJ, Mucciarone DA. 2009. Extreme longevity in proteinaceous deep-sea corals. Proc Natl Acad Sci USA. 106:5204-5208.

Roark EB, Guilderson TP, Dunbar RB, Ingram BL. 2006. Radiocarbon-based ages and growth rates of Hawaiian deep-sea corals. Mar Ecol Prog Ser. 327: 1–14.

Roark EB, Guilderson TP, Flood-Page S, Dunbar RB, Ingram BL, et al. 2005. Radiocarbon-based ages and growth rates of bamboo corals from the Gulf of Alaska. Geophys Res Lett. 32(4):L04606.

Roberts H, Carney R, Kupchik M, Fisher C, Nelson K, et al. 2007. *Alvin* explores the deep northern Gulf of Mexico slope. EOS. 88(35):341-342.

Roberts JM, Wheeler AJ, Freiwald A. 2006. Reefs of the deep: the biology and geology of cold-water coral ecosystems. Science. 312:543–547.

Roberts JM, Wheeler A, Freiwald A, Cairns S. 2009. Cold-water corals: The biology and geology of deep-sea coral habitats. Cambridge (GB): Cambridge University Press.

Roberts S, Hirshfield M. 2004. Deep-sea corals: Out of sight, but no longer out of mind. Front Ecol Environ. 2(3):123-130.

Robinson LF, Adkins JF, Keigwin LD, Southon J, Fernandez DP, et al. 2005. Radiocarbon variability in the western North Atlantic during the last deglaciation. Science. 310, 1469-1473.

Rogers AD. 1999. The biology of *Lophelia pertusa* (Linnaeus 1758) and other deep-water reef-forming corals and impacts from human activities. Int Rev Hydrobiol. 84:315-406.

Romero IC, Toro-Farmer G, Diercks AR, Schwing P, Muller-Karger F, et al. 2017. Large-scale deposition of weathered oil in the Gulf of Mexico following a deep-water oil spill. Environ Pollut. 228:179-189.

Rosenheim BE, Pendergraft MA, Flowers GC, Carney R, Sericano JL, et al. 2016. Employing extant stable carbon isotope data in Gulf of Mexico sedimentary organic matter for oil spill studies. Deep Sea Res Part II. 129: 249–258.

Rosenheim BE, Roe KM, Roberts BJ, Kolker AS, Allison MA, et al. 2013. River discharge influences on particulate organic carbon age structure in the Mississippi/Atchafalaya river system. Global Biogeochem Cycles. 27(1):154-166.

Rose NH, Seneca FO, Palumbi SR. 2015. Gene networks in the wild: identifying transcriptional modules that mediate coral resistance to experimental heat stress. Genome Biol Evol. 8:243-252.

Ross SW, Nizinski MS. 2007. State of deep coral ecosystems in the U.S. southeast region: Cape Hatteras to southeastern Florida. In: Lumsden SE, Hourigan TF, Bruckner AW, Dorr, G, (editors). The state of deep coral ecosystems of the United States. Silver Spring (MD): Department of Commerce, National Oceanic and Atmospheric Administration. NOAA Technical Memorandum CRCP-3. p.233–270.

Röthig T, Yum LK, Kremb SG, Roik A, Voolstra CR. 2017. Microbial community composition of deep-sea corals from Red Sea provides insight into functional adaptation to a unique environment. Sci Rep. 7:44714.

Ruiz-Ramos DV, Fisher CR, Baums IB. 2017. Stress response of the black coral *Leiopathes glaberrima* when exposed to sub-lethal amounts of crude oil and dispersant. Elem Sci Anth. 5:77.

Sampere TP, Bianchi TS, Allison MA. 2011. Historical changes in terrestrially derived organic carbon inputs to Louisiana continental margin sediments over the past 150 years. J Geophys Res Biogeosci. 116(G1):G01016.

Santschi PH, Oktay SD, Cifuentes L. 2007. Carbon isotopes and iodine concentrations in a Mississippi River delta core recording land use, sediment transport, and dam building in the river's drainage basin. Mar Environ Res. 63(3):278-290.

Santschi PH, Schwehr KA. 2004. 129i/127i as a new environmental tracer or geochronometer for biogeochemical or hydrodynamic processes in the hydrosphere and geosphere: The central role of organo-iodine. Sci Total Environ. 321(1–3):257-271.

Schiller RV, Kourafalou VH. 2014. Loop Current impact on the transport of Mississippi River waters. J Coast Res. 30(5):1287-1306.

Schink DR, Santschi PH, Corapcioglu O, Sharma P, Fehn U. 1995. 129I in Gulf of Mexico waters. Earth Planet Sci Lett. 135: 131-138.

Schlegel ML, Reiller P, Mercier-Bion F, Barré N, Moulin V. 2006. Molecular environment of iodine in naturally iodinated humic substances: Insight from x-ray absorption spectroscopy. Geochim Cosmochim Acta. 70(22):5536-5551.

Schmidt S, Debant A. 2014. Function and regulation of the Rho guanine nucleotide exchange factor Trio. Small GTPases. 5:e29769.

Schoener A, Rowe GT. 1970. Pelagic Sargassum and its presence among the deep-sea benthos. Deep-Sea Res. 17: 923–925.

Schroeder WW. 2002. Observations of *Lophelia pertusa* and the surficial geology at a deep-water site in the northeastern Gulf of Mexico. Hydrobiologia. 471(1-3):29-33.

Schwehr KA, Santschi PH. 2003. Sensitive determination of iodine species, including organo-iodine, for freshwater and seawater samples using high performance liquid chromatography and spectrophotometric detection. Anal Chim Acta. 482(1):59-71.

Schwing PT, Romero IC, Brooks GR, Hastings DW, Larson RA, et al. 2015. A decline in benthic foraminifera following the Deepwater Horizon event in the northeastern Gulf of Mexico. PLoS One. 10:e0120565.

Seidel M, Kleindienst S, Dittmar T, Joye SB, Medeiros PM. 2016. Biodegradation of crude oil and dispersants in deep seawater from the Gulf of Mexico: Insights from ultra-high resolution mass spectrometry. Deep Sea Res II. 129:108-118.

Sheng Y, Tang D, Pan G. 2011. Phytoplankton bloom over the northwest shelf of Australia after the Montara oil spill in 2009. Geomat Nat Hazards Risk. 2(4):329-347.

Sherwood OA, Lehmann MF, Schubert CJ, Scott DB, McCarthy MD. 2011. Nutrient regime shift in the western North Atlantic indicated by compound-specific δ15n of deep-sea gorgonian corals. Proc Natl Acad Sci USA. 108(3):1011-1015.

Sherwood OA, Jamieson RE, Edinger EN, Wareham VE. 2008. Stable C and N isotopic composition of cold-water corals from the Newfoundland and Labrador continental slope: Examination of trophic, depth and spatial effects. Deep Sea Res Part II. 55:1392-1402.

Sherwood OA, Scott DB, Risk MJ, Guilderson TP. 2005. Radiocarbon evidence for annual growth rings in the deep-sea octocoral *Primnoa resedaeformis*. Mar Ecol Prog Ser. 301:129-134.

Shichita T, Hasegawa E, Kimura A, Mortia R, Sakaguchi R. 2012. Peroxiredoxin family proteins are key initiators of post-ischemic inflammation in the brain. Nat Med. 18:911-917.

Shimamoto YS, Takahashi Y, Terada Y. 2011. Formation of organic iodine supplied as iodide in a soil−water system in Chiba, Japan. Environ Sci Technol 45, 2086-2092.

Shimamoto YS, Takahashi Y. 2008. Superiority of k-edge xanes over liii-edge xanes in the speciation of iodine in natural soils. Anal Sci. 24(3):405-409.

Shinzato C, Hamada M, Shoguchi E, Kawashima T, Satoh N. 2012. The repertoire of chemical defense genes in the coral *Acropora digitifera* genome. Zoolog Sci. 29:510–517.

Siddens LK, Krueger SK, Henderson MC, Williams DE. 2014. Mammalian flavin-containing monooxygenase (FMO) as a source of hydrogen peroxide. Biochem Pharmacol. 89:141-147.

Silva M, Etnoyer PJ, MacDonald IR. 2016. Coral injuries observed at mesophotic reefs after the Deepwater Horizon oil discharge. Deep Sea Res II. 129:96-107.

Simão F, Waterhouse RM, Ioannidis P, Kriventseva EV, Zdobnov EM. 2015. BUSCO: assessing genome assembly and annotation completeness with single-copy orthologs. Bioinf. 31(19):3210-3212.

Simister RL, Antzis EW, White HK. 2016. Examining the diversity of microbes in a deep-sea coral community impacted by the Deepwater Horizon oil spill. Deep Sea Res II. 129:157-166.

Smith DP, Peay KG. 2014. Sequence depth, not PCR replication, improves ecological inference from next-generation DNA sequencing. PLOS ONE. 9(2):e90234.

Snyder G, Aldahan A, Possnert G. 2010. Global distribution and long-term fate of anthropogenic 129i in marine and surface water reservoirs. Geochem Geophys Geosys. 11(4).

Soleimani M, Xu J. 2006. SLC26 chloride/base exchangers in the kidney in health and disease. Seminars Nephrol. 26(5):375-385.

Stallard RF. 1998. Terrestrial sedimentation and the carbon cycle: Coupling weathering and erosion to carbon burial. Global Biogeochem Cycles. 12(2):231-257.

Steenblock C, Heckel T, Czupalla C, Santo AIE, Niehage C, et al. 2014. The cdc42 guanine nucleotide exchange factor FGD6 coordinates cell polarity and endosomal membrane recycling in osteoclasts. J Biol Chem. M113. 504894.

Stanke M, Keller O, Gunduz I, Hayes A, Waack S, et al. 2006. AUGUSTUS: Ab initio prediction of alternative transcripts. Nucleic Acids Res. 34:W435–9.

Stuiver M, Polach HA. 1977. Discussion reporting of 14c data. Radiocarbon. 19(3):355-363.

Stuiver M, Reimer PJ. 1993. Extended 14c database and revised calib radiocarbon calibration program. Radiocarbon. 35:215-230.

Suárez-Suárez A, López-López A, Tovar-Sánchez A, Yarza P, Orfila A, et al. 2011. Response of sulfate-reducing bacteria to an artificial oil-spill in a coastal marine sediment. Environ Microbiol. 13(6):1488-1499.

Sulak KJ, Brooks RA, Luke KE, Norem AD, Randall M, et al. 2007. Demersal fishes associated with *Lophelia pertusa* coral and hard-substrate biotopes on the continental slope, Northern Gulf of Mexico. In: George Y, Cairns SD, editors. Conservation and adaptive management of seamount

and deep-sea coral ecosystems. Miami (FL): University of Miami Rosenstiel School of Marine and Atmospheric Science. p. 65-92.

Sulak KJ, Randall MT, Luke KE, Norem AD, Miller JM (editors). 2008. Characterization of northern Gulf of Mexico deepwater hard bottom communities with emphasis on *Lophelia* coral–*Lophelia* reef megafaunal community structure, biotopes, genetics, microbial ecology, and geology (2004–2006). Gainesville (FL): US Geological Survey; New Orleans (LA): US Department o the Interior Minerals Management Service. US Geological Survey Open-File Report 2008–1148; OCS Study MMS 2008–015. http://dx.doi.org/10.3133/ofr20081148.

Sunagawa S, Woodley CM, Medina M. 2010. Threatened corals provide underexplored microbial habitats. PLOS ONE. 5(3):e9554.

Takada H, Farrington JW, Bothner MH, Johnson CG, Tripp BW. 1994. Transport of sludge-derived organic pollutants to deep-sea sediments at deep water dump site 106. Environ Sci Technol. 28(6):1062-1072.

Tanner BR, Uhle ME, Mora CI, Kelley JT, Schuneman PJ, et al. 2010. Comparison of bulk and compound-specific δ13c analyses and determination of carbon sources to salt marsh sediments using n-alkane distributions (Maine, USA). Estuar Coast Shelf Sci. 86(2):283-291.

Thurber RLV, Barott KL, Hall D, Liu H, Rodriguez-Mueller B, et al. 2008. Metagenomic analysis indicates that stressors induce production of herpes-like viruses in the coral *Porites compressa*. Proc Natl Acad Sci USA. 105(47):18413-18418.

Thurber RLV, Correa AMS. 2011. Viruses of reef-building scleractinian corals. J Exper Mar Biol Ecol. 408:102-113.

Thurber AR, Sweetman AK, Narayanaswamy BE, Jones DOB, Ingels J, et al. 2014. Ecosystem function and services provided by the deep-sea. Biogeosci. 11:3941–3963.

Traylor-Knowles N, Rose NH, Palumbi SR. 2017. The cell specificity of gene expression in the response to heat stress in corals. J Exp Biol. 220:1837-1845.

Traylor-Knowles N, Granger BR, Lubinski TJ, Parikh JR, Garamszegi S, et al. 2011. Production of a reference transcriptome database (PocilloporaBase) for the cauliflower coral, *Pocillopora damicornis*. BMC Genomics. 12:585.

Trefry JH, Metz S, Nelsen TA, Trocine RP, Eadie BJ. 1994. Transport of particulate organic carbon by the Mississippi River and its fate in the Gulf of Mexico. Estuaries. 17(4):839-849.

Tsan M-F, Gao B. 2009. Heat shock proteins and immune system. J Leucocyte Biol. 85:905-910.

Tsunogai S, Sase T. 1969. Formation of iodide-iodine in the ocean. Deep Sea Res Oceangr Abstr. 16(5):489-496.

Turner RE, Rabalais NN, Alexander RB, McIsaac G, Howarth RW. 2007. Characterization of nutrient, organic carbon, and sediment loads and concentrations from the Mississippi River into the Northern Gulf of Mexico. EstuarCoasts. 30: 773-790.

Vargo GA, Hutchins M, Almquist G. 1982. The effect of low, chronic levels of no. 2 fuel oil on natural phytoplankton assemblages in microcosms: 1. Species composition and seasonal succession. Mar Environ Res. 6(4):245-264.

Valentine DL, Fisher GB, Bagby SC, Nelson RK, Reddy CM, et al. 2014. Fallout plume of submerged oil from Deepwater Horizon. Proc Natl Acad Sci USA. 111:15906-15911.

van Bleijswijk JDL, Whalen C, Duineveld GCA, Lavaleye MSS, Witte HJ, et al. 2015. Microbial assemblages on a cold-water coral mound at the SE Rockall Bank (NE Atlantic): interactions with hydrography and topography. Biogeosci. 12(14):4483-4496.

van de Ven R, Scheffer GL, Reurs AW, Lindenberg JJ, Oerlemans, et al. 2008. A role for multidrug resistance protein 4 (MRP4; ABCC4) in human dendritic cell migration. Blood. 112:2353-2359.

van de Water JA, Ainsworth TD, Leggat W, Bourne DG, Willis BL, et al. 2015. The coral immune response facilitates protection against microbes during tissue regeneration. Mol Ecol. 24(13):3390-3404.

van de Water JA, De Mares MC, Dixon GB, Raina J-B, Willis BL, et al. 2018. Antimicrobial and stress responses to increased temperature and bacterial pathogen challenge in the holobiont of a reef-building coral. Mol Ecol. 27(4):1065-1080.

van Eenennaam JS, Wei Y, Grolle KC, Foekema EM, Murk AJ. 2016. Oil spill dispersants induce formation of marine snow by phytoplankton-associated bacteria. Mar Pollut Bull. 104:294-302.

Vogel JS, Southon JR, Nelson DE. 1987. Catalyst and binder effects in the use of filamentous graphite for ams. Nucl Instrum Methods Phys Res, Sect B. 29:50-56.

Volkman JK. 1986. A review of sterol markers for marine and terrigenous organic matter. Org Geochem. 9:83-99.

Volkman JK. 2006. Lipid markers for marine organic matter. In: Volkman JK (editor). Marine organic matter: Biomarkers, isotopes and DNA: The handbook of environmental chemistry, volume 2N. Berlin, Heidelberg (DE): Springer. p. 27-70.

Vonk, SM, Hollander, DJ, Murk, A-TJ. 2015. Was the extreme and wide-spread marine oil-snow sedimentation and flocculent accumulation (MOSSFA) event during the Deepwater Horizon blow-out unique? Mar Pollut Bull. 100(1): 5-12, 10.1016/j.marpolbul.2015.08.023

Wade TL, Atlas EL, Brooks JM, Kennicutt MC, Fox RG, et al. 1988. NOAA Gulf of Mexico status and trends program: Trace organic contaminant distribution in sediments and oysters. Estuaries. 11(3):171-179.

Wagner AJ. 2009. Oxygen and carbon isotopes and coral growth in the Gulf of Mexico and Carribean Sea as environmental and climate indicators [dissertation]. College Station: Texas A&M University.

Wagner AJ, Guilderson TP, Slowey N, Cole JE. 2009. Pre-bomb surface water radiocarbon of the Gulf of Mexico and Carribean as recorded in hermatypic corals. Radiocarbon. 51:947–954.

Wakeham SG, Canuel EA. 2006. Degradation and preservation of organic matter in marine sediments. In: Volkman JK, editor. Marine organic matter: Biomarkers, isotopes and DNA: The handbook of environmental chemistry, volume 2N. Berlin, Heidelberg (DE): Springer. p. 295-321.

Wakeham SG, McNichol AP. 2014. Transfer of organic carbon through marine water columns to sediments- insights from stable and radiocarbon isotopes of lipid biomarkers. Biogeosci. 11(23):6895-6914.

Walker ND, Wiseman WJ, Rouse LJ, Babin A. 2005. Effects of river discharge, wind stress, and slope eddies on circulation and the satellite-observed structure of the Mississippi River plume. J Coast Res.1228-1244.

Waller R. 2005. Deep-water Scleractinia (Cnidaria: Anthozoa): Current knowledge of reproductive processes. In: Cold-water corals and ecosystems. Freiwald A, Roberts JM, editors. Berlin (DE): Springer. p. 691-700.

Warwick P, Zhao R, Higgo JJ, Smith B, Williams GM. 1993. The mobility and stability of iodine-humic and iodine-fulvic complexes through sand. Sci Total Environ. 130–131: 459-465.

Waterhouse RM, Seppey M, Simão FA, Manni M, Ioannidis P, et al. 2017. BUSCO applications from quality assessments to gene prediction and phylogenomics. Mol Biol Evol. 35(3):543-548.

Waterson EJ, Canuel EA. 2008. Sources of sedimentary organic matter in the Mississippi River and adjacent Gulf of Mexico as revealed by lipid biomarker and δ13ctoc analyses. Org Geochem. 39(4):422-439.

Wegley L, Edwards R, Rodriguez-Brito B, Liu H, Rohwer F. 2007. Metagenomic analysis of the microbial community associated with the coral *Porites astreoides*. Environ Microbiol. 9(11):2707-2719.

Wegley L, Yu Y, Breitbart M, Casas V, Kline DI, Rohwer F. 2004. Coral-associated Archaea. Mar Ecol Prog Ser. 273:89-96.

Weinbauer MG, Ogier J, Maier C. 2012. Microbial abundance in the coelenteron and mucus of the cold-water coral *Lophelia pertusa* and in bottom water of the reef environment. Aquat Biol. 16:209-216.

Weiss Y, Forêt S, Hayward DC, Ainsworth T, King R, et al. 2013. The acute transcriptional response of the coral *Acropora millepora* to immune challenge: Expression of GiMAP/IAN genes links the innate immune responses of corals with those of mammals and plants. BMC Genomics. 14:400.

White HK, Hsing PY, Cho W, Shank TM, Cordes EE, et al. 2012. Impact of the Deepwater Horizon oil spill on a deep-water coral community in the Gulf of Mexico. Proc Natl Acad Sci USA. 109:20303-20308.

Whitehead A, Dubansky B, Bodinier C, Garcia TI, Miles S, et al. 2012. Genomic and physiological footprint of the Deepwater Horizon oil spill on resident marsh fishes. Proc Natl Acad Sci USA. 109:20298-20302.

Williams B, Risk MJ, Ross SW, Sulak KJ. 2006. Deep-water antipatharians: Proxies of environmental change. Geology. 34: 773-776.

Williams B, Grottoli AG. 2010. Recent shoaling of the nutricline and thermocline in the western tropical Pacific. Geophys Res Lett. 37(22):L22601.

Williams B, Grottoli AG. 2011. Solution and laser ablation inductively coupled plasma–mass spectrometry measurements of br, i, pb, mn, cd, zn, and b in the organic skeleton of soft corals and black corals. Geochem Geophys Geosys. 12(3).

Williams B, Risk MJ, Ross SW, Sulak KJ. 2007. Stable isotope data from deep-water antipatharians: 400-year records from the southeastern coast of the United States of America. Bull Mar Sci. 81:437-447.

Witbaard R, Duineveld GCA, Kok A, van der Weele J, Berghuis EM. 2000. The response of *Oneirophanta mutabilis* (Holothuroidea) to the seasonal deposition of phytopigments at the Porcupine Abyssal Plain in the Northeast Atlantic. Prog Oceanogr. 50:423-441.

Wong GTF, Brewer PG, Spencer DW. 1976. The distribution of particulate iodine in the Atlantic Ocean. Earth Planet Sci Lett. 32(2):441-450.

Worthington JJ, Fenton TM, Czajkowska BI, Klementowicz JE, Travis MA. 2012. Regulation of TGFβ in the immune system: An emerging role for integrins and dendritic cells. Immunobiol. 217:1259-1265.

Wysocki LA, Bianchi TS, Powell RT, Reuss N. 2006. Spatial variability in the coupling of organic carbon, nutrients, and phytoplankton pigments in surface waters and sediments of the Mississippi River plume. Estuar Coast Shelf Sci. 69(1–2):47-63.

Xu EG, Mager EM, Grosell M, Pasparakis C, Schlenker LS, et al. 2016. Time- and oil-dependent transcriptomic and physiological responses to Deepwater Horizon oil in mahi-mahi (*Coryphaena hippurus*) embryos and larvae. Environ Sci Technol. 50(14):7842-7851.

Yakimov MM, Cappello S, Crisafi E, Trusi A, Savini A, et al. 2006. Phylogenetic survey of metabolically active microbial communities associated with the deep-sea coral *Lophelia pertusa* from the Apulian plateau, Central Mediterranean Sea.Deep Sea Res Part I. 53:62-75.

Yamaguchi N, Nakano M, Tanida H, Fujiwara H, Kihou N. 2006. Redox reaction of iodine in paddy soil investigated by field observation and the i k-edge xanes fingerprinting method. J Environ Radioact. 86(2):212-226.

Yum LK, Baumgarten S, Röthig T, Roder C, Roik A, et al. 2017. Transcriptomes and expression profiling of deep-sea corals from the red sea provide insight into the biology of azooxanthellate corals. Sci Rep. 7(1):6442.

Zhang LY, Hou XL. 2013. Speciation analysis of ^{129}I and its applications in environmental research. Radiochimca Acta. 101(8):525-540.

Zhang Q, Wang C, Liu Z, Liu X, Han C, et al. 2012. Notch signal suppresses toll-like receptor-triggered inflammatory responses in macrophages by inhibiting extracellular signal-regulated kinase 1/2-mediated nuclear factor κB activation. J Biol Chem. 287:6208-6217.

Zhang X-Y, He F, Wang G-H, Bao J, Xu X-Y, et al. 2013. Diversity and antibacterial activity of culturable actinobacteria isolated from five species of the South China Sea gorgonian corals. World J Microbiol Biotechnol. 29(6):1107-1116.

Ziegler M, Roik A, Porter A, Zubier K, Mudarris MS, et al. 2016. Coral microbial community dynamics in response to anthropogenic impacts near a major city in the central Red Sea. Mar Pollut Bull. 105:629-640.

Ziegler M, Seneca FO, Yum LK, Palumbi SR, Voolstra CR. 2017. Bacterial community dynamics are linked to patterns of coral heat tolerance. Nat Commun. 8:14213.

Ziervogel K, Joye SB, Arnosti C. 2016. Microbial enzymatic activity and secondary production in sediments affected by the sedimentation pulse following the Deepwater Horizon oil spill. Deep Sea Res II. 129:241-2.

Department of the Interior (DOI)

The Department of the Interior protects and manages the Nation's natural resources and cultural heritage; provides scientific and other information about those resources; and honors the Nation’s trust responsibilities or special commitments to American Indians, Alaska Natives, and affiliated island communities.

BOEM
Bureau of Ocean Energy Management

Bureau of Ocean Energy Management (BOEM)

The mission of the Bureau of Ocean Energy Management is to manage development of U.S. Outer Continental Shelf energy and mineral resources in an environmentally and economically responsible way.

BOEM Environmental Studies Program

The mission of the Environmental Studies Program is to provide the information needed to predict, assess, and manage impacts from offshore energy and marine mineral exploration, development, and production activities on human, marine, and coastal environments. The proposal, selection, research, review, collaboration, production, and dissemination of each of BOEM’s Environmental Studies follows the DOI Code of Scientific and Scholarly Conduct, in support of a culture of scientific and professional integrity, as set out in the DOI Departmental Manual (305 DM 3).